Application of Probabilistic Damage Identification to Civil Engineering Structures

T. (Tianxiang) Wang

Technische Universiteit Delft

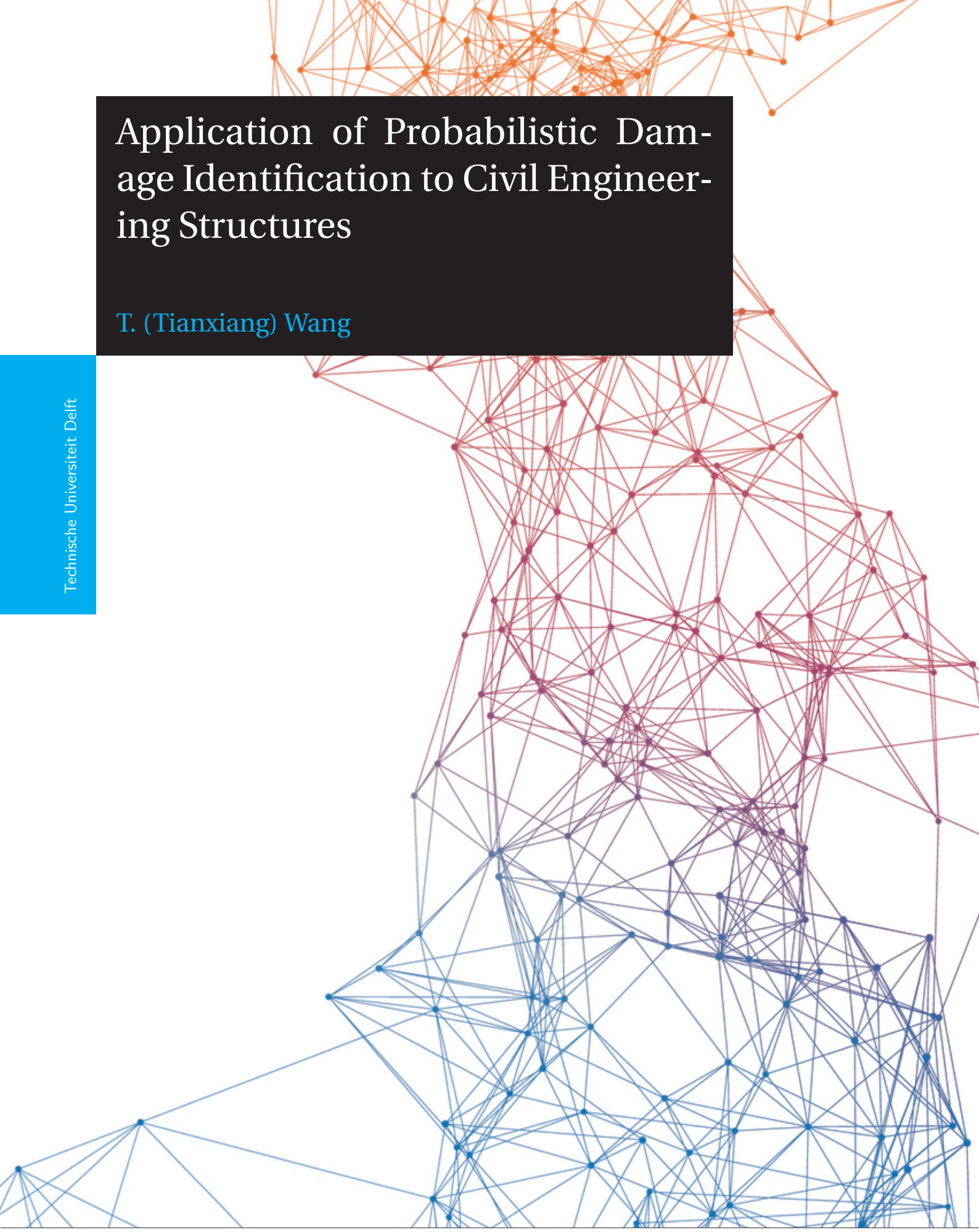

TU Delft Delft University of Technology

Challenge the future

Application of Probabilistic Damage Identification to Civil Engineering Structures

A Marriage of Structural Health Monitoring and Bayesian statistics

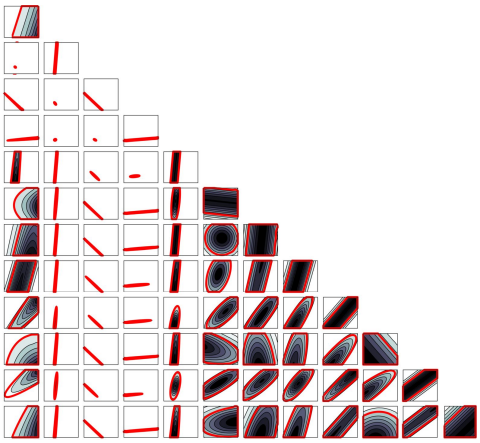

APPLICATION OF PROBABILISTIC DAMAGE IDENTIFICATION TO CIVIL ENGINEERING STRUCTURES

A MARRIAGE OF STRUCTURAL HEALTH MONITORING AND BAYESIAN STATISTICS

by

T.(Tianxiang) **Wang**

in partial fulfillment of the requirements for the degree of

Master of Science

in Structural Engineering (Structural Mechanics)

at the Delft University of Technology,

to be defended publicly on 2018-11-29.

The chair of the master thesis assessment committee:

Dr. ir. M.A.N. Hendriks	Delft University of Technology

Committee members:

Prof. dr. ir. J.G. Rots	Delft University of Technology
Dr. ir. Morales Napoles Oswaldo	Delft University of Technology
Dr. ir. A.T. (Arthur) Slobbe	TNO
Dr. ir. Árpád Rózsás	TNO
Dr. ir. Helder Sousa	HS Consulting / BRISA Group, Portugal

An electronic version of this dissertation is available at
http://repository.tudelft.nl/.

PREFACE

I started my structural engineering master program at TU Delft two years ago. This master thesis is one of the outcomes of this journey which consists of hard work, progress, and joy. The graduate thesis, which is really appealing and interesting to me, is co-supervised by TNO and TU Delft. Here I would like to express my greatest gratitude to those who assisted me to accomplish this graduate program.

First, I would like to thank the chair of my committee Dr. Max Hendriks who kindly introduced me to TNO where I grew and progressed rapidly during the graduate thesis. I appreciate the effort he made to coordinate the committee, giving me valuable feedback after each meeting and keeping me on track and result-oriented. At the beginning of the graduate internship, it was really challenging for me to acquire the statistical and machine learning knowledge that are needed for the completion of this work. With a lot of mathematics and programming involved it is a totally different field than civil engineering with which I am more familiar. I have to mention that Arpad really helped me out in this situation by showing me the tricks and smart ways of programming. There are countless times he taught me how to debug efficiently and how to organize data types. Sometimes, I even got inspired while reading his code, and then generalized them to my case. Thanks to those experience, I felt more fun in programming and really enjoyed it. As the project going, Arthur and Arpad helped me a lot in how to present my work clearly. From the countless internal presentations, I have improved a lot for my presentation skills which is extremely important for my further career based on their advice. Additionally, I also would like to thank Dr. Oswadlo Morales and Dr. Helder Sousa who were really enthusiastic to provide technical advise on my project in their expertise and offer me help when I encountered problems.

Thank to all my friends who have always supported me behind. It is you guys that carry me through. Especially my girlfriend Lizzyzhou, who has always been there for me.

Lastly, I would like to express the greatest thank to my parents. The reason why I am optimistic, confident, and positive, is that I always know that I have you supporting me, which gives me infinite courage to get over difficulties and move forward.

Tianxiang Wang
Delft, November 2018

SUMMARY

The rapid development in statistics, information technology, and computational power have enabled numerous innovative methods to emerge in Structural Health Monitoring (SHM) for structural damage detection, both in practical application and research. The intention of such methods is to use the data obtained from the monitoring system to extract sufficient information to identify damage types that may appear in the structure. However, the following type of questions are mostly unanswered for realistic structural types and monitoring systems: Which responses of the structure should be monitored? Which sensor locations and sensor combinations carry the most information? Among the currently available computational algorithms, which one is the most suitable one in this context? Hence, this study aims to contribute on this front and provide answers for practical applicability. A comprehensive study of a realistic, prestressed concrete bridge built by the cantilever method - the Lezíria Bridge in Portugal is undertaken to provide insight into these questions.

The engineering challenge is studied in a probabilistic framework where the uncertainty sources are model uncertainty and measurement uncertainty. The Bayesian paradigm is used to handle the uncertainty component and a validated Finite Element (FE) model is applied to capture the mechanical behavior. The influence of the potential damage scenario, severity of damage, sensor type, the combination of sensors, prior knowledge of the structure, and the extent of uncertainty of the FE model and measurements are analyzed in this thesis. The informativeness of the Damage Identification (DI) process is reflected by the information content of its resulting posterior distributions. The information content is quantified using measures based on information entropy and the area of credible regions.

It is demonstrated that selecting different responses to monitor may lead to a significant change in the informativeness of the result. It is also shown that for all analyzed cases using the most informative sensor type provides adequate information that reflects the damage state, while the rest types could only complement very limited information. In addition, the hybrid Markov Chain Monte Carlo(MCMC) seems more efficient and effective to conduct Bayesian inference. The findings provide valuable, quantitative insight into the design of new monitoring systems.

Key words: *Structural Health Monitoring, Damage Identification, Bayesian Statistics, Information Content Analysis*

GLOSSARY

Credible region (or interval): a credible region(interval) is a range of values within which an unobserved parameter value falls with a particular probability. We use 90% CR throughout this study which means 0.9 probability mass of the distribution of the random variable in contained in this region. This means that the real value of the parameter is within the 90%-level credible interval with 0.9 probability. Out of the infinitely many credible intervals only the highest density interval (hdi) is considered in this study.

Damage identification: refers to detect the damage which is the changes of the material or geometric properties of the structural system, which may in turn significantly influence the performance of a structure.

Damage scenario: refers only to the type of the damage but does not concern the severity of that. It is used as a hypothesis where the damage type is specified.

Highest density interval (hdi): a special credible interval with the smallest region that contains the given subjective probability (0.9). In two-dimensional cases it is called highest density region.

Likelihood: expresses how likely is the data can fit the model given a set of parameter values.

Measurement uncertainty: describes the difference between a measured value of a quantity and its true value. It is assumed that the measurement uncertainty follows a normal distribution which is quantified in Sousa *et al.* [1].

Model parameters: are the variables that can define a unique FE model in this study. The location and severity of damage can be expressed through changes in model parameters. The FE model can be parameterized by the considered damage scenarios.

Statistical inference: "the process of drawing conclusions about populations or other collections of objects about which we have only partial knowledge from samples" [2]

CONTENTS

List of Abbreviation

Acr	Area of the prior/posterior credible interval/region
ADVI	Automatic Differentiation Variational Inference
BI	Bayesian inference
cdf	cumulative distribution function
CR	Credible Region (highest density)
DH	Horizontal Displacement
DI	Damage Identification
DS	Damage Scenario
FE	Finite Element
FEM	finite element method/model
hpd	highest probability density
HMC	Hamiltonian Monte Carlo
MC	Monte Carlo
MCMC	Markov Chain Monte Carlo
MH	Metropolis Hastings
RO	Rotation
RS	Response Surface
pdf	probability density function
SHM	Structural Health Monitoring
VI	variational inference

List of Figures

LIST OF TABLES

1

INTRODUCTION

1.1. MOTIVATION

Structural monitoring is of great importance, not only for newly built structures but even more importantly for the numerous aging ones. Most recently, a large section of the Morandi bridge collapsed amid heavy rainfall in Italy. Dozens of vehicles plunged 45m amid heavy traffic and forty-three people lost their lives in this disaster. It is reported that the bridge had been suffering from degradation. Due to the degradation and corrosion of existing infrastructure such as bridges and roads, the state of a structure should be clearly known to judge if it is still in good condition to prevent collapse. At present, the decision to repair or replace a damaged structural member of a Civil Engineering structure is prevalently made on the basis of the inspector's or engineer's evaluation of the particular situation with little-published information available for guidance [8]. However, such local inspections may be insufficient to make decisions when the inspection interval is long, and the damage could not be explicitly observed. Other than that, site visits and inspections are time-consuming and costly. For instance, after an extreme event, assigning inspectors to determine which part of the structure needs to be replaced or strengthened could cost days. In terms of efficiency, traditional methods of visual inspection and analysis could often lead to unnecessary maintenance on structural components that are still sufficiently safe. These considerations form one of the reasons why SHM is introduced as a systematic method using monitoring data acquired from sensors on the structure to gain information on the current condition of a structure.

Typically, SHM is able to detect damage that refers to the changes of the material or geometric properties of the structural system, which may in turn significantly influence the performance of a structure. This method increases public safety by detecting damage state of infrastructure more accurately and effectively using the monitoring data collection and analysis. In addition, most SHM systems provide real-time monitoring data details, presenting reliable information on the integrity of the structure, which is extremely crucial after an immediate damage event. Generally, SHM has vastly improved the effectiveness of Damage Identification (DI).

Numerous researches of SHM have emerged in recent decades. Considering the currently available methods, probabilistic approaches of SHM are promising and innovative as it can further improve quantitative assessment. Although lots of methods are developed and discussed, most of them are investigated on greatly simplified examples where the feature of these approaches can be well captured and easy to manipulate under different interested hypotheses, such as introduce different damage severity or scenarios. In contrast, few studies focus on realistic, large-scale civil engineer-

ing structures. Therefore, the availability of such methods applied to a realistic structure and its performance are of great interest.

1.2. RESEARCH QUESTIONS

Condition assessment or damage identification problems can be divided into two groups based on what one can measure. We distinguish direct and indirect assessments. In case of direct assessment, the relevant damage properties can be (quasi-)directly measured, e.g. loss of tendon force from a strain gauge or a load cell applied directly to the tendon in question. In case of the indirect assessment, the measured quantity is only a proxy of the variable of interest (damage), e.g. the increased deflection of a bridge can indicate tendon force loss. Indirect assessment problems are more common than direct ones as (i) we do not know in advance where damage will occur and we cannot put sensors everywhere; and (ii) some damage types cannot or expensive to be directly measure. In this thesis the boundary between direct and indirect assessment problems is defined as follows: if the connection between the directly measured parameter and variable of interest requires the knowledge of the large part of the analyzed structural system we talk about indirect problems, otherwise the problem is direct. The subject of this indirect assessment problems.

With the assistance of a detailed finite element (FE) model that can simulate the structural behavior, SHM can be realized in a manner that the collected monitoring data is used to update the FE model such the model results match the measured values as closely as possible. This is often referred to as the global approach of damage identification (DI) [8].

However, during this process, the data gathered by sensors and calibrated FE models are inevitably burdened by uncertainties. Since computational limitations are becoming less of a concern with increased computing power and enhanced algorithms, it is now possible to conduct the probabilistic analysis of engineering problems where uncertainties can be taken in to account. Bayesian inference is widely used to explicitly incorporate uncertainties. The monitoring data is the input for Bayesian inference which will yield a distribution of parameters that reflect the damage state. Especially for a civil engineering structure, there are various responses that can be potentially measured to acquire the monitoring data.

This study focuses on the application of Bayesian inference to DI. Therefore, factors that may influence the Bayesian inference of detecting damage of a structure will be discussed in this thesis. The main research question arises from these considerations:

- *Given a specific large-scale bridge and available sensors that can be installed to measure the responses, how to set up the possible sensor configurations so that the most information on the damaged condition can be revealed based using Bayesian approach?*

Further questions could be derived from the main research question, such as: Which type of sensor carries the most information? How many sensors should be used at least to detect the damage in an acceptable accuracy and where to put them? Beyond questions about the monitoring data, two more sub-questions are formulated:

- *How to measure the information carried by a sensor in relation to a damage state? How do different measures compare?*

In order to have an explicit definition of how much information is carried by the outcome of Bayesian inference, a proper criterion which can quantitatively measure the information content should be established. Only then the main research question could be resolved appropriately. Another sub-research question is based on the consideration of which algorithms should be used to conduct the Bayesian inference:

- *Which available Bayesian computational algorithms perform better considering the fact that computational demanding FE model is involved in damage identification?*

Thanks to advancements in applied statistics, many computational algorithms are available to solve different Bayesian problems. Unlikely the typical statistical inference problem, Bayesian inference in DI normally involves a detailed FE model which is considered computational expensive if thousands of times evaluation is needed during the inference process. Explained from an engineering point of view, for example, one could not afford to wait days for decision-making after severe damage has occurred on a structure, which leads the demand of using more effective and efficient algorithm to conduct the Bayesian inference. The better performance refers to within the same computational effort, the closer to the exact solution or more effective samples are drawn. This study will be focusing on giving appropriate answers to those research questions through a simple benchmark problem and a realistic full-scale bridge. The overview of the research questions are shown in Figure 1.1.

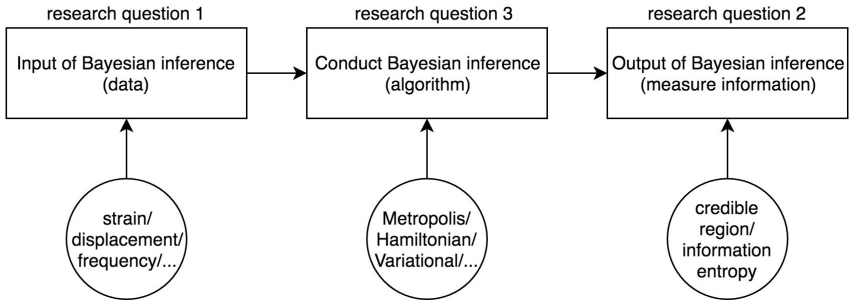

Figure 1.1: Overview of research questions.

1.3. SCOPE

This study uses two structures to illustrate a process of answering the research questions. The methodology can be easily generalized to any other structures. Even though this study mainly focuses on DI in the elastic phase, the idea behind is to collect available data and apply statistical models on the data to solve engineering problems. In this research, pseudo data is created by FE model, while Bayesian approach is employed to represent and propagate model uncertainty and measurement uncertainty. Although using Bayesian techniques for DI contains a detailed and complex FE model, it is still could be seen as a particular Bayesian regression problem with random variables and responses following a relationship that is built through FE model. The Bayesian approach suits particularly well the engineering field such that every mathematical term is assigned a corresponding engineering interpretation. For example, likelihood function accounts for measurement uncertainty while observations are monitoring data. Similarly, the Bayesian approach could be applied to other fields with other engineering interpretations.

1.4. APPROACH

In order to answer the research questions, the following objectives should be achieved.

- Survey of related SHM, Bayesian statistics, and information theory literature for solving the Bayesian inference problem in damage identification.
- Formulation of the desired properties of a benchmark problem. The benchmark problem should illustrate the using Bayesian paradigm is able to detect damage with uncertainties

taken into account. Illustration of the necessity to further investigate the influence of different monitoring data, versatile criterion for information content and efficient computational algorithms.

- Formulation of a realistic problem where Bayesian inference can be used to detect the damage of a full-scale civil engineering structure. Selection of measurement of information content to compare the different monitoring data acquisitions. Selection of computational algorithms to conduct Bayesian inference based on their statistical performance.
- Quantitative comparisons in terms of monitoring data, computational algorithms.

1.5. THESIS STRUCTURE

Firstly, in chapter 2 the literature is studied in the field of SHM for DI, especially the frequently-used deterministic methods, after which Bayesian approach is introduced with successful applications to take into account uncertainties. Afterward, Bayesian inference for DI is outlined in a rigorous, theoretical manner in chapter 3 where the background of research questions is elaborated.

In order to thoroughly explore of the research questions, a simple but illustrative benchmark example which is easy to tune has been studied in chapter 4 to capture the features. Due to its simplicity to parameterize, insights can be gained after numerous tests under different hypotheses. Through this benchmark shear frame problem, different responses show notably different performance in terms of information content. In parallel, the performance of various algorithms is discussed. Generally, the benchmark problem provides sufficient evidence that it is worthwhile to further investigate a realistic structure.

As a step further in the level of complexity, and based on recent work done by Sousa *et al.* [1] in the application of advanced FE models and probabilistic methods on damage identification on a full-scale prestressed concrete bridge - Lezíria Bridge in Portugal, this chapter extends the features and conclusions drawn from the shear frame example by addressing some of the research questions outlined in the above-mentioned work. Although it still follows a similar methodology to gain insights of the DI of a bridge, new problems and features arise due to the complexity and variability of the Bayesian inference applied on a detailed and full-scale civil engineering structure. Selection of computational algorithms as well as improving the measures of information content is made according to those problems. Most importantly, conclusions can be drawn not only in accordance to research questions themselves, but interesting engineering perspectives of the DI could also be summarized for a specific structure. Finally, limitations and recommendations are discussed.

2

Literature Review

2.1. Overview

First, the relevant literature is reviewed to understand the current state of SHM for Damage Identification (DI). Several common deterministic methods of DI are studied. However, deterministic methods cannot address uncertainties associated with the structural model and measurement, which Bayesian statistics can incorporate. Then, a number of applications using Bayesian techniques to solve DI problems have been exhibited with their innovations and limitations. Finally, the contribution of this study is presented.

2.2. Deterministic Methods of DI

Ideally, a monitoring system would be able to identify the damage at a very early stage, locate the damage within the available sensor distribution, provide an estimation of the severity of the damage, and predict the responses in the future [9]. A common practice for DI is parameter estimation where normally a refined FE model is included. After obtaining measured test data, the FE model would be calibrated by parameters based on optimization methods to minimize the error between the FE model response and the measured data. Parameters of FEM can be generalized such as geometric or material properties according to its potential damage scenario so that damage state can be reflected by its value. For instance, Sanayei and Saletnik [10] selected strain to be measured, where a truss and a frame structure are created to illustrate changes in element stiffness parameters can be identified by elemental strain measurement. Besides unique monitoring data type, a combination of experimental static test data and changes in frequencies is used to detect damage in a planar truss model proposed by Wang *et al.* [11]. Doebling *et al.* [9] has summarized vibration-based identification techniques that are deterministic and their applications in specific structures comprehensively.

All of these above-mentioned studies treat parameters that reflect damage as deterministic quantities by minimizing the error between the FE model responses and measured responses. The parameters are expected to represent the current condition of a realistic structure through a FE model.

2.3. Bayesian Approach of DI

In reality, there are always errors associated with the process of constructing a theoretical model of a structure, for instance, FE model [12]. This is due to simplifications and assumptions made during

the model process, i.e. the idealized model may not truly represent all the aspects of an actual structure [13]. Moreover, measurement uncertainties arise from the presence of noise while measuring the responses, which will propagate to the output data. Therefore, it is necessary to account for uncertainties. A Bayesian model updating approach that based on the foundation of Bayes' theorem provides a robust and rigorous framework to incorporate the modeling uncertainty and measurement uncertainty [14]. Bayesian approach updates a specified set of models with their corresponding probability that reflects the likelihood between the predicted response and measured response [15]. The probability distribution of model parameters is first assumed based on prior knowledge. Then it is updated based on Bayes' theorem by using available measured data.

A variety of applications of Bayesian approach for DI are published. Starting with the availability for less complex structures, Sohn and Law [16] has shown Bayesian approach is valid to detect multiple damage locations for a 6-story shear frame. Beck and Au [17] applied Bayesian model updating problem to a 2-story shear frame model, where frequencies are measured to infer changes of stiffness. Similarly, Cheung and Beck [18] expanded the amount of uncertain parameters to 31 with mass, stiffness and damping parameters for a 10-story linear shear building. It has been shown that even though with large measurement uncertainty where deterministic methods might yield less accurate results due to the noise, parameters are still well approximated by the sample mean of Bayesian inference. Other than truss and frame structures, Straub and Papaioannou [15] aplplied the Bayesian approach to a cantilever beam, the authors used the deflection data to infer the reciprocal of bending rigidity of the beam. Moving into realistic applications, Bayesian approaches have been successfully applied in bridge engineering. In the DI of steel truss bridges, the modeling uncertainties of the joint configuration are tackled with Bayesian approach by Zheng and Yu [19]. It is worth mentioning rather than measuring the realistic structure, a FE model of truss bridge is created through OpenSees to simulate the damage scenarios and collect the monitoring data in this literature. Mustafa and Matsumoto [13] created FE model for an existing, damaged bridge where the experimental data is obtained from. They demonstrated that after obtaining the experimental data and its corresponding FE model, Bayesian model updating is able to detect the local damage of the real structure through the updated model parameters. Moreover, Figueiredo *et al.* [14] shows detecting damage in the Z-24 bridge in Switzerland at an early stage is still possible by using pattern recognition to distinguish that the variation of frequency is caused by damage, but not the variability of temperature or traffic load. Above mentioned studies focus on inferring parameters within a specific model, whereas competing models in a 2-story frame and 10-story building are also investigated by model selection to determine the most appropriate model among several candidate models [20]. During the process of DI, limitation that the number and location of measurement sensors are not properly addressed is brought up. Optimizing sensor location to extract the most information of the uncertain parameters is discussed by Papadimitriou *et al.* [21] where information entropy is introduced as a criterion of optimality using simplified truss and shear structures.

2.3.1. COMPUTATIONAL METHODS

Mathematicians and statisticians have found numerous algorithms to conduct Bayesian analysis, each of these algorithms have their strengths and weaknesses. Mackay [3] has summarized several commonly used computational methods including the Markov Chain Monte Carlo (MCMC) and variational inference (VI). Unlikely the typical statistical problems, using Bayesian statistics in DI usually involves computational demanding FE models. Cheung and Beck [18] introduced improved Markov Chain convergence criterion to increase the acceptance rate while using hybrid Monte Carlo simulation. Beck and Au [17] applied adaptive simulation Markov Chain Monte Carlo method to explore the parameter space more effectively. Interestingly, Straub and Papaioannou [15] validates the availability of using structural reliability method instead of MCMC with the same structure [17]

showing that different computational algorithms are applicable for the same problem. However, no comparison is made between different methods in terms of the performance of sampling.

2.4. KNOWLEDGE GAPS

Although Bayesian approach for DI has been widely investigated, there is limited knowledge regarding:

- Exploration of monitoring different responses for a full-scale bridge considering different damage scenarios.
- Discussion of information gain using a subset of all available sensors.
- Comparing the performance of different computational algorithms to conduct Bayesian inference when a detailed and computational demanding full-scale FE model is involved.

The above-mentioned aspects are related to the corresponding research questions that will be answered through this study.

3

CONCPETS, METHODS, AND TOOLS

3.1. OVERVIEW

The methodology to answer the research questions is introduced in this chapter. First, basic definitions are explained, after which the Bayesian paradigm is elaborated as the connection of those definitions. An overview of Bayesian approach for DI is shown in Figure 3.1. Following the flowchart, several computational algorithms are selected to conduct Bayesian analysis.

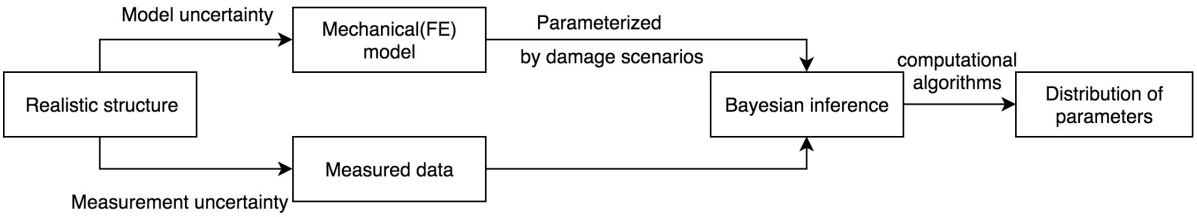

Figure 3.1: Flowchart of DI using Bayesian inference.

Then, after obtaining the posterior distribution of parameters, methods that will be used to gain insight into the outcome in terms of information content are presented. Two criteria are investigated for this purpose namely, the area of credible region and information entropy. Other than the information contained by the joint distribution of variables, the dependence structure of those variables is worth being explored. Copula is used to describe the dependence between random variables. Therefore, the inference outcome is analyzed in these three aspects , as shown in Figure 3.2.

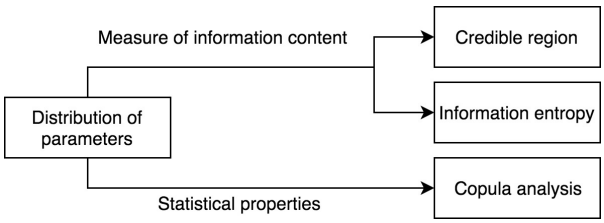

Figure 3.2: Framework of analyzing inference outcome.

3.2. MECHANICAL MODEL

In this study, all structures are modeled using the Finite-Element Method (FEM) assuming linear-elastic behavior. The advantage of FE models is that it is easy to parameterize the model with relevant damage configurations and to introduce damage on element-level. For example, if the stiffness loss of a certain part of a structure is of interest, it can be parameterized by a group of element stiffness variation. In this context, one specific parameter, which will be named model parameter throughout this study, defines a unique FE model. Therefore, the location and severity of damage can be expressed through changes in model parameters. The model parameters are associated with the damage of a real structure, being the proxy of damage extent. Additionally, a specific parametrization scheme is called a model class. For example, given a bridge, if the settlement of a support is of interest, then the model can be parameterized by pier settlement with the parameters representing the extent of settlement. Similarly, if the loss of stiffness for bridge components is considered, the bridge can be parameterized with the variation of stiffness, where the parameters reflect the extent of stiffness loss, as shown in Figure 3.3.

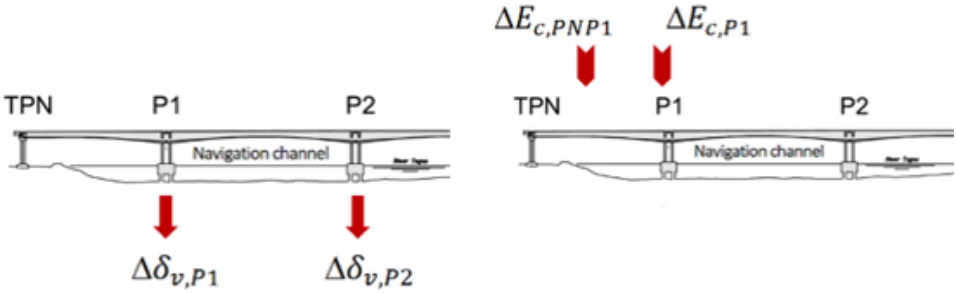

Figure 3.3: Different parametrizations for the same structure [1]

.

3.3. UNCERTAINTIES

In general, how uncertainty is modeled in this work isexpressed by the following equation:

$$\begin{aligned} y^{\text{measured}}(\mathbf{x}) &= y^{\text{real}}(\mathbf{x}) + \varepsilon \\ y^{\text{real}}(\mathbf{x}) &= y^{\text{FEmodel}}(\mathbf{x}) + \delta(\mathbf{x}), \end{aligned} \tag{3.1}$$

where $y^{\text{measured}}(\mathbf{x})$ denotes the measured responses of a structure, which is also called observations or monitoring data, $y^{\text{FEmodel}}(\mathbf{x})$ denotes the responses from the FE model, $\delta(\mathbf{x})$ denotes the discrepancy function between the analytical responses (FE model) and the experimental responses (without noise), ε denotes the measurement uncertainty. In Eq. 3.1, the first equation shows the measured responses are the combination of real responses and the measurement noise, while the second equation indicates the real responses consist of the simulated responses by FE model and a term describes the discrepancy between FE model responses and experimental responses due to the model uncertainty. In other words, the measured responses are the summation real responses related to FE model and an independent additive term – measurement uncertainty.

3.3.1. MODEL UNCERTAINTY

Model uncertainty refers to the discrepancy between the theoretical model, specifically, FE model in this study, and the real structure. It occurs during the process of constructing a representative

model of the real structure through FE modeling. It is because of the simplifications of FE model and the uncertain environment of the structure, such as no perfect support, variation of materials during manufacture when it is assumed the material properties are homogeneous. In Eq. 3.1, $\delta(\mathbf{x})$ accounts for model uncertainty, where x in this study, refers to the model parameters.

3.3.2. MEASUREMENT UNCERTAINTY

Measurement uncertainty – also called measurement noise or observation noise – describes the difference between a measured value of a quantity and its true value. If no measurement uncertainty presents, there would be a unique mapping between the parameters and responses. It is supposed that measurement uncertainty always exists, which means data is contaminated by noise during measurement. For simplicity, in this study, the assumption that the measurement uncertainty for different sensors is independent of each other is made. More specifically, it is assumed that the measurement uncertainty can be expressed in an additive form (Eq. 3.1) and normally distributed with zero mean in Eq. 3.2. The σ for different sensors may change, but there is no correlation between different sensor measurement.

$$\varepsilon \sim \mathcal{N}(0, \sigma^2). \tag{3.2}$$

3.4. BAYESIAN INFERENCE

Bayesian inference is a statistical inference approach where Bayes' theorem is applied to update the probability of a hypothesis using data. It is an extremely powerful set of tools for modeling any random variable when the data is limited and some prior knowledge is provided. Bayesian statistics treats all inference about the unknown quantities as random variables by assigning a probability distribution to each. The Bayesian model draws the latent variables (parameters) from a prior distribution where the initial belief is taken into account, then relates them to the observations (data) through a likelihood function. There is an underlying relationship between the latent variables and the observable data, in this study, the measurable responses of a structure are controlled by the model parameters through the FE model. After observing the data, the prior knowledge of the latent variables will be updated by the data, which results in the posterior distribution. The goal of Bayesian inference can be summarized in three categories, parameter estimation, prediction of data values, and model selection [22]. In this study, we focus on parameter estimation and model selection.

3.4.1. PARAMETER ESTIMATION

Bayes' theorem is the fundamental theorem for Bayesian statistics to incorporate the information carried by observed data and prior information about the event, through the likelihood function and prior distribution of parameters, respectively. Bayesian statistics allows newly observed data to update the initial belief of an event.

Bayes' theorem with discrete events:

$$\begin{aligned} P(A|B) &= \frac{P(B|A) \cdot P(A)}{P(B)} \\ P(B) &= \sum_n P(B|A_n) \cdot P(A_n) \end{aligned} \tag{3.3}$$

Where

- $P(A|B)$ is the probability of an event A occurs given that B occurred;
- $P(A)$ or $P(B)$ is the probability of event A or B occurs , which is also called marginal probability;
- $P(B)$ is called evidence, which can be calculated by the low of complete probability;

In Bayesian inference, parameters are treated as random variables and assigned a probability distribution. By substituting the event A and B with parameters and observations, the Eq. 3.3 expression will be:

$$P(\theta|x) = \frac{P(x|\theta) \cdot P(\theta)}{P(x)} = \frac{P(x|\theta) \cdot P(\theta)}{\int_{\Theta} P(x|\theta) \cdot P(\theta) \cdot \mathrm{d}\theta} \tag{3.4}$$

where

- x is the observed data or observations;
- θ is the parameters to be inferred;
- $P(x|\theta)$ denotes the likelihood of getting the observations given a set of parameters;
- $P(\theta)$ denotes the prior distribution that reflects the prior knowledge on the parameters;
- $P(x)$ is also known as evidence which is a constant by marginalizing the production of prior and likelihood function over the entire parameter space;
- $P(\theta|x)$ is the posterior distribution of parameters after taking into account the observed data.

The main goal of Bayesian inference in DI is to estimate the representative model parameters using the monitoring data of a structure with prior knowledge. It is widely known as model updating, which involves choosing the parameters within a class of model to match the measured data with its corresponding responses. This is an inverse way of modeling a structure by a set of parameters and then simulating the responses. In contrast with deterministic approach, the model parameters are no longer constant values but a distribution of all possible parameters with their own weights according to the monitoring data, where uncertainties have been taken into account. The FE models by identified parameters are supposed to be capable of producing responses which are close to, but not necessarily equal to, the measured data. If a FE model is built for a structure, there are various choices regarding the parametrization of the model which depends on the considered damage scenario. Bayesian inference is to infer the distribution of model parameters if an explicit parameterized scheme for the structure is given and monitoring data is available. The corresponding engineering explanations of Bayesian inference are listed in Table 3.1.

Mathematics	**Engineering**
Hypothesis/Model	A parameterized FE model
Parameters θ	Unobservable quantities that define the FE model
Observations x	The measured responses from a structure
Priors $P(\theta)$	The prior knowledge of parameters before measuring responses
Likelihood $P(x\|\theta)$	The likelihood of observing the responses given a certain FE model
Posteriors $P(\theta\|x)$	A distribution of model parameters of a structure considering initial belief and the measured responses

Table 3.1: Engineering definition of its corresponding mathematical quantity.

3.4.2. MODEL SELECTION

There may exist several possible hypotheses or models to describe a problem, which involves a hierarchical dependency of variables. The second goal of Bayesian inference in this thesis is to deter-

mine which model has the higher magnitude of belief to fit the observable data. As mentioned in Table 3.1, the inference of parameters is conditional on the model class or hypothesis, which can be tackled with Bayes' rule again. Essentially, model selection is a case of parameter estimation, it can expressed as following, which is an expansion of Eq. 3.4:

$$P(\theta|x,\mathcal{M}) = \frac{P(x|\theta,\mathcal{M})\cdot P(x|\mathcal{M})}{P(x|\mathcal{M})} = \frac{P(x|\theta)\cdot P(\theta|\mathcal{M})}{\int_{\Theta} P(x|\theta,\mathcal{M})\cdot P(\theta|\mathcal{M})\cdot \mathrm{d}\theta} \tag{3.5}$$

$$P(\mathcal{M}|x) = \frac{P(x|\mathcal{M})\cdot P(\mathcal{M})}{P(x)} \tag{3.6}$$

In DI, model class can be explained as a certain scheme of parametrizing the undamaged mechanical model. There are various model classes that can be generated based on different possible damage scenarios, for example, if a bridge is suspected to be damaged, it can be parametrized as in Fig.3.3 based on different hypothesis. If both model classes are reasonable to be established, it becomes extremely important to identify which model class has a higher probability of observing the measured data, equivalently, to determine which damage scenario does it belong to according to the measured data. If all the damage scenarios are considered equivalently, which means the prior probability is equal to each other, the denominator does not influence the value of $P(\mathcal{M}|x)$. The only contributing part is the model evidence $P(x|\mathcal{M})$. It is also worth noticing that calculating model evidence requires integration over the parameter space , which is intractable when the parameter dimension is high (dim>5).

Models are often compared using the Bayes factor that is a probability ratio of two models, as shown in Equation 3.7, which is the ratio of Eq. 3.6 for two competing models. Table 3.2 contains a recommendation on how to use the Bayes factor for model comparison.

$$B_{2,1} = \frac{p(\mathcal{M}_1|\mathbf{x})}{p(\mathcal{M}_2|\mathbf{x})} = \frac{p(\mathbf{x}|\mathcal{M}_1)\cdot p(\mathcal{M}_1)}{p(\mathbf{x}|\mathcal{M}_2)\cdot p(\mathcal{M}_2)} \tag{3.7}$$

Bayes factor	**Evidence against model i**
1-3.2	Not worth more than a bare mention
3.2-10	Substantial
10-100	Strong
>100	Decisive

Table 3.2: Bayesian factor for model selection [6].

3.4.3. BAYESIAN COMPUTATIONAL ALGORITHMS

In Equation 3.4, the denominator of posterior density involves integrating the product of the likelihood and prior over the parameter space, which is normally unfeasible in moderately high dimensions (>4). Therefore, a class of Markov Chain Monte Carlo (MCMC) simulation methods have been developed for obtaining an asymptotic approximation of the posterior distribution without calculating the denominator. Representative samples can be drawn from the posterior by random walk, as long as the random walk chains reach stationarity. The general process of random walk can be described as algorithms use different schemes to draw next potential sample, and then judge if accept the next sample or reject it based on a certain criteria which are related to the probability density of the current sample and the next tentative sample. For example, the Metropolis-Hastings

(MH) uses a customized proposal function to draw the a candidate sample, then the probability density of the proposed candidate is evaluated to be compared with the current one. We accept the candidate if its density is greater. However, if the target distribution is smaller, we accept it with a customized probability α, as shown in Fig .3.4. By doing so, the random walk will draw more samples in the area where the probability density is high. As soon as the stationary criterion has been reached, a sample of the target distribution by observing the chain after a certain number of steps can be obtained. The larger the sample size is, the more closely the distribution of the sample matches the actual desired distribution. Another advantage of drawing representative sample is it becomes easier to obtain important quantities such as mean and variance, where integration is normally required for analytical results. In addition, marginalizing becomes easier by discarding the irrelevant variables since sample is vector of parameters where different variables are recorded separately. The availability of such approximation methods has been widely studied in terms of convergence diagnostics mathematically.

MCMC methods	Strength	Limitation
Metropolis	1. no need to explore the conditional distributions for each random variables 2. versatile, as long as the target PDF can be evaluated	1. sensitive to the algorithm parameters (have to tune with the accept rate or adjust the proposal function if it rejects too many samples)
Gibbs sampling	1. does not have algorithm parameters to tune	1. not available when the conditional distributions are not known 2. the conditional distribution is not a parametric distribution (can't directly sample from) 3. not efficient for multiple clusters
Slice sampling	1. the random walk would always move forward 2. the step size is self-tunning	1. the likelihood is evaluated multiple times within one step (extremely expensive for our model)
Hamiltonian MC	1. reduces the random walk behavior, and explores the target more quickly the MH	1. requires the gradient of likelihood function can be evaluated 2. evaluate likelihood and its gradient every step

Table 3.3: Comparison of different MC methods

Several most commonly used MCMC algorithms are listed in this Table 3.3 , where their strengths and limitations are also mentioned. Two of them are selected in this study to test their behavior when a FE model is involved, Metropolis-Hastings (MH) and Hamiltonian MC (HMC), namely. The Gibbs sampling is excluded due to the conditional distribution is not known, while for slice sampling, it is not considered since it evaluates the likelihood function which is extremely computational expensive for multiple times within one step. First, convergence diagnostics will be conducted, after which comparison is made based on the performance of each algorithm. Specifically, with the same amount of evaluations for the likelihood which is considered the most computationally demanding part, effective sample size and MC error are compared as they demonstrate the effectiveness and efficiency of Monte Carlo chains. Besides, another approximation method: Variational Inference(VI) is also investigated, where posterior is approximated by minimizing the variational free energy of a parametric distribution. The algorithms of MH and HMC are detailed in Fig 3.4 and Fig 3.5.

Algorithm 1 Metropolis-Hastings algorithm

Initialize $x^{(0)} \sim q(x)$
for iteration $i = 1, 2, \ldots$ **do**
  Propose: $x^{cand} \sim q(x^{(i)}|x^{(i-1)})$
  Acceptance Probability:
    $\alpha(x^{cand}|x^{(i-1)}) = \min\{1, \frac{q(x^{(i-1)}|x^{cand})\pi(x^{cand})}{q(x^{cand}|x^{(i-1)})\pi(x^{(i-1)})}\}$
  $u \sim \text{Uniform}\ (u; 0, 1)$
  if $u < \alpha$ **then**
    Accept the proposal: $x^{(i)} \leftarrow x^{cand}$
  else
    Reject the proposal: $x^{(i)} \leftarrow x^{(i-1)}$
  end if
end for

Figure 3.4: Metropolis Hastings sampling procedure [3]

Algorithm 1 Hamiltonian Monte Carlo

Given θ^0, ϵ, L, $\mathcal{L}$, M:
for $m = 1$ to M **do**
  Sample $r^0 \sim \mathcal{N}(0, I)$.
  Set $\theta^m \leftarrow \theta^{m-1}, \tilde{\theta} \leftarrow \theta^{m-1}, \tilde{r} \leftarrow r^0$.
  for $i = 1$ to L **do**
    Set $\tilde{\theta}, \tilde{r} \leftarrow \text{Leapfrog}(\tilde{\theta}, \tilde{r}, \epsilon)$.
  end for
  With probability $\alpha = \min\left\{1, \frac{\exp\{\mathcal{L}(\tilde{\theta}) - \frac{1}{2}\tilde{r}\cdot\tilde{r}\}}{\exp\{\mathcal{L}(\theta^{m-1}) - \frac{1}{2}r^0\cdot r^0\}}\right\}$, set $\theta^m \leftarrow \tilde{\theta}$, $r^m \leftarrow -\tilde{r}$.
end for

function Leapfrog(θ, r, ϵ)
Set $\tilde{r} \leftarrow r + (\epsilon/2)\nabla_\theta \mathcal{L}(\theta)$.
Set $\tilde{\theta} \leftarrow \theta + \epsilon\tilde{r}$.
Set $\tilde{r} \leftarrow \tilde{r} + (\epsilon/2)\nabla_\theta \mathcal{L}(\tilde{\theta})$.
return $\tilde{\theta}, \tilde{r}$.

Figure 3.5: Hamiltonian Monte Carlo sampling procedure [3]

After drawing samples from the target distribution, we would like to know if the simulation reaches stationary. One way of confirming this is to see if multiple chains initialized from different initial conditions give similar results of the target distribution. Considering the fact that the starting point

may be far away from the target distribution, we may discard first certain amount of samples, which allows Markov Chain to cost some time to reach its equilibrium distribution. The discarded samples is called burn-in period. Back to the problem if the MC simulation is converged, Gelman *et al.* [23] has introduced a convergence diagnostics which require the Gelman factor of MC simulation equals to 1. Once the MC chains are converged, we can assume that the stationary distribution of simulation is the target distribution. Apart from the highest density credible interval of parameters, we analyze the behavior of MC simulation in terms of effective sample size and standard error which is defined as follow:

- Standard error (MC error): the standard error equals the sample standard deviation divided by the square root of the sample size, it is a measure of the dispersion of sample means (MC sample) around the population mean (According to central limited theory, the sample mean will be close to population mean if the sample size is large enough)
- Effective sample size: it is the equivalent amount of samples which are drawn independently from the target distribution

3.5. INFORMATION CONTENT OF POSTERIOR DISTRIBUTION

This section provides methods that will be employed to evaluate the information contained in the posteriors. The aim of measuring information content is to show how much information can be extracted from the outcome of Bayesian inference, in other words, how well can the measured data explain the damage scenario. Credible region and information entropy are selected as indicators for measuring the information content of posteriors.

3.5.1. CREDIBLE REGION

In Bayesian statistics, a credible region(interval) is a range of values within which an unobserved parameter value falls with a particular probability. It is a region in the domain of a posterior probability distribution that constitutes a given amount of the posterior (probability) mass. The credible region throughout study is the smallest region that contains the given subjective probability mass for the two-variable joint distribution, which is analogized by the narrowest credible interval for 1D case. Mathematically, an α % of credible region is defined: first, find $P*$ that satisfies:

$$\alpha = \int_{\theta:P(\theta|x)>P*} P(\theta|x)\mathrm{d}\theta$$

then obtain the credible region:

$$C_\alpha(\theta) = \{\theta : P(\theta|x) > P*\}$$

In this study, the area of 90% credible region where the inferred parameters would fall with a probability of 0.9, is used to evaluate the information contained as a proxy for different posteriors. The smaller the credible region is, which means the parameter would fall into the smaller constrained area with a subject probability, the more informative the posterior is. By comparing the credible region of different posteriors, a desirable posterior could be selected as the most information included. Accordingly, its observation is valuable since it tells which responses to be measured can identify the damage of a structure best. The credible region could also be visualized to be an auxiliary criterion for engineers making decisions. In the following chapters, within a damage scenario, the CR using different pair of sensors is compared through the Equ .3.8 which is proposed in Sousa *et al.* [1].

$$\eta_i = \left(\frac{A_{\text{CR,ref}}}{A_{\text{CR},i}} - \frac{A_{\text{CR,ref}}}{p_{CR} \cdot A_{\text{sup}}} \right) \cdot \frac{1}{1 - \frac{A_{\text{CR,ref}}}{p_{CR} \cdot A_{\text{sup}}}} \tag{3.8}$$

where

- η_i is the relative explanatory power
- $A_{\text{CR},i}$ area of the posterior credible region (A_{CR}) considering the nth set of sensors
- $A_{\text{CR,ref}}$ is the area of the posterior credible region considering the reference set of sensors
- $A_{\text{sup}}$is the the total area of the support of the inferred parameters
- P_{CR} is the probability/credible mass corresponding to the credible regions

3.5.2. INFORMATION ENTROPY

Information entropy quantifies the uncertainty involved in the value of a random variable or the outcome of a random process. An intuitive interpretation of information entropy: if a lower probability event occurs it conveys more information than the occurrence of a higher probability event. The entropy of a probability distribution is simply the weighted average of information carried by variables over their probability distribution. Higher entropy represents a lack of information, which is also considered to be more uncertain and unpredictable [24]. Mathematically, the entropy is defined:

$$h(P) = -\sum P_i \log(P_i) \tag{3.9}$$

For a continuous probability density functions:

$$h(P) = -\int_{Support} p(x) \log p(x) dx \tag{3.10}$$

Subsequently, entropy will be utilized to measure how much information does a selected posterior of two variables to present a quantitative comparison between different posteriors. The smallest entropy represents the least uncertainty of inferring the parameters. Entropy of continuous variables:

$$h(p(x_1, ..., x_n)) = -\iint_{X_1,...,X_n} p(x_1, ..., x_n) \log p(x_1, ..., x_n) dx_1 ... dx_n \tag{3.11}$$

3.6. COPULA

After obtaining a set of posteriors, dependency of the variables is of interest from a statistical perspective. Copula is a function that is used to describe the dependence structure between random variables by eliminating the effect of marginal distribution. It could potentially provide valuable information giving the engineering background. For example, copula is widely used to investigate tail dependency. Given the context of DI, it could be explained that if two parameters are selected to describe the damage scenario, will one parameter reach extremely large values, given severe damage has occurred in terms of the other parameter. According to Sklar's theorem, multivariate distribution can be written in terms of its marginal distribution and copula. Therefore, multivariate joint distributions can be decomposed into marginal distributions and copula function.

Given a random vector = $(X_1, X_2, ..., X_n)$, with marginal CDFs $(F_1(x), F_2(x), ..., F_n(x))$

According to the probability integral transformation:

$$F_1(x), F_2(x), ..., F_n(x) \sim \text{Uniform}(0,1)$$

.

Using Sklar's theorem the joint cumulative distribution can be defined with a copula function:

$$C(F_1(X_1), F_2(X_2), ..., F_n(X_n)) = \Pr(F_1(x) < F_1(X_1), ..., F_n(x) < F_n(X_n)) \tag{3.12}$$

In addition, there is a class of parametric family such as Gaussian copula, Gumbel copula whose properties have been extensively studied. Among these copulas, each of them may capture different dependence structures, such as, Clayton can only capture negative tail dependencies while Frank can model negative and positive dependencies. Therefore, the parametric copula families provide references to explore the dependence structure non-parametric distribution. Kendall rank correlation coefficient is calculated as a parameter to match the non-parametric copula and parametric family. The definition of Kendall tau coefficient is defined in Eq. 3.13 between two measured quantities(X_i, Y_i), where the concordant pair means $X_i > X_j and Y_i > Y_j$; or $X_i < X_j and Y_i < Y_j$, the discordant pair means $X_i > X_j and Y_i < Y_j$ or $X_i < X_j and Y_i > Y_j$. If If $x_i = x_j or y_i = y_j$, the pair is neither concordant nor discordant.

$$\tau = \frac{\text{(number of concordant pairs)} - \text{(number of discordant pairs)}}{n(n-1)/2}. \tag{3.13}$$

First, drive the copula density equation using Eq. 3.14 based on the knowledge of joint distribution and marginal distributions,

$$c(F_1(X_1), F_2(X_2), ..., F_n(X_n)) = \frac{f(x_1, ..., x_n)}{f_1(x_1) \cdot f_2(x_2) ..... f_n(x_n)} \tag{3.14}$$

After obtaining the copula density, a set of samples can be drawn according to the density using rejection sampling [3]. Then the Kendall tau coefficient of the copula density samples can be calculated, after which five common parametric copulas are selected as reference with the same coefficient. The parametric family contains the Gaussian copula, Gumbel copula, student-T copula, Clayton copula, and Frank copula.. The copula density of matching parametric family is controlled by the parameter θ, which can be determined through the relationship in the last column of Table .3.4, where $D_1(\theta) = 1/\theta \cdot \int_0^\theta t/(e^t - 1) \cdot dt$. Therefore, the procedure of finding the matching parametric copula for a non-parametric copula is summarized as:

- Calculate the non-parametric copula density so that samples can be drawn accordingly
- Determine the τ parameter of non-parametric copula based on the samples using Equ. 3.13
- Determine the corresponding θ parameter by $\theta(\tau)$
- Calculate the parametric copula with the same Kendall tau parameter
- Compare the copula density and correlations in different quadrants

Parametric copula	**Copula distribution**	$\theta(\tau)$
Gaussian	$\Phi_{Ga}\left(\Phi^{-1}(u_1),\Phi^{-1}(u_2);\theta\right)$	$\sin(\pi/2\cdot\tau)$
Student T	$t_2\left(t^{-1}(u_1;\nu),t^{-1}(u_2;\nu);\theta\right)$	$\sin(\pi/2\cdot\tau)$
Clayton	$\left(\max\left\{{u_1}^{-\theta}+{u_2}^{-\theta}-1;0\right\}\right)^{-1/\theta}$	$2\cdot\tau/(1-\tau)$
Gumbel	$\exp\left(-\left(-\log(u_1)^{\theta}+-\log(u_2)^{\theta}\right)^{1/\theta}\right)$	$1/(1-\tau)$
Frank	$-\frac{1}{\theta}\cdot\ln\left(1+\frac{(e^{-\theta\cdot u_1}-1)\cdot(e^{-\theta\cdot u_2}-1)}{e^{-\theta}-1}\right)$	$1+4\cdot(D_1(\theta))-1)/\theta$

Table 3.4: Parametric copula controlled by Kendall tau parameter [7]

The contour of copula density for each copula is visualized first with the same color gradient. This is to determined which parametric copula has the close density gradient with the non-parametric one. Afterward, the copula space has been divided into four quadrants to visualize the density distribution over four quadrants and correlation of each quadrant. The best match parametric copula would be the one who has the same tendency of all aspects mentioned above. Then the dependence structure of two variables could be estimated by the best matching parametric copula.

4

BENCHMARK PROBLEM: TWO-STORY SHEAR FRAME

4.1. OVERVIEW

A two-story structure in Fig. 4.1 is created which is simple but illustrative to show interesting features of damage identification using Bayesian inference. According to the main research question, two responses are selected to be measured as measurable data sources. Performance of measuring different responses is evaluated by quantifying the information content and visualizing the posterior distributions. Approximation tools of Bayesian computation are investigated to explore higher dimensional parameter space, in the meanwhile, to explore the sub-research-questions. Their behaviors are compared in terms of convergent rate, MC error, and effective sample size. This section is a preliminary analysis for further research where interesting features are extended in chapter 5.

4.2. FE MODEL

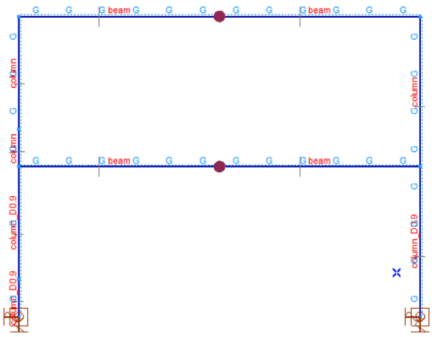

Figure 4.1: Model in the Axis FE program (reality).

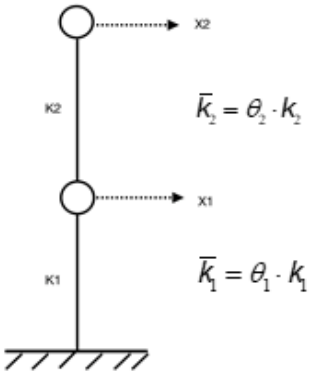

Figure 4.2: FE model.

The mechanical example is a two-story shear frame inspired by Beck and Au [17]. Both measurement uncertainty and model uncertainty are taken into account, an initial value of mass and stiffness should be set up based on engineering knowledge as shown in Table 4.1. The initial value will be updated using Bayes' rule to reflect the state after measuring certain responses.

The structure is two-story frame, each story is modeled as a rigid (relatively high Young's modules, $10 * E$) beam with length of 8m, the beam cross-section is $A_{beam} = 10.5 \times 10^{-3} m^2$, with same density $\rho = 7850 kg/m^3$, young's modules$E = 20000 N/mm^2$. The inter-story is modeled as a column with cross-section $A_{column} = 18.8 \times 10^{-3} m^2$, $I_{column} = 0.167 \times 10^{-3} m^4$ and its stiffness $\frac{12EI}{l^3}$ is to be updated based on the monitoring data.

Bay width	8m
Story height	3m
Column area	$A_{column} = 18.8 \times 10^{-3} m^2$
Moment of inertia	$I_{column} = 0.167 \times 10^{-3} m^4$
Beam area	$A_{beam} = 10.5 \times 10^{-3} m^2$
Moment of inertia	$I_{beam} = 0.562 m^4$
Mass density	$\rho = 7850 kg/m^3$
Lumped mass of floor	$m = 15 \times 10^3 kg$
Youngs Modulus	$E = 20000 N/mm^2$

Table 4.1: Parameters for Axis VM model

Mass of column	$m_{column} = 3 \times 18.8 \times 10^{-3} \times 7850 = 442 kg$
Mass of beam	$m_{beam} = 8 \times 10.5 \times 10^{-3} \times 7850 = 659 kg$
Mass of First floor	$m_{first} = 2m_{column} + m_{first} = 16500 kg$
Mass of Second floor	$m_{second} = 2m_{column} \times \frac{1}{2} + m_{first} = 16100 kg$
Equivalent stiffness	$k_1 = k_2 = \frac{12EI}{l^3} = 2.9689 \times 10^7 N/m$

Table 4.2: Parameters for FE model.

To be specific, the model is built in FEM software Axis VM, which is considered reality used herein to generate pseudo real responses. A Python code is created based on FE knowledge as a FE model to be able to generate responses of different parameters using the corresponding element type and boundary conditions. In the FE model, the shear frame has been modeled as a 2-DOF mass-spring system with concentrated mass and clamped support in the bottom. Timoshenko beam element is applied for columns in Fig 4.2. Additionally, the rotation angle of the connections has been set to zero to model the shear behavior because of the connected, much stiffer beam in Axis VM model. The stiffness of the column remains unknown and to be inferred. Table 4.3 shows that the deviations of responses (displacement of each story and the first two natural frequency) are around 5 %. It is reasonable to simplify the real structure into such a model. Hereafter, the notation of FE model refers to the model created by Python code. The discrepancy of responses obtained from the FE model and Axis is considered as model uncertainty.

Model	**Mid_disp**$[mm]$	**Top_disp**$[mm]$	**Freq_1**$[Hz]$	**Freq_2**$[Hz]$
Reality (Axis VM)	3.325	6.775	4.037	10.391
FE model (Python code)	3.367	6.734	4.210	10.963
Error	1.2%	0.6%	4.1%	5.2%

Table 4.3: Validation of the Python based FE model.

4.3. MEASUREMENT UNCERTAINTY

It is assumed that the responses are contaminated with measurement uncertainty. As mentioned in section 3.4.1, the mathematical relationship between the true responses and contaminated responses follows a zero-mean Gaussian distribution with a specific standard deviation conditional on the extent of measurement uncertainty. Lumping the measurement uncertainty and model uncertainty together, uncertainties are taken into account in the likelihood function which calculates the likelihood of proposed parameters could yield the measured data. The likelihood function is taken from Beck and Au [17], which could be simply interpreted as the square of the ratio between observations and responses obtained from parameters follows a Gaussian distribution with a mean of 1 and a varying standard deviation.

$$\frac{{x_\theta}^2}{{x_{\text{measured}}}^2} \sim \mathcal{N}(1, {\sigma_0}^2) \tag{4.1}$$

In this case, for the sake of simplicity and comparability, it is supposed both measuring frequency and displacement has the same uncertainty. It is plausible to assume the uncertainty of measurement for both observations are identical, which yields:

$$|\sigma_{disp,1}| = |\sigma_{disp,2}| = |\sigma_{freq,1}| = |\sigma_{freq,2}| = |\sigma_0|$$

The mathematical expression of calculating the likelihood is:

$$P(\{x_1, x_2, ..., x_m\}|\theta_1, \theta_2, ..., \theta_n) = \prod_{i=1}^{m} P(x_i|x_\theta) \propto e^{-\frac{1}{2{\sigma_0}^2} \cdot (\sum_{i=1}^{m} (\frac{{x_\theta}^2}{{x_i}^2} - 1)^2)} \tag{4.2}$$

where x_θ is the responses generated by the FE model given a set of parameters.

In order to be consistent with the notation defined in literature, the following mapping is applied: $\ln \sigma_0 = \frac{1}{2}(\ln 2)(1-i)$, three levels of uncertainty have been selected, $i = [1, 5, 9]$, for ε in equation 3.2, its corresponding distribution is shown in 4.3.

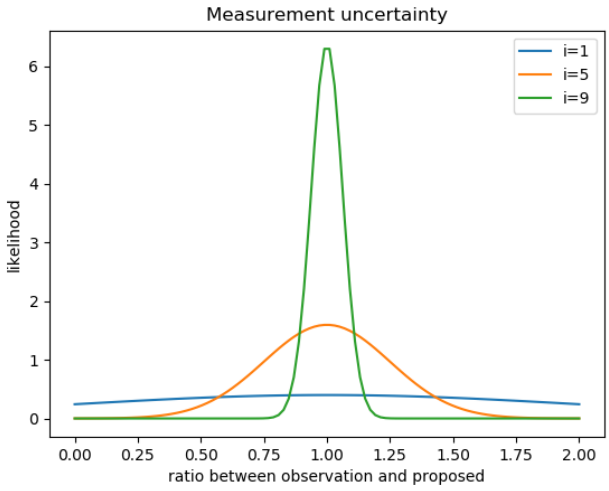

Figure 4.3: Measurement uncertainty.

4.4. MONITORING DATA

Natural frequency and displacement are selected as monitoring responses. The first two natural frequencies are observed. They are obtained from the simplified model by solving an eigenvalue problem, while in common practice, this can be done by installing accelerometers on the structure. The displacement of each story is obtained by adding an external force $F = 100KN$ on the top story. In this case, the loading condition is assumed to be fully known. The displacement of each floor is measured. The monitoring data is created by generating responses from Axis, and then added a random number sampled from its measurement uncertainty distribution (Figure 4.3). Particular realizations of monitoring data are shown in Table 4.4.

Top Damage (%)	**Bottom Damage** (%)	**Mid_disp**$[mm]$	**Top_disp** $[mm]$	**Freq_1**$[Hz]$	**Freq_2**$[Hz]$
0	0	3.325	6.775	4.037	10.391
0	50	6.420	9.850	3.108	9.691
50	0	3.324	9.851	3.575	8.488
50	50	6.419	12.945	2.912	7.535

Table 4.4: Monitoring data

4.5. DAMAGE SCENARIOS

A set of damage scenarios is created by adjusting the moment of inertia of columns that either between beams (second story column) or between a beam and support (bottom story) in Axis model, which simulates integrate stiffness reduction of each story. It is worth mentioning that after the Bayesian inference, the damage state of Axis model can be presented by the model parameter of FE model, where model uncertainty and measurement uncertainty are taken into account.

	Damage Scenarios
1	The stiffness of bottom inter-story is reduced by 50%
2	The stiffness of top inter-story is reduced by 50%
3	The stiffness of both top and bottom inter-story is reduced by 50%

Table 4.5: Damage scenarios

4.6. NUMERICAL INTEGRATION PERFORMANCE

Numerical integration is feasible for two dimensions case where the model evidence can be integrated. Three damage scenarios are simulated in Axis, and their responses have been used as observations for Bayesian inference.

4.6.1. POSTERIOR

In order to calculate the posterior probability, the expression of the likelihood function and prior distribution are required. The former is discussed in equation 4.2, while for the prior distribution, it is presumed there is bias for the initial guess of the stiffness. A 30% overestimation and 20% underestimation of the nominal undamaged stiffness are assumed by introducing two independent lognormal distribution with standard deviation equals 1 and $mode = [1.3, 0.8]$ respectively, for both frequency and displacement. The joint prior distribution is plotted in Figure 4.4.

After acquiring the monitoring data, priors are updated consequently. As shown in Figure 4.5, uncertainty level influences the posterior significantly for the undamaged state. With uncertainty level 1, the measurement uncertainty is so large that it barely gives more information than the prior itself for both displacement and frequency. As the uncertainty is decreasing, the shape of posterior shrinks as the information carried by data becomes dominating over the prior, which represents for less uncertainty in inferring the parameters. The posterior trends to bifurcate as the uncertainty decreasing for measuring frequency, which would yield two separated cluster. In contrast, if displacement monitoring data is used as input for Bayesian inference, the circle-like posterior would not separate.

For other damage scenarios, the posteriors are plotted with uncertainty parameter of 9. Regard as bottom columns damaged case, measuring frequency yields two separated clusters that indicate

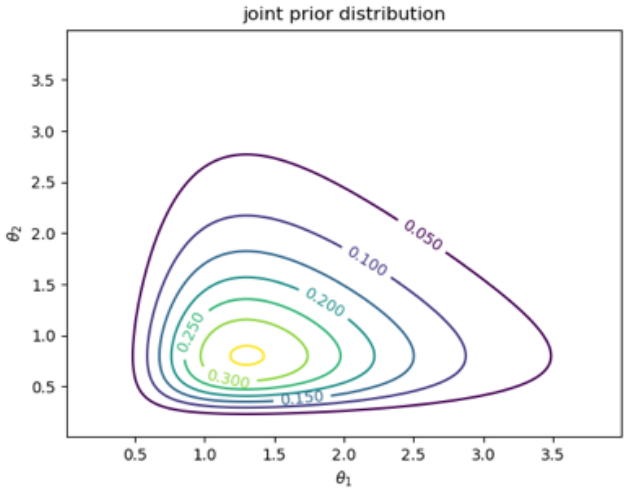

Figure 4.4: Joint prior distribution.

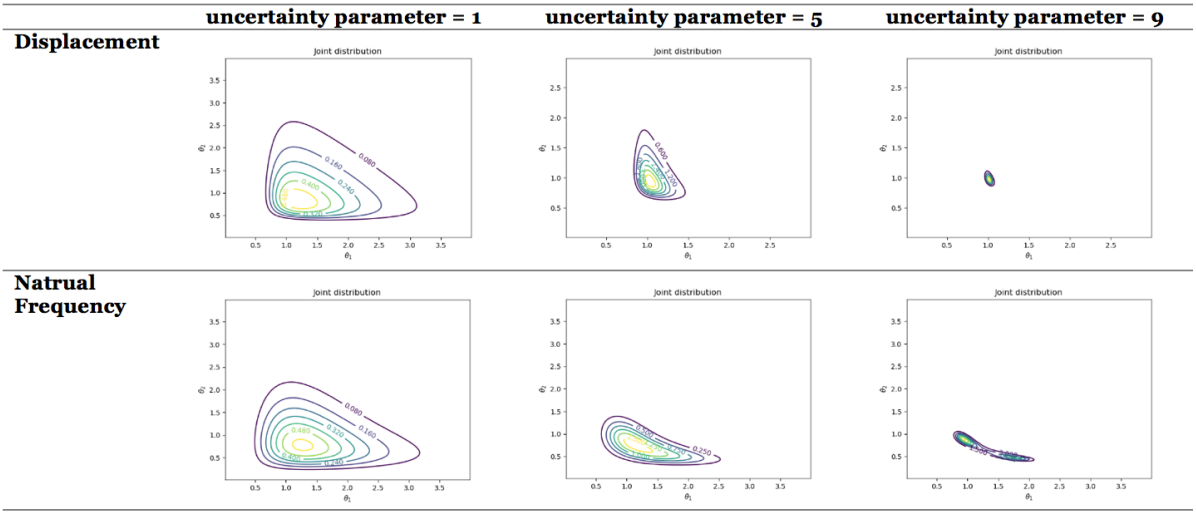

Figure 4.5: Posterior distribution for different monitoring data and measurement uncertainty.

given the monitoring data, two most probable sets of parameters are identified. Intuitively, if the simplified model is calibrated with both sets of parameters, the updated model is able to represent the behavior of the real structure. One possible explanation is as the uncertainty decreases, the posterior would end up with the deterministic solution where there is no measurement uncertainty. Solving the deterministic equation of natural frequency sometimes yields two possible solution, which results in a multimodal distribution of posteriors for this specific monitoring data. This is due to to quadratic term in the characteristic equation of the eigenvalue problem. In contrast, measuring displacement yields one unique concentrated cluster for all three damage scenarios which is more favorable than multiple clusters for DI as the unique mode is identified.

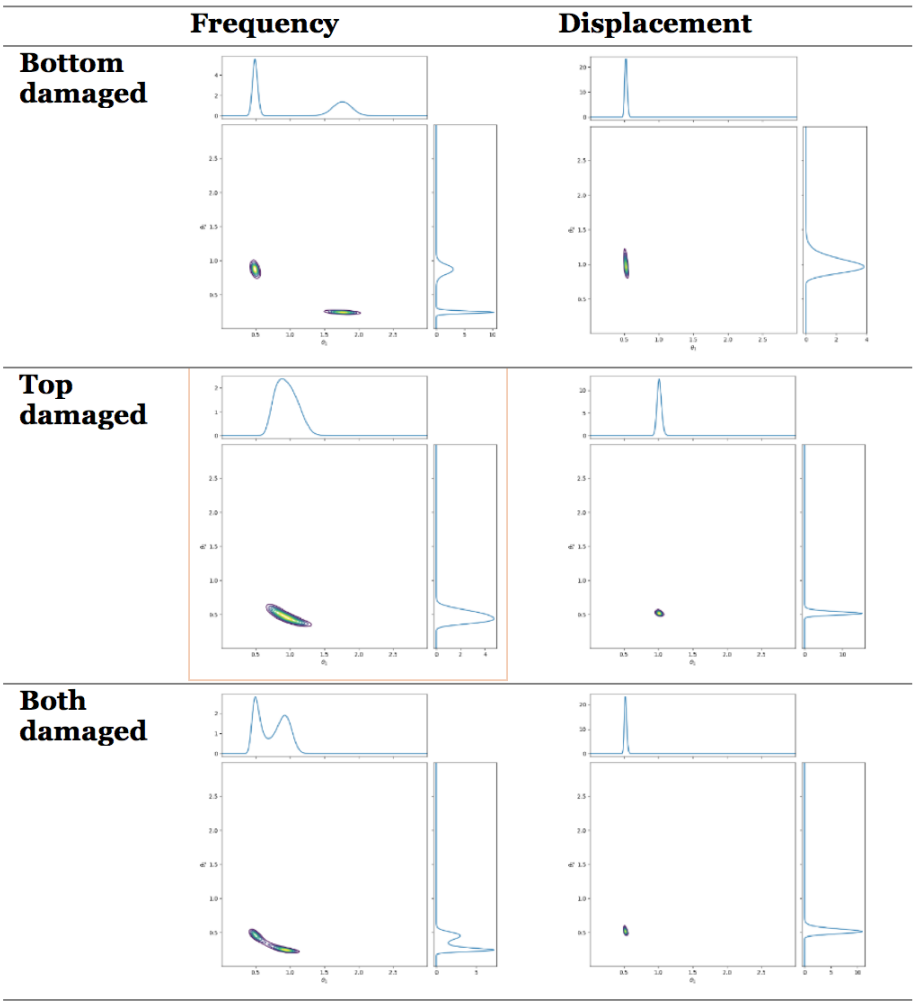

Figure 4.6: Posterior distribution for different monitoring data and damage scenarios.

4.6.2. CREDIBLE REGION

The 90% credible region of above posteriors are plotted in figure 4.7 with the applied damage severity. For all cases, the 90% credible region where the parameters have 0.9 probability to fall into this region is drawn by the red line, the applied damage severity indicated by the green dot is well recognized as it is included within the credible region. The area of credible region is a measurement of information content, as illustrated in Chapter 3, smaller credible region refers to less uncertainty of inferring parameters. It is notable that for the bottom damaged case where the 90% credible region consists of two separated clusters, the applied damage value fall into one of them. It demonstrates that although the credible region is separated for this case, the damage state could still be identified.

After a straightforward visualization of the credible region for all damage scenarios, the ratio of area between measuring displacement and frequency is first calculated and plotted in Figure 4.8. It can be clearly seen the credible region of frequency is considerably larger than that of displacement, specifically, around 8 times larger for three out of four scenarios. In other words, measuring displacement gives a much narrower region that the stiffness parameters would fall into. It illustrates that for this shear frame, measuring the displacement of two stories outperforms measuring natural frequency in terms of detecting damage of the columns. However, in this simple example, a

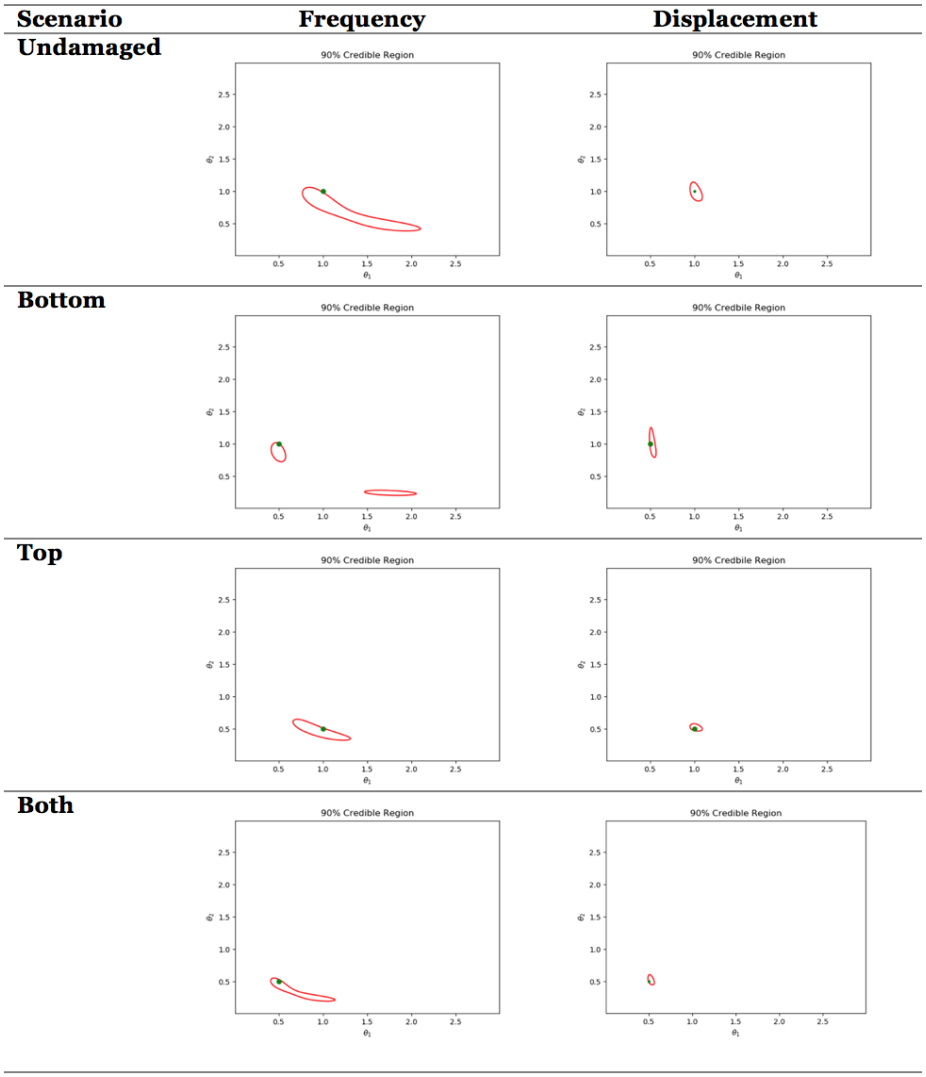

Figure 4.7: Posterior distribution for different monitoring data and damage scenarios.

known load that can result in a visible deformation is applied, which is unusual to be applied on a damaged structure in reality. To summarize, although in terms of information contained by the inference outcome, measuring the displacement of two stories outperforms measuring the natural frequency, considering the load condition in this case might not be feasible in real application and the fact that particular spots are selected to measure the displacement, we could not reach a conclusion that measuring displacement overwhelmingly outclass measuring natural frequency. But the result provides insight into that monitoring different responses would influence the informativeness of Bayesian inference.

4.6.3. MODEL SELECTION

After parameter inference, now the model selection problem is addressed. A simple test demonstrates the necessity of model selection where different parametrizations are used. This analysis aims to find the most likely parameterization scheme among several candidates given the monitoring data. Specifically, pseudo data is generated by Axis inducing 50% stiffness reduction from the support to the $\frac{1}{4}$ position of the bottom column, as shown in Figure 4.9. Displacement is measured

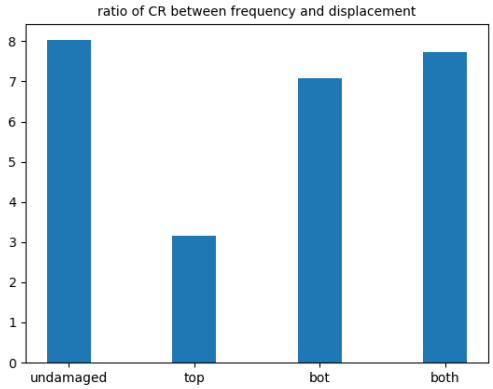

Figure 4.8: The CR ratio between frequencies and displacement

as a monitored response in this selection, listed in table 4.6.

Figure 4.9: Inducing partial damage for model selection.

Observations	Mid (mm)	Top (mm)
Displacement	3.812	7.231

Table 4.6: Monitoring data.

Three different parameterizations under its corresponding hypotheses are created as candidate models to describe the real damage scenario. Specifically, the first model is under the hypothesis that the bottom column segment can be both damaged with different severity for each half of the segment while the top segment stays intact. The second model keeps the bottom segment intact while the top is damaged with each half of it can have a reduced stiffness. The last model is the original parameterization with treating both columns as a single unit that can be damaged separately as shown in 4.10. It is examined which one is the most probable hypothesis under the observations in Table 4.6 by calculating the evidence (Eq. 3.5).

The three models are compared and explanations are given according to Table 3.2. The first model is so dominating and the second model is almost negligible. Since model 3 also includes the possibility that the bottom segment is damaged, it still remains a moderately probable. The above conclusions come from the fact that bottom segment is set to be damaged, the model where the bottom segment

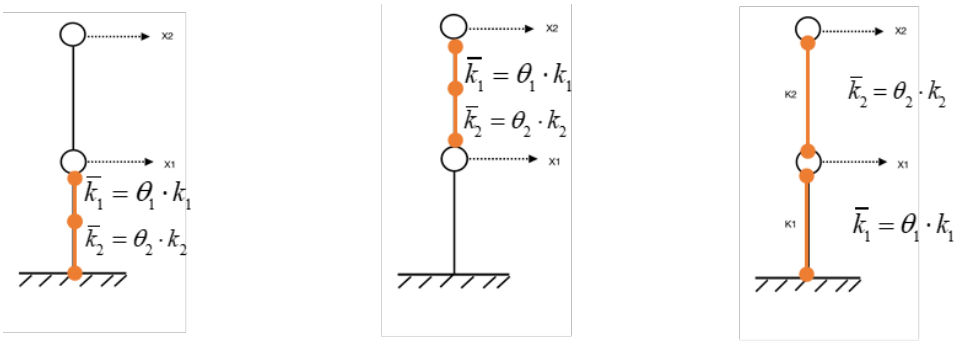

Figure 4.10: Candidate models. Model 1,2, and 3 from left to right.

is parameterized would have a higher probability of generating the monitoring data, while model itself has a better representativeness of the real damage state. From the engineering point of view, the model selection is a process that selects the most likely one over competing parameterization schemes of the FE model and given observations. This can be used to analyze the potential damage scenario for a civil structure after measuring some responses.

Model	Evidence	Bayesian factor
1	0.0310	218 (decisive)
2	0.000142	1 (a bare mention)
3	0.00285	20 (strong)

Table 4.7: Bayes factors for the three considered models.

4.7. APPROXIMATE BAYESIAN COMPUTATION

In higher dimensions, the numerical integration in the denominator of Bayes' rule is practically intractable. Therefore, other – often approximate – methods are used to draw samples from the posterior distribution. In this section, the number of uncertain parameters are extended to four by introducing two mass parameters whose prior follows a Gaussian distribution with a mean of 1 and standard deviation of 0.1. The engineering interpretation behind choosing this prior is based on that engineers are more confident giving mass estimation in FEM than stiffness. This section is carried out by implementing the python code inside the customized likelihood function in the statistical package Pymc3. The log-normal distribution is set with a $\sigma = 1$ of its underlying normal distribution of both θ_1 and θ_2. These four parameters are assumed to be independent from each other. Therefore, the prior marginals are:

$$\begin{aligned}
&\text{bot stiffness}: \theta_1 \sim lognormal(mode = 1.3)\\
&\text{top stiffness}: \theta_2 \sim lognormal(mode = 0.8)\\
&\text{bot mass}: \theta_3 \sim \mathcal{N}(\mu = 1, \sigma = 0.1)\\
&\text{top mass}: \theta_4 \sim \mathcal{N}(\mu = 1, \sigma = 0.1)
\end{aligned}$$

There are four parameters to be inferred, two stiffness parameters and two mass parameters. Two Bayesian computational methods, Metropolis-Hastings, and Hamiltonian Monte Carlo are selected to investigate the behavior of different computational algorithms. The pseudo data generated in 2D case is still used in this session, shown in Table 4.8. In order to capture the features of the higher dimensional problem, the unimodal distribution and multimodal distribution are discussed separately. The frequency is chosen as the monitored response due to the multimodal posterior observed

in Figure 4.5.

Mode	**Scenarios**	**Frequency**$[Hz]$
unimodal	top damaged	(3.575, 8.488)
multimodal	undamaged	(4.037, 10.391)

Table 4.8: Input monitoring data for high-dimension problem.

4.7.1. UNIMODAL POSTERIOR

It is assumed that the computational cost of a single iteration step in the HMC algorithm is 2, 1 being the cost of a single evaluation of the FEM. This is due to the need to evaluate the gradient of likelihood as well in every iteration step. To keep the number of evaluations constant, the sample size of Metropolis-Hastings is doubled than that of Hamiltonian Monte Carlo. The sampling process is executed with two parallel chains and 500 burn-in samples. The sample size is 5000 for HMC and 10000 for MH. First, the MCMC convergence is checked by Gelman diagnostics. All chains have reached stationary as the Gelman factor equals to 1. The trace plot where the sampling process is visualized and the scatter plot are shown below. The performance of sampling is compared with respect to 95% credible interval, standard error, and effective sample size.

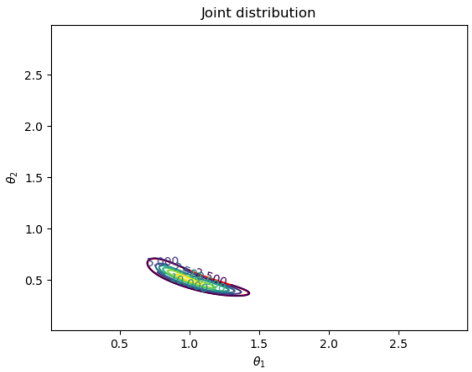

Figure 4.11: Posterior of stiffness parameters(2D)

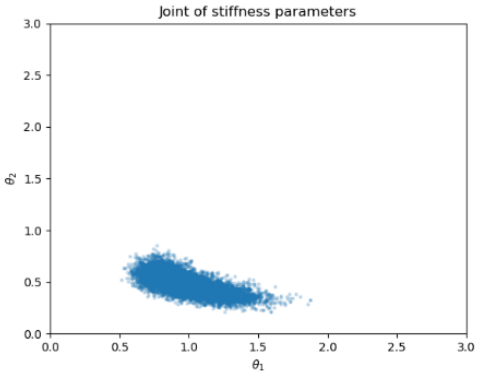

Figure 4.12: Scatter of stiffness parameters(HMC)

In order to reduce the uncertainty of result when only conducting the inference for once, the inference is iterated for 50 times independently. The quantities that will be discussed below are averaged first. As shown in Figure 4.14 where red dots represent the applied damage severity, they perform equally well since the posterior mean is sufficient to estimate the applied damage. Standard error shows that despite the credible interval for both cases are close to each other, HMC outperforms MH with a considerably lower standard error for three out of four parameters. Moving into effective sample size, which equals the amount of sample drawn independently from the posteriors, HMC has a significant superiority than MH in all parameters. In other words, the samples drawn from MH are more correlated to each other. Overall, in this section, HMC has a better performance considering all above-mentioned aspects. Subsequently, we move to multimodal posterior.

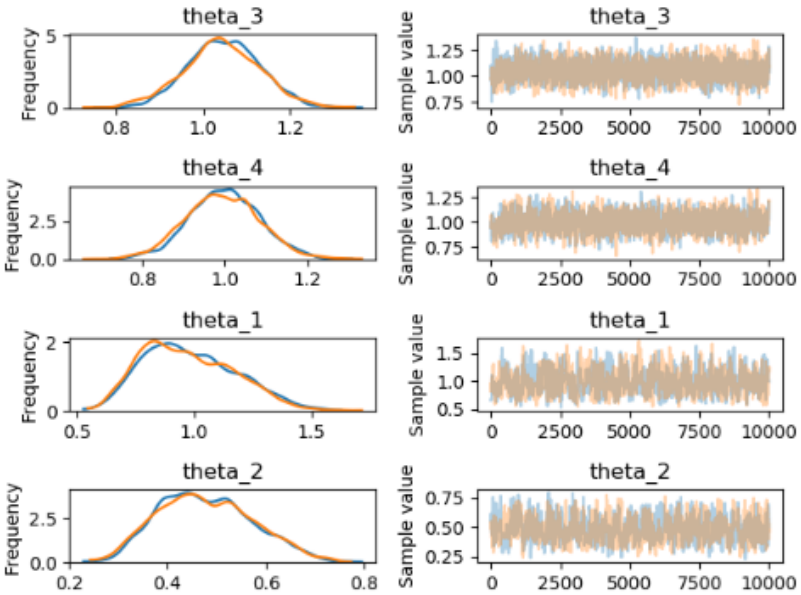

Figure 4.13: Trace plot of parameters (HMC).

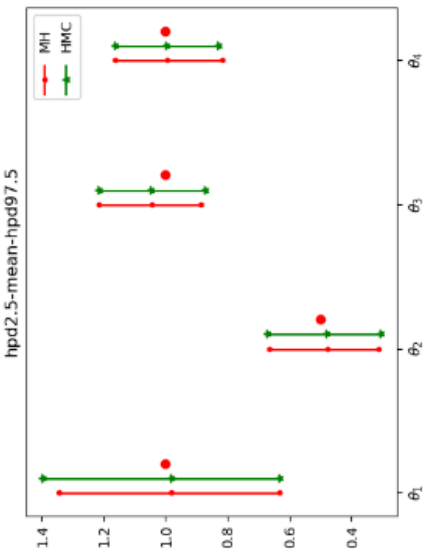

Figure 4.14: 95% credible interval.

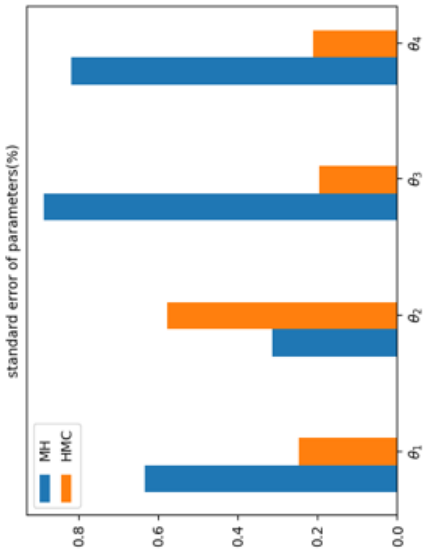

Figure 4.15: Standard error.

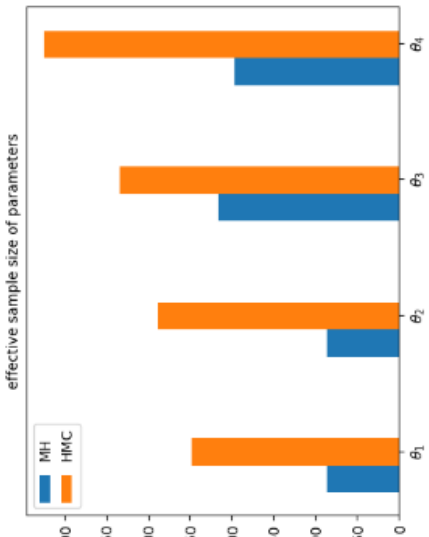

Figure 4.16: Effective sample size.

4.7.2. MULTIMODAL POSTERIOR

The availability and efficiency for different algorithms to explore multiple mode posteriors have been discussed in this session. Similarly, the 95% credible interval, standard error and effective sample size of the two algorithms are compared with the same evaluations. The monitoring data is the same as the undamaged case where two peaks can be observed in the posterior for two uncertain parameters. First, the Gelman factor is verified showing that it still equals one, which assures the sampling process has reached stationary. Then, the trace of sampling and the scatter of two stiffness parameters are plotted. In Figure 4.18 a similar two-mode shape of the 2-dimensional case can be observed despite the mass parameters are also uncertain.

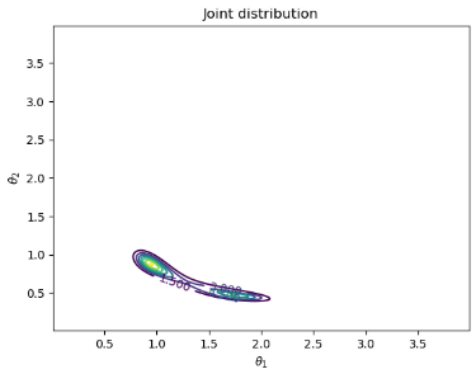

Figure 4.17: Posterior of stiffness parameters(2D)

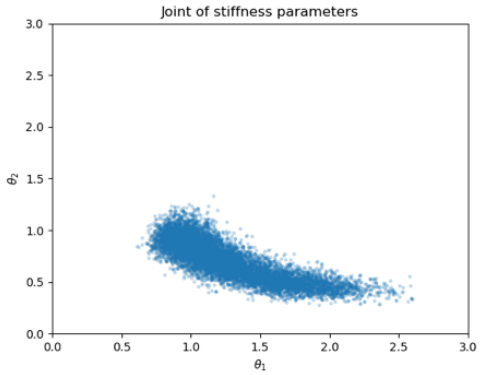

Figure 4.18: Scatter of stiffness parameters(HMC)

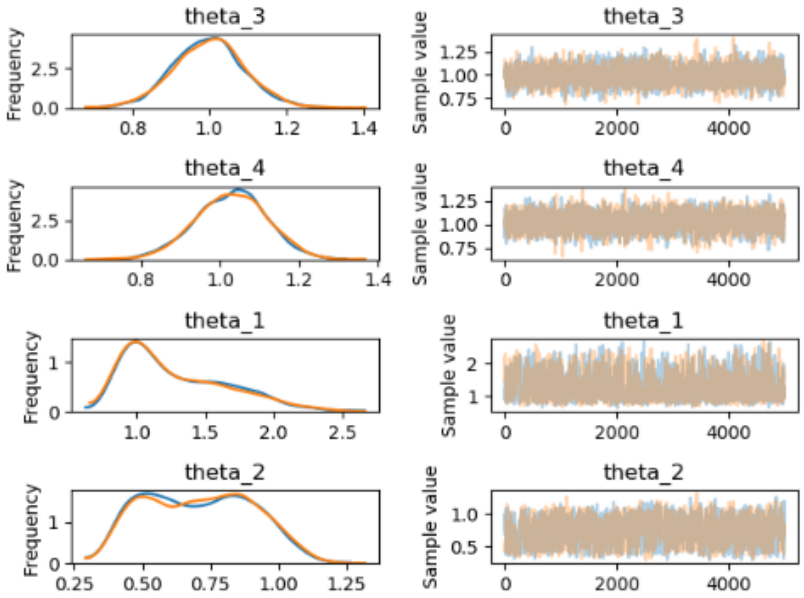

Figure 4.19: Trace plot of parameters (HMC).

For multimodal distribution, a similar conclusion can be drawn based on figures below. In terms of credible interval, both of them involve the applied damage indicated by red dot illustrating the availability of identifying damage in high-dimensional parameter space. It also demonstrates that these methods are capable of exploring the whole posterior. Secondly, HMC has a smaller standard error for all parameters. As can be clearly seen in the figure of effective sample size, HMC is able to draw samples with a considerably weaker correlation than MH. In general, HMC outperforms MH

with respect to effective sample size and standard error, while they perform equally well if credible interval is considered. Therefore, in this example, the hybrid Monte Carlo (HMC) is more efficient than traditional random walk based MH with the same evaluation times. However, if the modes are separated by a very low likelihood valley as shown in Fig.4.21, neither of the considered methods would be able jump between the modes in reasonable steps within one chain. Illustrated in Fig 4.20 and 4.21 with four chains in different colors, apart from the orange chain, the rest is not able to move to the second mode.

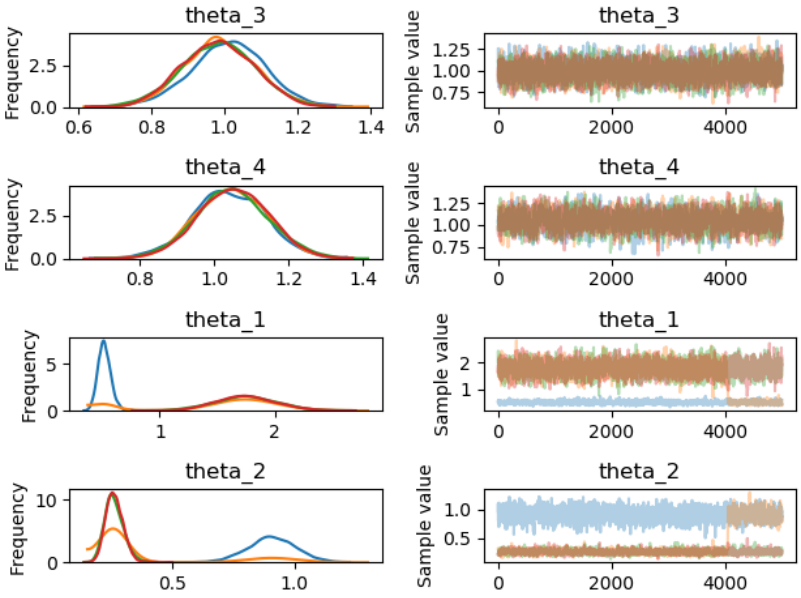

Figure 4.20: Trace plot of parameters)

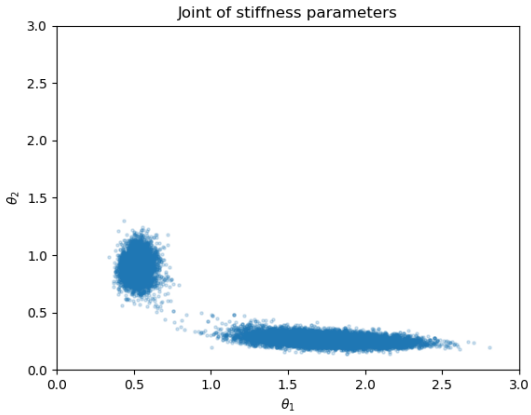

Figure 4.21: Scatter of stiffness parameters(HMC)

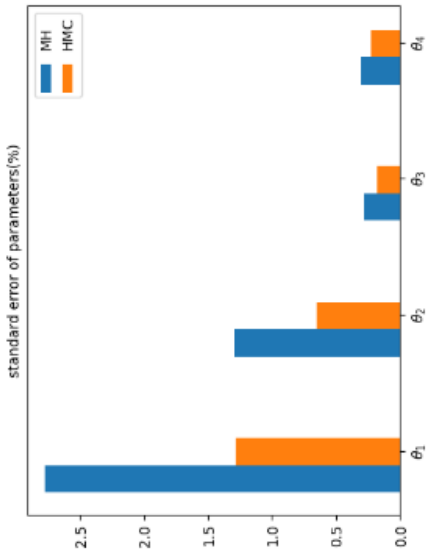

Figure 4.23: Standard error.

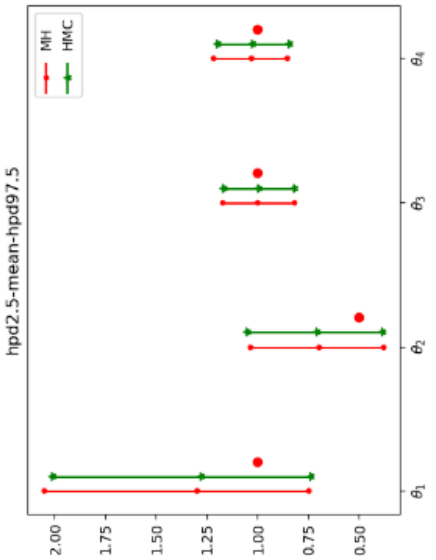

Figure 4.22: 95% credible interval.

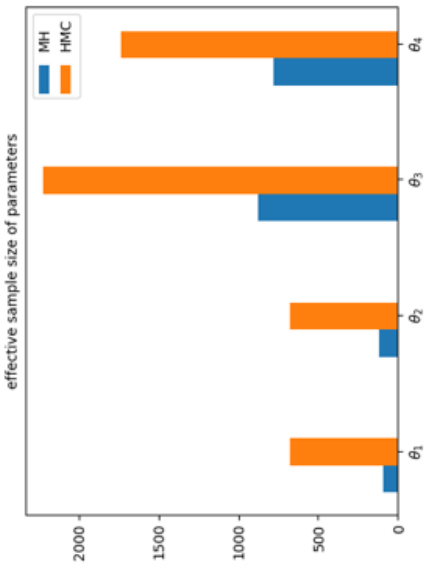

Figure 4.24: Effective sample size.

5

FULL-SCALE CASE: PRESTRESSED CONCRETE BRIDGE BUILT BY THE CANTILEVER METHOD

5.1. OVERVIEW

After a comprehensive Bayesian analysis being conducted to the simple benchmark problem, the findings remain questionable if the simple shear frame is replaced by a real civil engineering structure. As a continuation, in this chapter, the following questions related to the chapter 4 will be answered. First, in the shear frame example, measuring displacement and natural frequency performed distinctively in the context of Bayesian DI where the stiffness of the column is considered damaged and parameterized. For a real-life structure, there are plenty of possible damage scenarios that can occur and various properties can be measured. Which responses should be measured to gain more information? Apart from these questions, it is discussed measuring displacement would always have a considerable small credible region. In this chapter, how to evaluate the posteriors will be addressed not only in terms of credible region, but in information entropy which is more numerically robust. An extension of Bayesian approach for DI will be performed in terms of sensor management, information content and identifiability for a combination of damage scenarios. Finally, if the HMC is still efficient than MH when a complex and detailed FE model involved is discussed. This chapter is an extension of Sousa *et al.* [1] where large part of the modelling work has been done, as shown in Fig 5.2.

5.2. PHYSICAL MODEL

5.2.1. THE BRIDGE

The Leziria Bridge (Portuguese: Ponte da Lezíria) in Fig.5.1 is a box-girder bridge, which is one of longest bridges in the world, with a total length of 12 km, which is part of the A10 motorway in Portugal that forms an outer boundary to the Lisbon metropolitan area. A brief introduction of the bridge is given below. It is composed of three segments:

- the north approach viaduct with 1700 m of length;
- the main bridge substructure, crossing the river Tagus, with a total length of 970 m;
- the south approach viaduct, with a total length of 9160 m.

Figure 5.1: Leziria bridge [4]

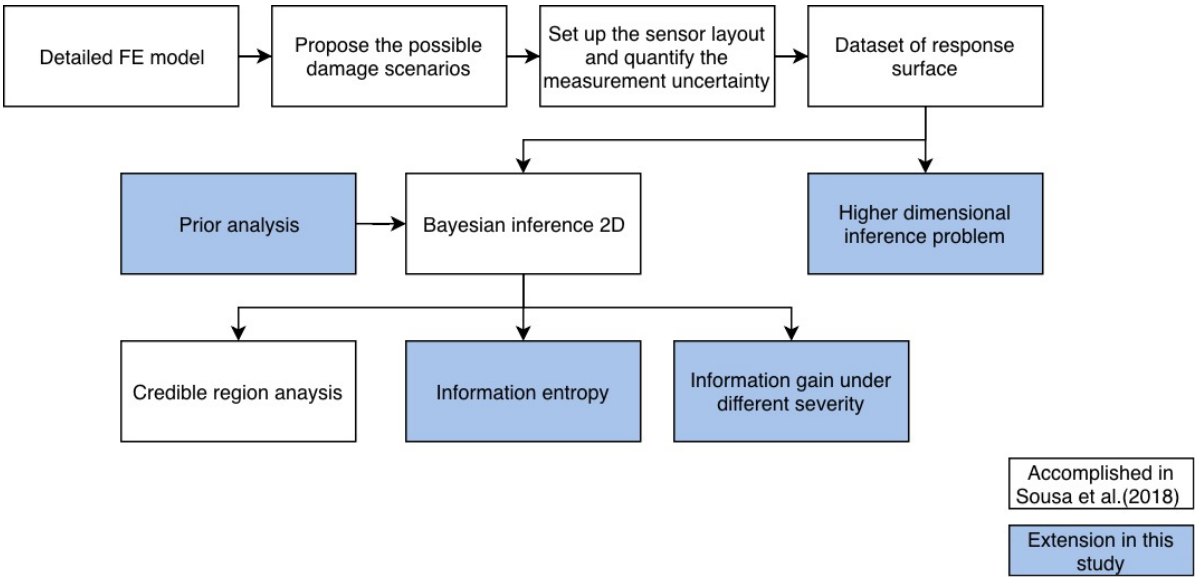

Figure 5.2: Flowchart of work assignment

The main bridge consists of eight spans and seven interior piers which are standing on pile caps in the riverbed. The concrete piers are formed by four walls with constant thickness and variable width. The bridge girder is a box section of variable height ranging from 4 to 8m and constant widht of 10m. The superstructure is monolithically connected to the piers except at piers TPN, P6, P7, and TPS. The dimensionals of each component are recorded in Figure 5.3. Details of the construction process of Leziria bridge is in Sousa *et al.* [5].

5.2.2. FE MODEL

A detailed and rigorous Diana FE model is built for the main bridge part of the Leziria bridge. Beam elements with approximately 1 to 2 m long have been selected for the discretization of the structure. The embedded prestressing cables of the bridge girder are modeled with parabolic elements, while the soil-pile interaction is represented by elastic springs. The construction process is simulated with 105 stages by updating the FE model based on the collected information from the contractor consortium [5]. Overall, the numerical model has 1804 beam elements, 633 truss elements 5106 re-

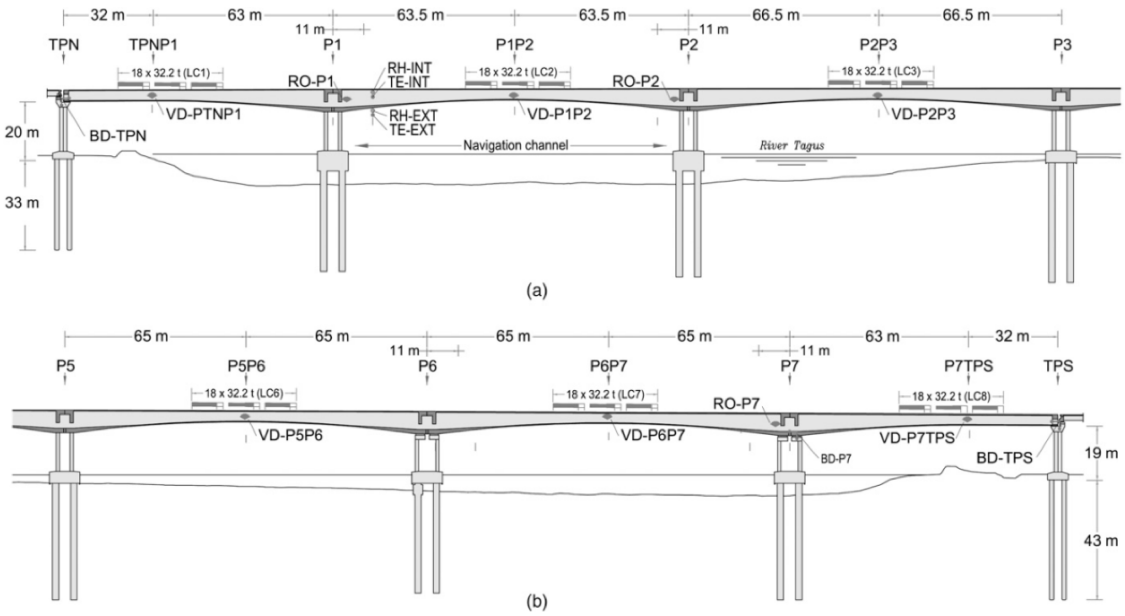

Figure 5.3: Main bridge substructure of Leziria Bridge[5].

inforcement elements including ordinary reinforcements and prestressing cables, 248 springs, and 16 supports. The details and verification can be found in Sousa *et al.* [5]. In this chapter, due to it is impractical and expensive to apply damage to a real structure, the FE model is applied to simulate different damage scenarios.

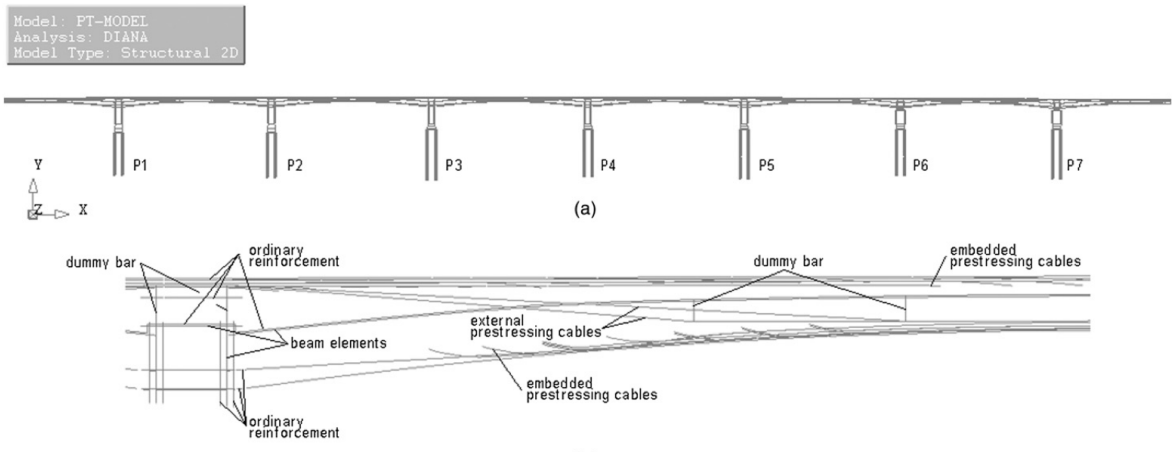

Figure 5.4: Detailed FE model of Leziria bridge.[1]

5.3. MEASUREMENT UNCERTAINTY

The range of measurement uncertainty has been allocated into three levels to explore the effect of different measurement uncertainty extents, a basic uncertainty vector has been set up in section 5.4. The rest of levels are obtained by simply multiplying a scale factor with the unit uncertainty, whose value is shown in the last column of Table .5.1. The quantification of measurement uncertainty is presented in Sousa *et al.* [1]. A scale factor [1,5,10] is selected to represent small, intermediate, and

large uncertainties.

Taken into account the lumped uncertainty, the likelihood function $\{x_n\}$ follows a normal distribution where the mean is the response $\{x_\theta\}$ generated from FE model and the standard deviation σ is dependent on the sensor type and uncertainty extent.

$$\begin{aligned} \{x_n\} &\sim \mathcal{N}(\{x_\theta\}, \sigma) \\ \{x_\theta\} &= FEM(\theta) \end{aligned} \tag{5.1}$$

5.4. MONITORING DATA

An integrate monitoring system has been installed on Lezíria bridge where the data such as relative humidity, rotation and joints displacement is recorded. The whole configuration of the monitoring system is detailed in Sousa *et al.* [5]. From Sousa *et al.* [1], twelve measure points are selected with various type of sensors as listed in Table.5.1. The sensor type has four categories as shown below, containing horizontal and vertical displacement of piers, rotation of piers, and strain of top or bottom slab. The measurement uncertainty is given according to its corresponding sensor type [25]. Specifically,

- One bearing displacement at the supporting section TPN
- Three vertical displacements in the first three spans TPNP1, P1P2 and P2P3
- Three rotations of the deck girder above the supporting sections TPN, P1, and P2
- Five concrete strains located on the deck girder at mid-span sections and supporting sections

Due to the mechanical behavior of hogging and sagging moment, it is reasonable to measure the strain in the bottom slab for mid-span and bottom slab when it comes close to the piers. The layout of sensors are listed below in accordance with figure 5.3.

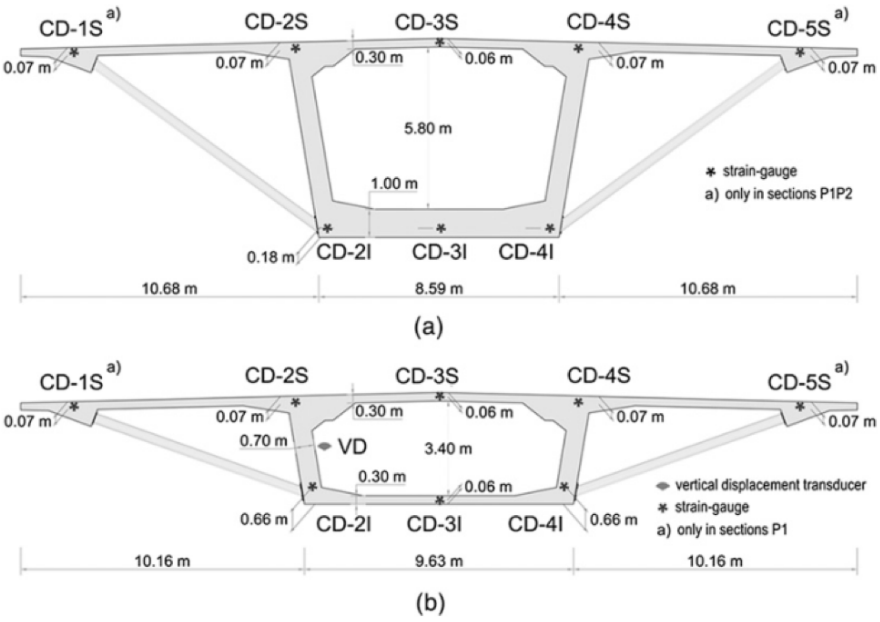

Figure 5.5: Details of cross section[5]

Sensor number	Sensor name	Location	Type	Unit uncertainty
1	OUT1_DH_PTN	TPN	Horizontal Displacement (mm)	0.075 (mm)
2	OUT2_DV_PTNP1	PTNP1	Vertical Displacement (mm)	0.075 (mm)
3	OUT3_DV_P1P2	P1P2		
4	OUT4_DV_P2P3	P2P3		
5	OUT5_RO_PTN	PTN1	Rotation (10^{-3})	5.0 (10^{-3})
6	OUT6_RO_P1	P1		
7	OUT7_RO_P2	P2		
8	OUT8_EX_PTNP1I	PTNP1 (bottom slab)	Strain (10^{-6})	0.35(10^{-6})
9	OUT9_EX_P1S	P1 (top slab)		
10	OUT10_EX_P1P2I	P1P2 (bottom slab)		
11	OUT11_EX_P2S	P2 (top slab)		
12	OUT12_EX_P2P3I	P2P3 (bottom slab)		

Table 5.1: Measurement points for the analysis[1]

5.5. DAMAGE SCENARIOS

From the literature review [1] of long-term monitoring of a large-scale prestress bridge and the specificity of Leziria bridge, e.g., water infiltration and corrosion due to the maritime environment. Four likely damage scenarios have been enumerated as the most typical ones which are outlined in Table 5.2.

Number	Damage
1	Deterioration of bearing devices
2	Prestress loss due to failure of external tendons
3	Pier settlements due to liquefaction of the foundation soil
4	Loss of stiffness on the deck girder above the piers

Table 5.2: Considered damage scenarios [1]

5.5.1. DETERIORATION OF BEARING DEVICES

The first damage scenario is due to the consideration of the abnormal restrained movement behavior on the bearing devices. Specifically, the bearing device at δ_{TPN} and θ_{TPN} is simulated by elastic springs K_{tra} and K_{rot}. The parameterization is done by assigning the upper bound and lower bond of the stiffness of springs, which refers to the movement is free to occur and the movement is completely restrained respectively. A sensitivity analysis is done to quantify the upper bounds which are 10^{+11} N/rad and 10^{+13} N/rad correspondingly [1].

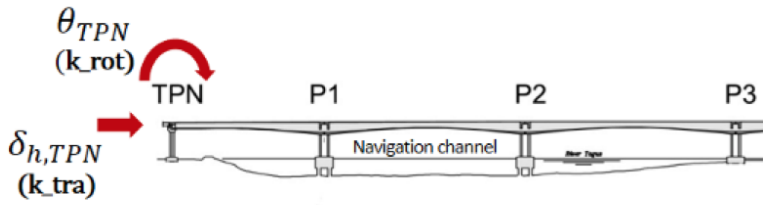

Figure 5.6: Bearing malfunctioning - damage scenario 1[1].

5.5.2. PRESTRESS LOSS

Moving to the second damage scenario, the model is parameterized by reduction of the external prestress tendon due to the prestress loss. Two external tendons along the first span of the bridge, ΔP_{TD1}, and in one of the external tendons along spans P1P2 and P2P3, ΔP_{TD1}, are considered. The prestress force of two external prestress tendons in undamaged status are 1341 MN and 1270 MN individually. Whereas the completely damaged case is there is no longer prestress force in those tendons.

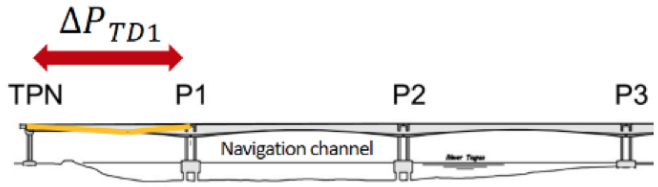

Figure 5.7: Pier settlement - damage scenario 2[1]

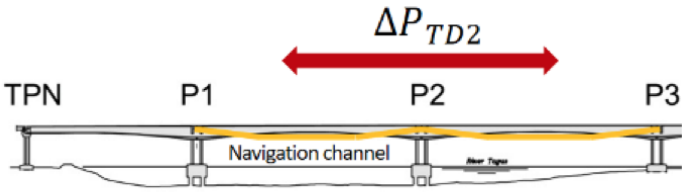

Figure 5.8: Prestress Loss - damage scenario 2[1]

5.5.3. PIER SETTLEMENTS

Considering the environment of the piers, it is probable that pier settlement occurs due to liquefaction of the foundation of the soil. The parameterization is realized by setting the pier settlement from 0 to a maximum 50 m for the first two piers.

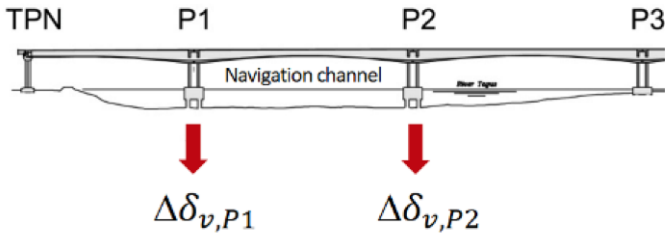

Figure 5.9: Pier Settlements - damage scenario 3[1].

5.5.4. LOSS OF STIFFNESS

Finally, the loss of stiffness of critical sections of the deck girder is considered. In accordance with the previous damage cases, the critical area is the deck girder regions near of the mid-span section PTNP1 and above pier P1. By setting the maximum loss of 50% of Young's modulus in the concrete,

the model is parameterized by stiffness varying from 19.5Gpa to 39.1GPa and 19.4Gpa to 38.7GPa respectively.

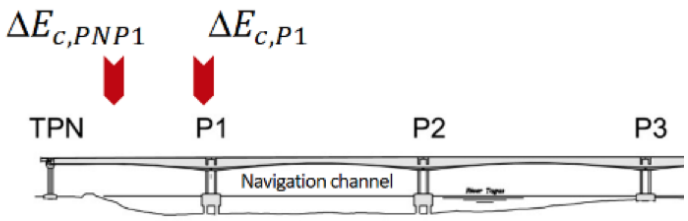

Figure 5.10: Reduction of the stiffness - damage scenario 4[1].

To summarize, four damage scenarios are enumerated considering the typical damage scenarios for a prestressed bridge as well as the environment of Leziria bridge. Table 5.3 summarizes the parameter settings for each damage scenario. The damage state of the bridge is defined by two model parameters that represent the severity of corresponding damage. It is worth mentioning the parameter has been normalized with a reasonable upper bound and lower bound so that it is a non-dimensional variable.

Damage Scenarios	**Parameters**	**Lower bound (no damage)**	**Upper bound (full damage)**	**Normalization (range)**
Bearing deterioration	K_{tra}	0 N/m	$10^{+11} N/m$	(0, 0.1)
	K_{rot}	0 N/m	$10^{+11} N/rad$	(0, 0.1)
Prestress loss	PTD1	1341 MN	0 MN	(0, 1)
	PTD2	1270 MN	0 MN	(0, 1)
Pier settlement	ΔP_{TD1}	0.0 m	0.5 m	(0, 1)
	ΔP_{TD2}	0.0 m	0.5 m	(0, 1)
Stiffness loss	$\Delta E_{c,PTNP1}$	39.1 GPa	19.5 Gpa	(0, 0.5)
	$\Delta E_{c,P1}$	38.7 GPa	19.4 Gpa	(0, 0.5)

Table 5.3: Normalized parameters for each damage scenario[1].

It is necessary to mention that for bearing deterioration and stiffness loss of concrete, in order to perform the differences of responses, a live load of 200 kN/m, along 28.5 m, is applied in the span TPNP1 of the Lezíria bridge. Further details can be found in Sousa *et al.* [5]. For the pier settlement, an imposed deformation is applied at pier 1 and pier 2 with the maximum magnitude of 0.5m. Finally, the loading condition for the external prestress loss is set with a range from no damage (1341$MNan$ and 1270MN respectively) to totally damaged (0 external prestress force).

5.6. NUMERICAL INTEGRATION PERFORMANCE

In order to use numerical integration for Bayesian analysis, the responses generated by all the hypothetical parameters must be known. For this case, Sousa *et al.* [1] simulated the structure response by applying Response Surface instead of looping all parameters through Diana model to reduce the computational effort substantially. Hence, Sousa *et al.* [1] generated responses surfaces for all twelve sensors based on four aforementioned damage scenarios. The error of Response Surface fitting has been analyzed showing that the maximum error is below 5%, which is acceptable in this

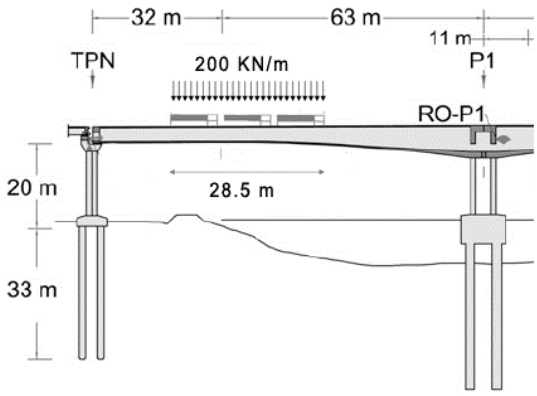

Table 5.4: Applied live load [1].

context. Essentially, the data read from sensors is the responses of that location contaminated with measurement uncertainty.

5.6.1. POSTERIOR

This part of work was done by the Sousa *et al.* [1] where more details can be found. Due to all damage scenarios are parametrized with two parameters, numerical integration is still feasable. Given the monitoring data from twelve sensors, the Bayesian approach can be used to infer the posterior distribution of the normalized parameters that reflect the actual damage in the structure. Hence, the posterior distribution of parameters for different damage scenarios with various uncertainty is shown in Figure 5.11 where the blue dash line indicates the applied damage. The solid red line is the 90% highest density credible region of parameters. Each row represents a measurement uncertainty, while each column indicates the considered damage secnario.

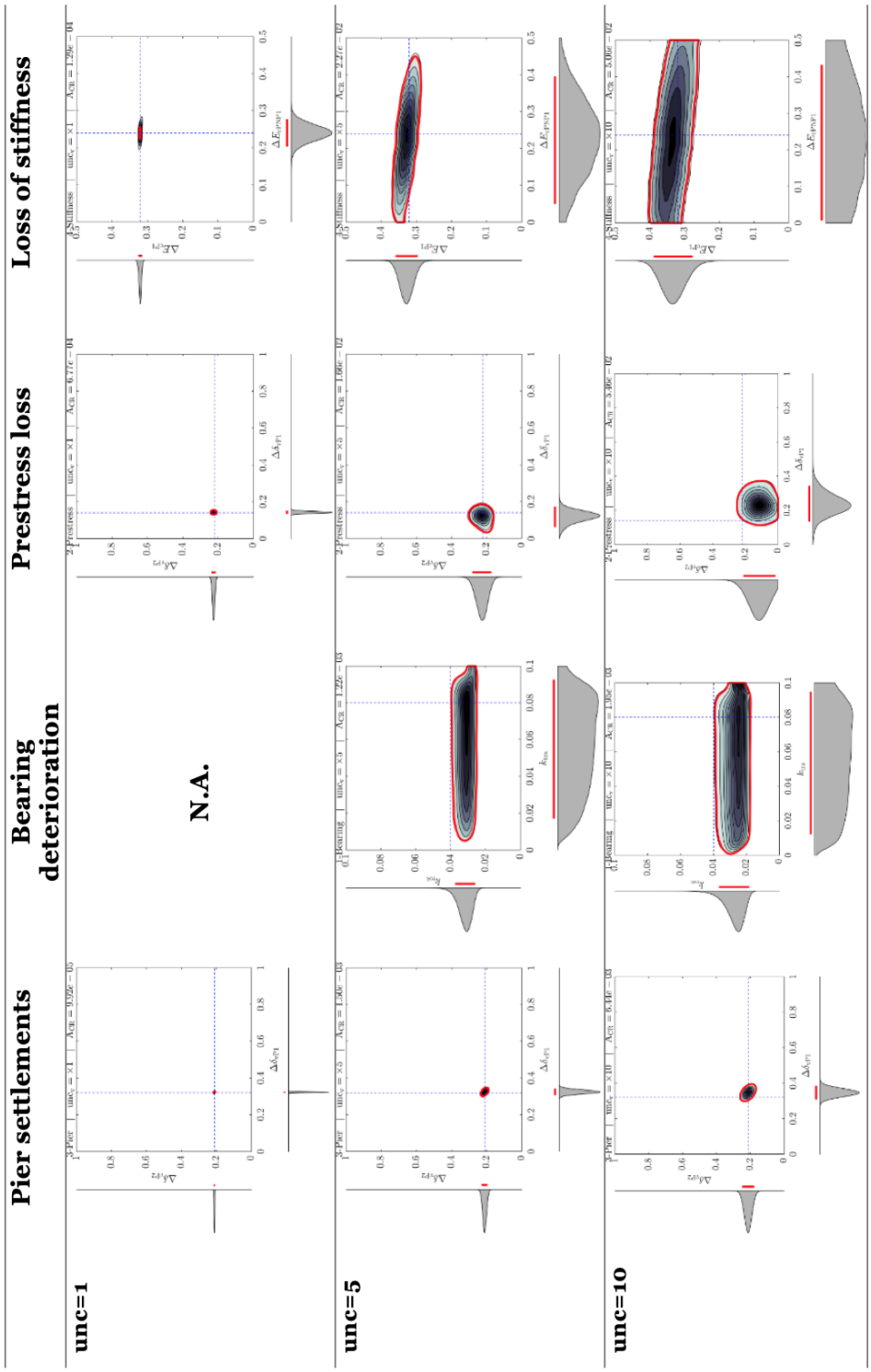

Figure 5.11: The posteriors for different damage scenarios and measurement uncertainty [1]

Uniform prior has been applied for aforementioned inference. From a general perspective, in all cases the damage severity has been identified successfully, with the preset value falling into the 90% credible region for different damage scenarios and extent of measurement uncertainty. The details are explained first within a damage scenario, and then across the proposed scenarios. For the pier settlement, the CR is a concentrated circle-like shape. Even though when the measurement uncertainty is small, the CR of posterior is fairly small area, the preset value is still contained in this CR. Increasing the measurement uncertainty, the CR of posterior gradually expands. For the bearing deterioration, it has to be pointed out that the "N.A." where uncertainty is level one is caused by numerical issue, which will be discussed later in this study. As shown in the figure, the marginal distribution for the first parameter is wide, which reflects the identifiability for the first parameter is poor compared to the other one. It seems like increasing the measurement uncertainty will not influence the CR significantly. Moving to the prestress loss case, although when the uncertainty is small, the damage is well identified, increasing the uncertainty will decrease the identification accuracy essentially. It is demonstrated by the preset value barely touching the boundary of CR when the uncertainty is high. If the loss of stiffness is considered, increasing the measurement uncertainty will affect the identifiability of the first parameter more significantly than the other one. The conclusion that the area of CR will normally be larger by increasing measurement uncertainty can be drawn considering all damage scenarios. Nevertheless, the expansion of the credible region is still conditional on its damage scenario. For instance, the increment of the measurement uncertainty for stiffness loss would enlarge the credible region more significantly, if compared to that of pier settlement.

5.6.2. EFFECT OF PRIOR

Uniform prior has been applied for aforementioned inference. Therefore, with a non-informative prior where all parameters have the same probability to be inferred, the posterior probability is proportional to that of the likelihood. Given the fact that prior distribution incorporates the subjective beliefs about a parameter, different prior probability may also influence the result of inference. In this context, the prior distribution is based on the related engineering knowledge of a structure. Subsequently, two informative priors are herein investigated as a step further to study the effect of priors with all sensors available. An improper asymmetric and slightly skewed prior has been selected as to be representative of not significant damage case, following lognormal distribution with mode 0.4, a unit standard deviation. Due to the prior assigns probability to the value which out of the support region, the density is normalized within the scale of support, so the integral over support is 1. A normal distribution with a mean equal to the midpoint of the support and a standard deviation whose magnitude is 0.2 for all scenarios is investigated to represent intermediate damage case. The density of two informative priors is shown as below when the support is from 0 to 1.

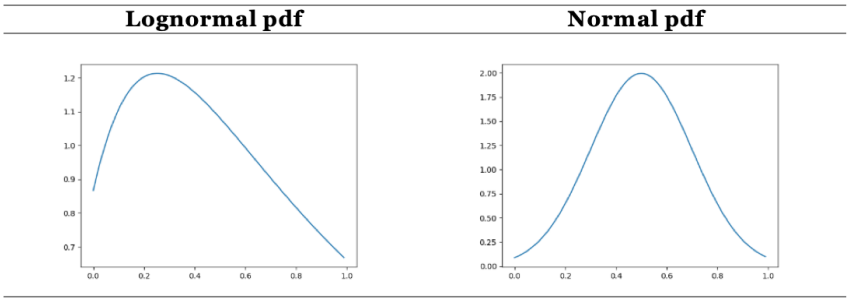

Figure 5.12: The two, considered, informative prior distributions.

By replacing the prior, a consistent similar pattern to uniform prior of the posterior contour is observed for pier settlement in Figure 5.13, while for prestress loss, the contour pattern has changed significantly. In order to have an insight into the effect of priors with different damage severity as well as damage scenarios, the damage extent is preset from 0.1 to 0.9 for both parameters with a discrete interval of 0.1. Pier settlement and prestress loss are analyzed to demonstrate the effect of prior. By comparing the deviation of credible region, the shift of mean for those damage scenarios, the influence of different informative priors has been visualized.

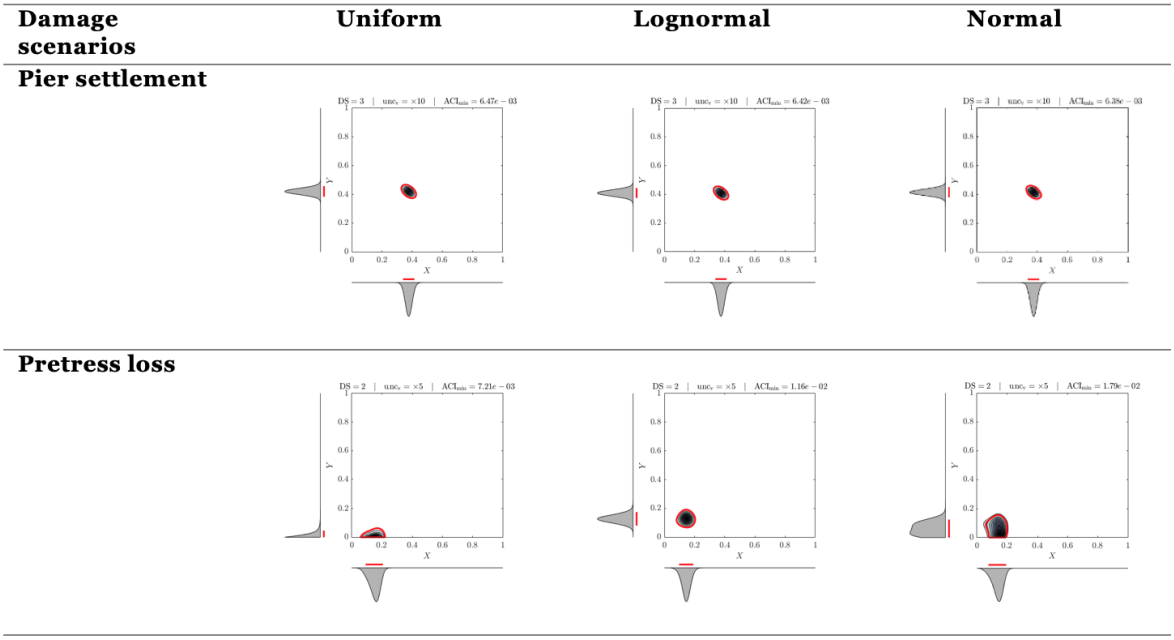

Figure 5.13: Prior effect for different damage scenarios.

The effect of changing prior is quantified in terms of credible region and posterior means. The damage severity is preset by an increment of 0.1 for one of two parameters each time. So over the entire parameter space, there are 100 points being selected to capture the tendency of credible region and parameter mean shifts for different damage severity. The ratio of credible region area and parameter mean for informative prior and uniform prior is plotted in Figure 5.14 respectively.

For pier settlement, with the uncertainty level of 5, the changes of credible region quantified by the ratio between uniform prior and two informative priors are within the scale of $(-5\%, +5\%)$. The same conclusion can also be applied to both posterior means. The figure presents for such a damage scenario, data is so overwhelmingly dominating over the prior and hence using informative priors do not affect the outcome significantly. One possible explanation is that in this case, the monitoring data is distinctive for applied damage severity, so the likelihood for parameter who is away from the preset value will be extremely small. In practice, the subjective initial belief for this scenario would not be decisive as the data information will be dominating eventually.

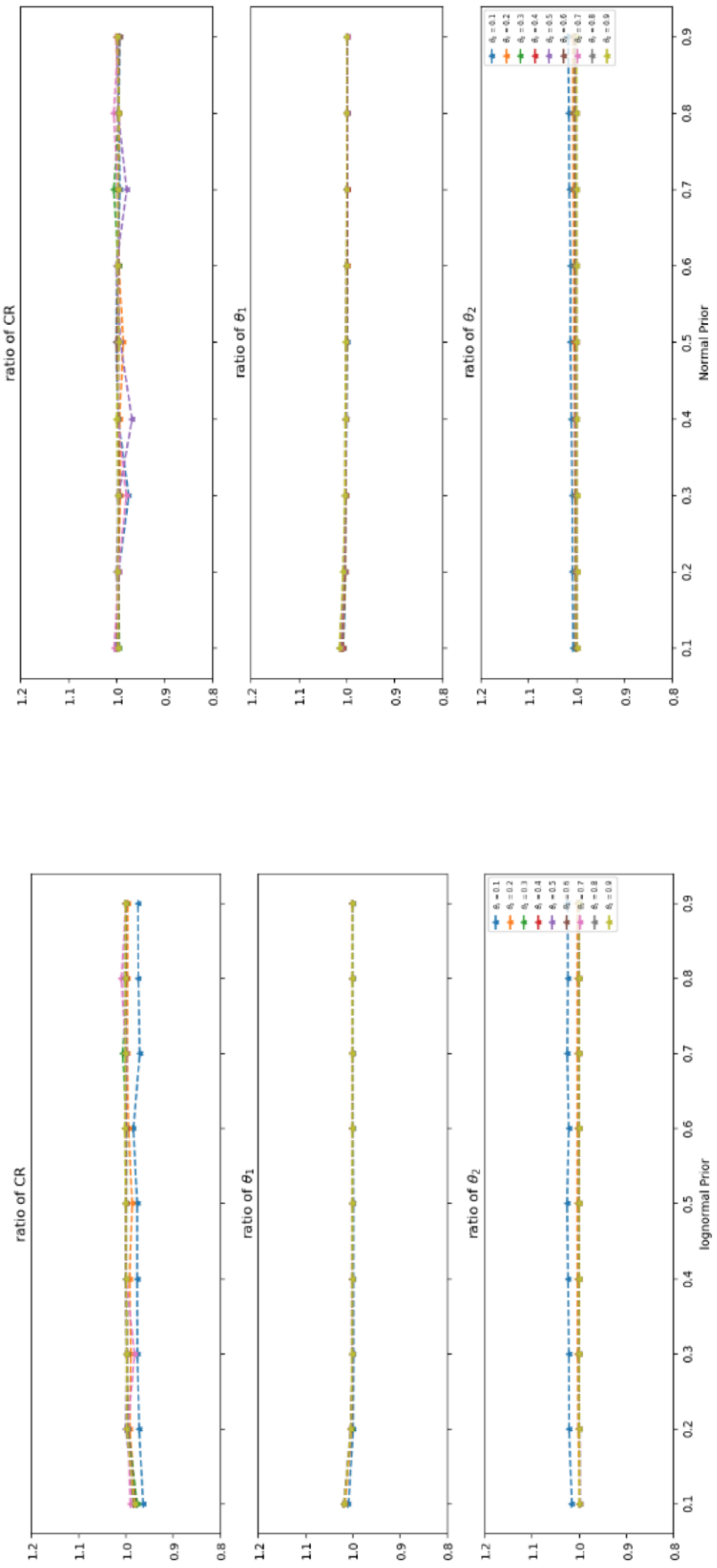

Figure 5.14: The ratio of inference outcomes between informative priors and uniform priors.

In contrast, for the prestress loss damage scenario, the posterior is a mixture of monitoring data and prior, where both data and prior play an important role. As can be seen in Figure 5.15 the ratio of credible region indicated by the first dot of the blue dash line where slight damage occurs, is around 200% greater than that of uniform prior, and the mean of the first parameter using lognormal prior is four times higher than that of uniform prior. Take the second row of Figure 5.13 as an example, the informative prior would result in the credible region moving away from the edge of the support due to the information it provided. The evidence from those figures suggests that when a damage state that is defined by the parameters near the edge of support is observed, the prior information should be considered carefully as it will considerably change the results of posterior. As this section illustrated, prior sensitivity for different damage scenarios is worth to be discussed for DI. For those scenarios that are sensitive to the change of prior, extra attention should be devoted to the selection of prior distribution.

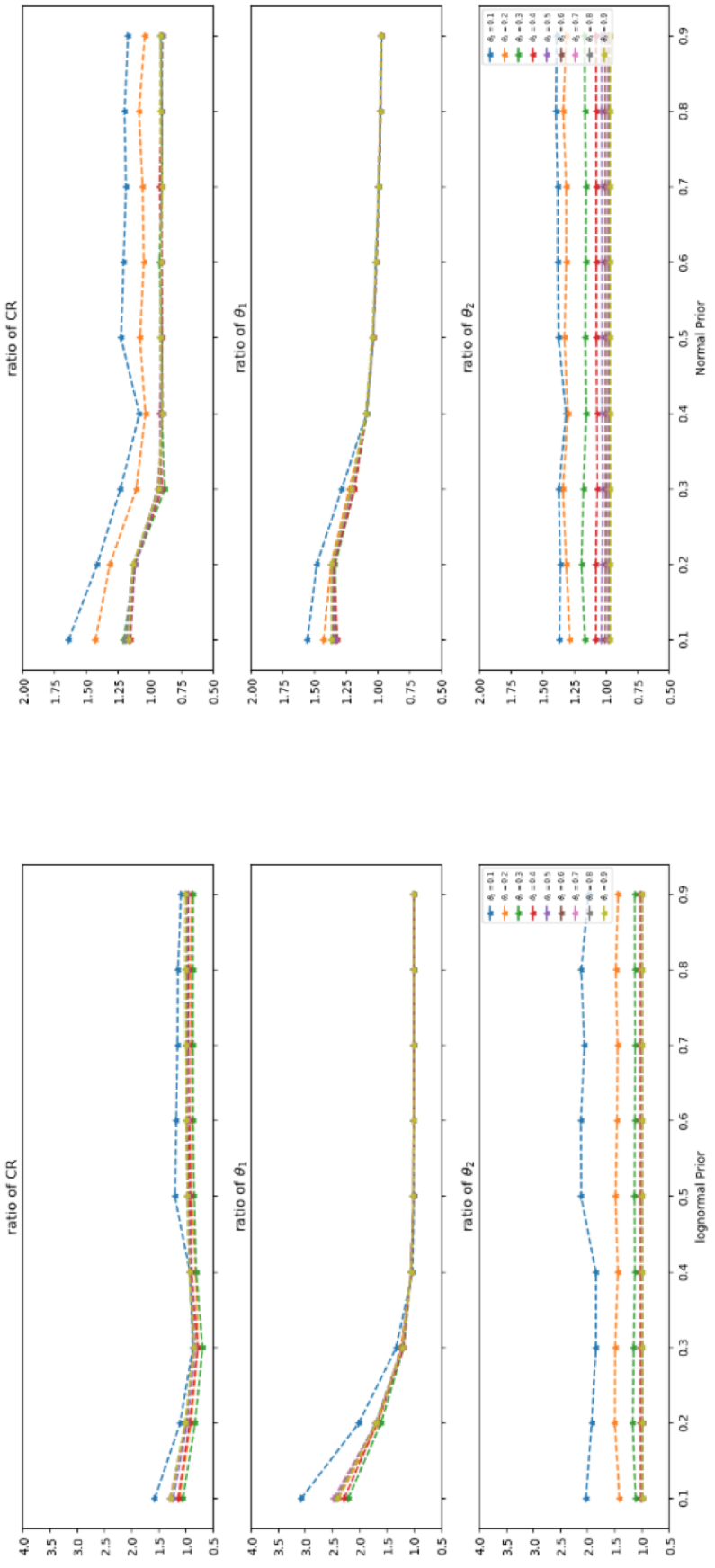

Figure 5.15: Prior effect for prestress loss.

5.6.3. INFORMATION ENTROPY

In Sousa *et al.* [1], an analysis has been conducted to determine which two sensors are the most informative sensor pair that the most information of damage state can be extracted. A short description will be given in this section, in the meantime, there are several defects arising in this analysis. An optimized solution will be given correspondingly. Moreover, as an extension, a comparison of information gain between the most informative sensor and the reference sensors will be evaluated.

INTRODUCTION OF PREVIOUS WORK

For each damage scenario, two out of twelve sensors have been selected as one pair to investigate which combination would give the most information of damage state. This analysis aims to gain insight of how a subset of sensors contributes to the available information carried by all sensors. The potential benefit is to manage sensors more efficiently, for example, which type of sensors can provide more information compared to others within a damage scenario. The information carried by the posterior distribution is evaluated by the area of credible region for different sensor pairs. The CR is normalized from 0 to 1, where 0 means the support region, 1 is the area of credible region of reference sensor set (all twelve available sensors) times the probability mass defined subjectively (90%), shown in Equ 3.8. In Figure 5.16, each item in the heatmap is the normalized information content using its corresponding index of sensors. For pier settlement with measurement uncertainty level 5, the matrix plot exhibits that measuring vertical displacement would yield the minimum area of credible region. So choosing the sensor 3 and 4 is the most informative pair in this case. The matrix plot provides a clear evidence of which pair to pick to gain the most information of the damaged condition.

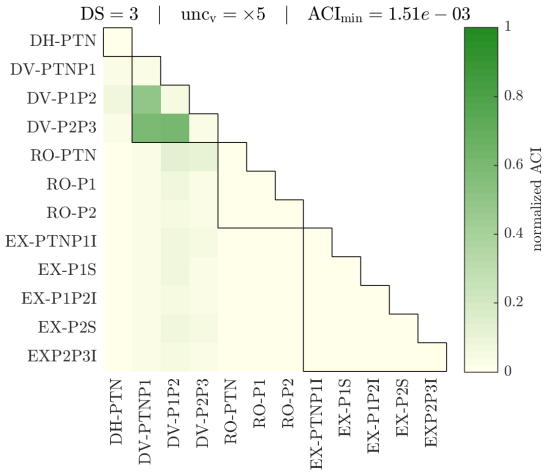

Figure 5.16: Matrix plot of the most informative pair [1].

However, the above-mentioned methodology has deficiency as shown in the Figure 5.18. The first figure reveals that it has a poor scaling in this specific damage scenario. The second figure exhibits if the uncertainty level is set to 1 for pier settlement, there are unexpected values along the column 4. Apparently, the result is not as reliable as the minimum credible region equals to 0, which is caused by the numerical issue when determining the credible region. Although this analysis could visualize the informativeness of sensor combinations, it is not robust enough when tackling with all the posteriors.

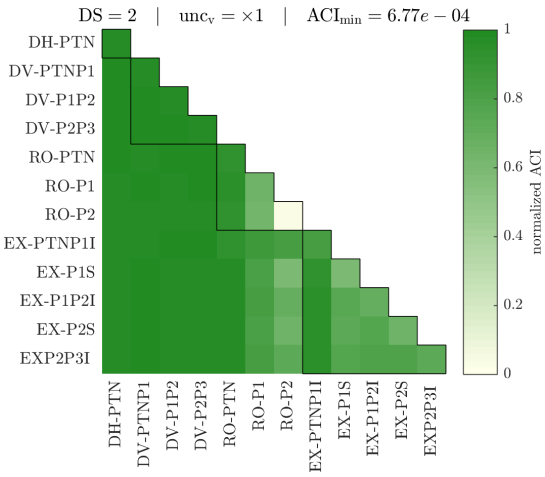

Figure 5.17: Poor separation behavior. (DS: prestress loss)

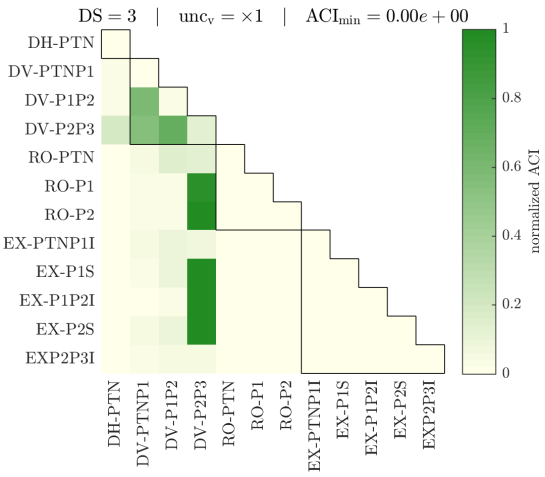

Figure 5.18: Numerical issue occurs while determining the credible region. (DS: pier settlement)

5

EXTENSION OF PREVIOUS WORK

As can be seen in Figure 5.17, the scaling behavior is poor in some of the damage scenarios. The matrix plot does not give a clear separation of different pairs using the normalized credible region area. Most of them perform similarly under the CR criterion. In addition to the numerical difficulties of determining the credible region for posteriors as in Figure 5.19, another measure of information content is introduced: information entropy. Subsequently, it will be demonstrated that entropy is a more numerically robust measure than credible region. In addition, it has a better scaling compared to credible region. After exploring which pair of sensors could reveal the most information regarding the damage state, a comparison of information content between using all available sensors and the most informative pair is made to gain insight of information gain under different damage severity.

The information carried by a pair is evaluated using equation 3.11 through entropy to perform the most informative combination assuming the measurement uncertainty is averaged with level 5 for all cases. A heatmap is plotted to compare the information contained by different pairs. The diagonal of heatmaps refers to the entropy using only one sensor, while each element represents the entropy obtained from its corresponding index of the sensors. Besides, the detailed posterior distribution of each pair has been plotted to aid the information content analysis.

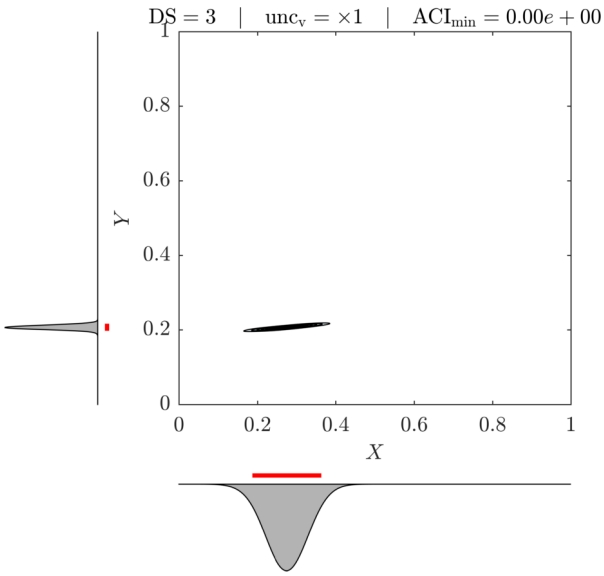

Figure 5.19: The posterior that causes numerical issue of finding credible region.

PIER SETTLEMENT

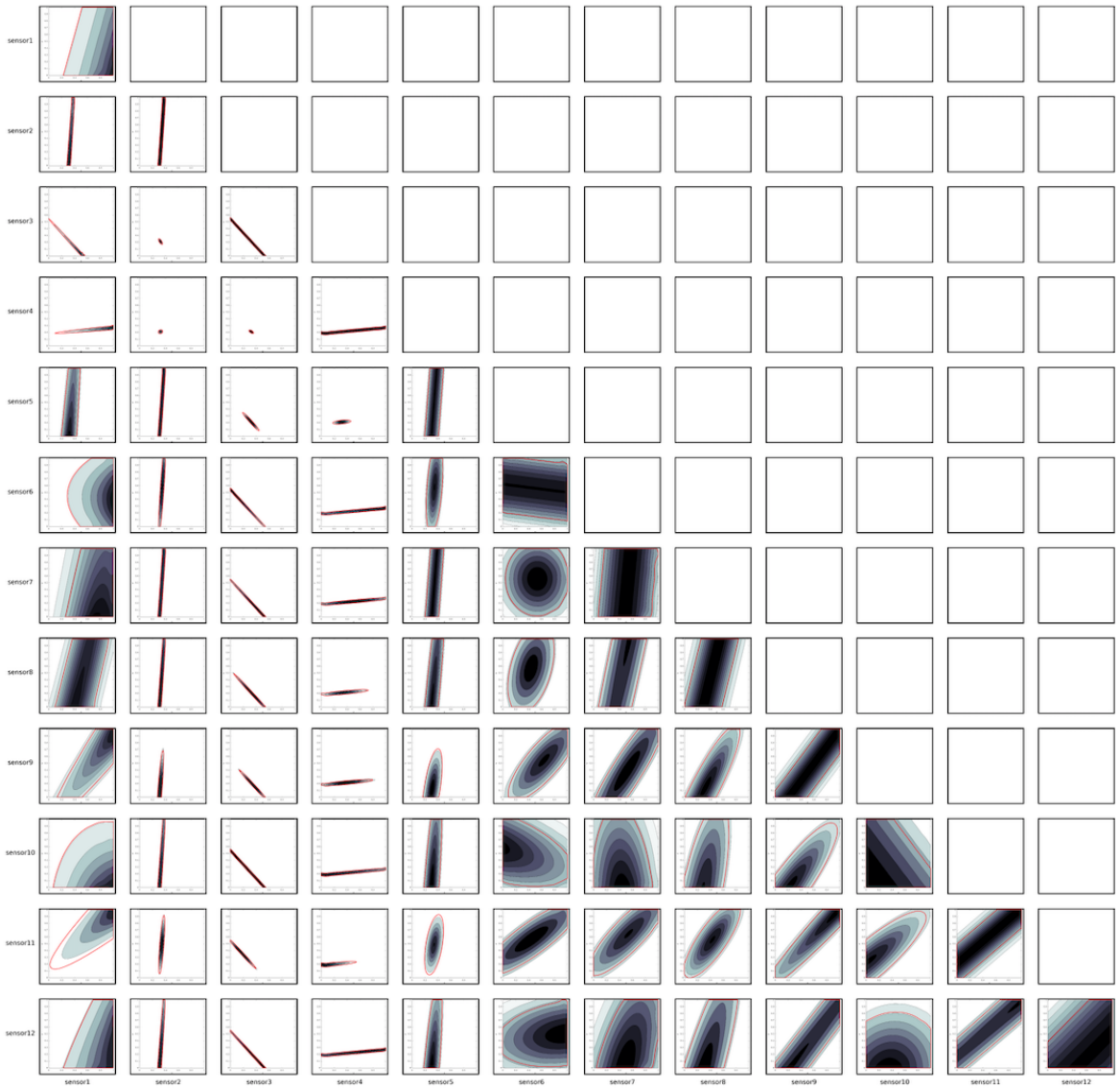

Figure 5.20: Matrix plot of posterior distribution using different pairs for pier settlement.

Figure 5.20 shows all details of posteriors and credible region for different sensor pairs if pier settlement is considered. As can be seen in Figure 5.22, using sensor 3 and 4 as a pair has the smallest entropy, which means the most information regarding the pier settlement can be extracted. As for the sensor types, both of them measure vertical displacement. From a mathematical point of view, using the monitoring data of sensor 3 and 4 could lead the lowest uncertainty in inferring the model parameters, while in engineering perspective, the sensor management has to give priority to the sensors measuring vertical displacement where either two out of three can provide relatively sufficient information of damage.

In comparison, the evaluation of information content using the area of credible region is shown in Figure 5.21. Similarly, it demonstrates that sensor 3 and 4 is still the most informative pair and the combination of vertical displacement sensor outperforms the rest type of sensor. For the rest pair, it seems that they perform equally with almost the same normalized value for the area of credible

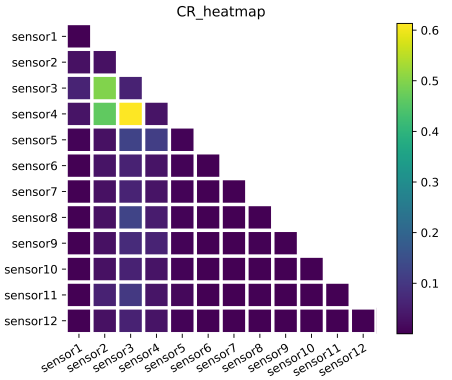

Figure 5.21: Information content using credible region of different pairs.

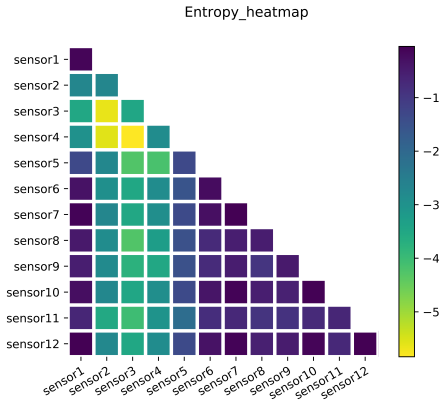

Figure 5.22: Information content using entropy of different pairs.

region. However, due to its lower degree of discrimination, it overlooked some acceptable pairs from an engineering perspective where a concentrated circle shape posterior is observed using sensor 4 and 5 in figure 5.20. It illustrates that using entropy as a measure of information content would present a better separation of sensor pairs.

In order to explore the capability of inferring parameters with other damage severity for the most informative pair, the damage severity has been set up from 0 to 1 while keeping the values of the two parameters equal, with an interval of 0.1 for both parameters each increment. The most informative pair and the pair providing least information are recorded to be compared to explore the relationship of information gain using the informative pair with the reference set.

The red dot represents the reference case of all twelve sensors (reference) the green dot represents the most informative sensor pair (minimum value of entropy/CR), and the blue dot represents the sensor pair with the least information (maximum value of entropy/CR), the figure 5.23 shows the gap of information content in different preset damage scenarios. It can be clearly seen that even though the damage severity increases from 0.1 to 0.9, the most informative sensor pair still remains the same (sensor 3 and 4) for this scenario. Another striking point is that in this figure, using more than the most informative pair of sensors provides very limited information gain as the gap between the red line and green line is relatively small.

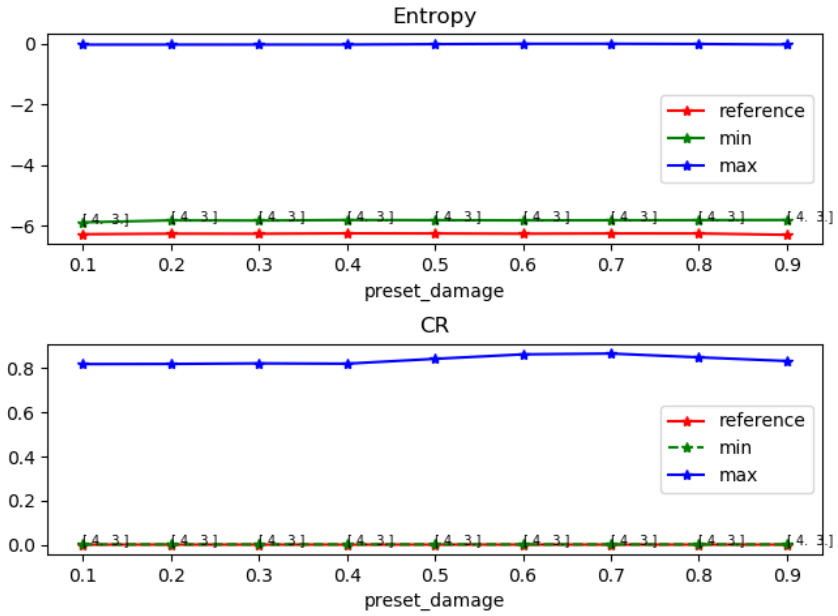

Figure 5.23: Information gain for the most informative pair.

BEARING DETERIORATION

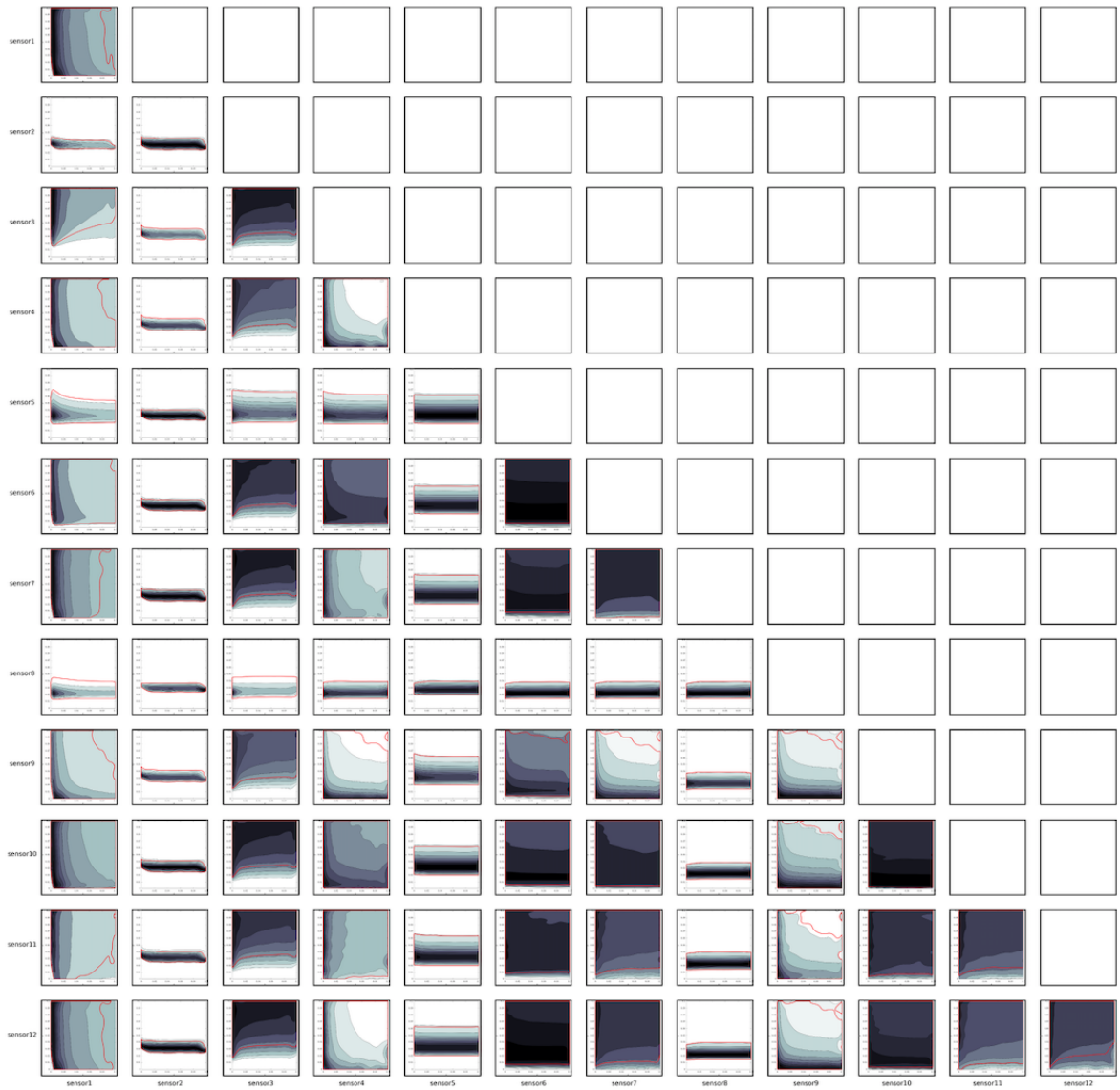

Figure 5.24: Posterior distribution of different pairs.

Figure 5.24 shows all details of posteriors and credible region for different sensor pairs if bearing deterioration is considered. It is visible that for the rotational spring parameter can be identified by some sensors, for example, the combination contained sensor 2 or 8. However, not all sensor pairs can identify the transversal displacement parameter accurately. This may be attributed to that the transversal displacement could barely affect the monitoring data, which leads the parameter to be unidentifiable.

As can be seen in Figure 5.26, using sensor 2 and 8 as a pair has the smallest entropy. It tends to be that the pair that contains either sensor 2, 5, or 8 slightly outperforms the rest of the sensor types. Although they come from totally different sensor types, the common feature for those sensors is that they are the closest sensors in their type to the pier TPN where the deterioration is considered. It can be generally concluded that in this damage scenario, the sensor close to the damage position tends to provide more information on the damage state.

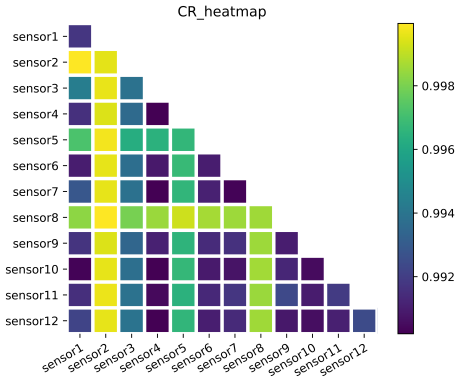

Figure 5.25: Information content using credible region of different pairs.

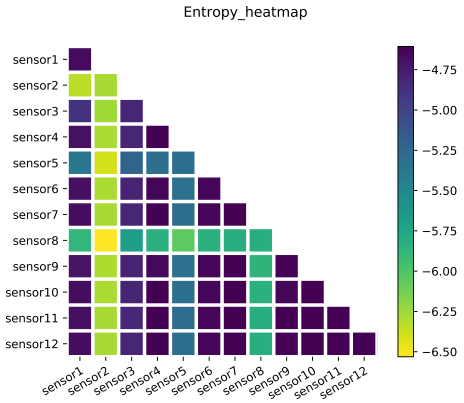

Figure 5.26: Information content using entropy of different pairs.

5

In comparison, the evaluation of information content using the area of credible region is shown in Figure 5.25. It verifies that sensor 2 and 8 is still the most informative pair. Interestingly, a similar conclusion that the closer sensors could extract more information can be drawn. Different with the pier settlement case, the credible region shows a great similarity with entropy in this case.

Moving to the most informative pair under different applied damage extent, Figure 5.27 presents sensor 2 and 8 would constantly be the most informative pair with regards to information entropy. Interestingly, the most striking point is this figure is the inconsistency in the credible region that the most informative pair could take over the reference set where all sensors are used in terms of the minimum credible region. Apparently, it is impossible that using two of the twelve sensors can provide more information than using all. The cause of this unexpected inconsistency is the numerical issue of determining the credible region mentioned in Section 5.6.3. Meanwhile, it illustrates that entropy is more numerically robust than credible region.

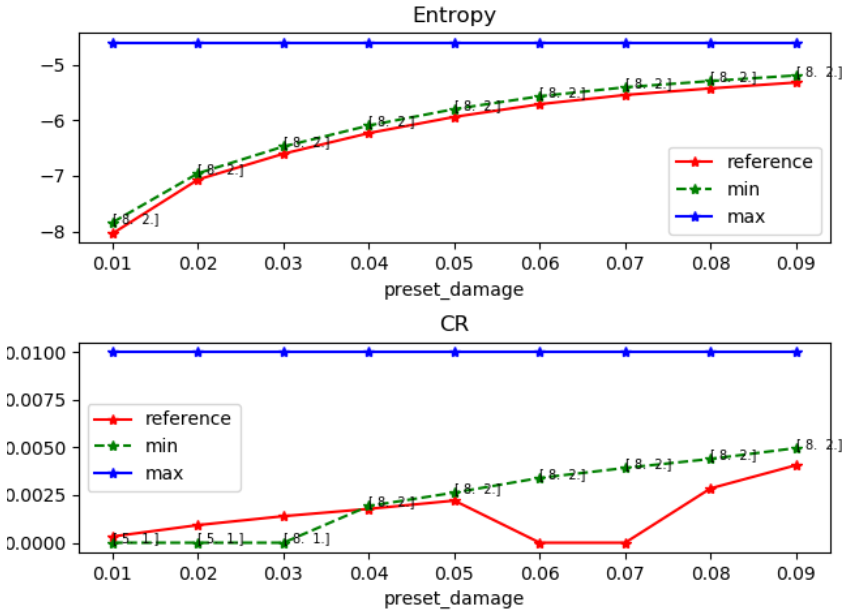

Figure 5.27: Information gain for the most informative pair.

PRESTRESS LOSS

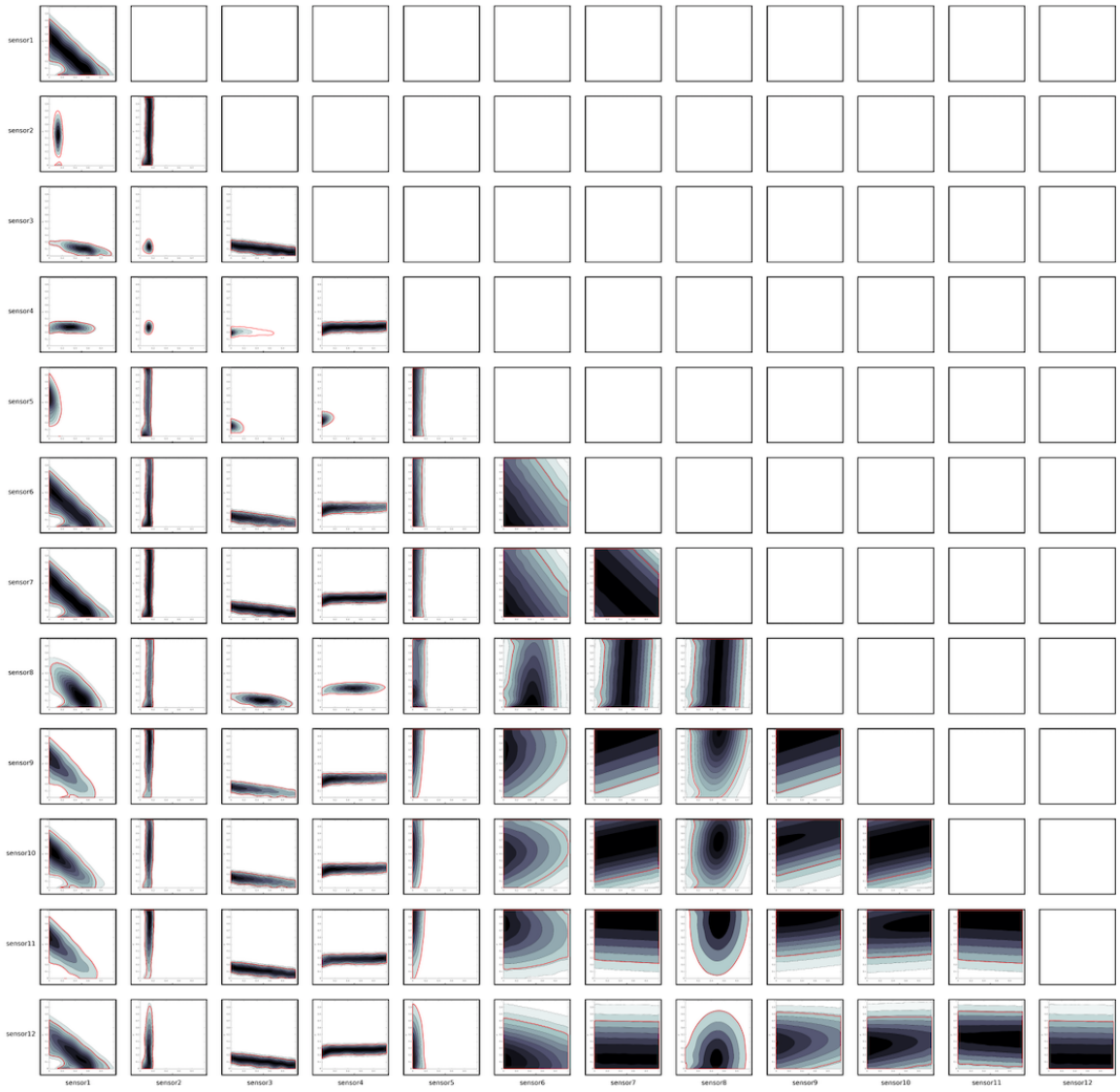

Figure 5.28: Matrix plot of posterior distribution using different pairs for prestress loss

Figure 5.28 shows all details of posteriors and credible region for different sensor pairs if prestress loss of the first segment and segment along Pier 1 and Pier 3 is considered. Apparently, using a combination of vertical displacement sensor could identify both parameters better as other contours of posteriors tend to be more dispersed.

As can be seen in the figures below, using sensor 2 and 4 as a pair has the smallest entropy, which is the same sensor pair for pier settlement damage scenario. As for the sensor types, both of them measure vertical displacement. It shows that measuring the vertical displacement is a relatively effective and efficient proxy of detecting the prestress loss along the considered part of Leziria bridge. It is also worth noticing that sensor 2 where the vertical displacement of the midspan $TPN-P1$ is measured appears in all above-mentioned case. Apart from the transducer sensor type, measuring the rotation of the TPN could at least provide a good inference for the first segment prestress loss, which may due to the fact that prestress loss would result in an inclination of support section TPN.

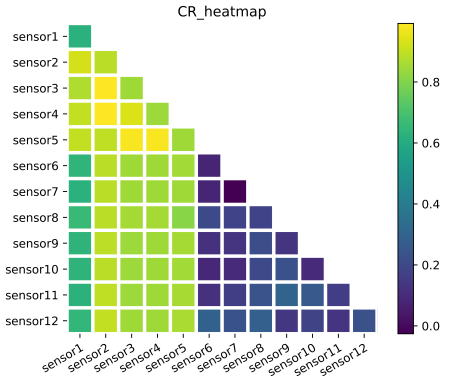

Figure 5.29: Information content using credible region of different pairs.

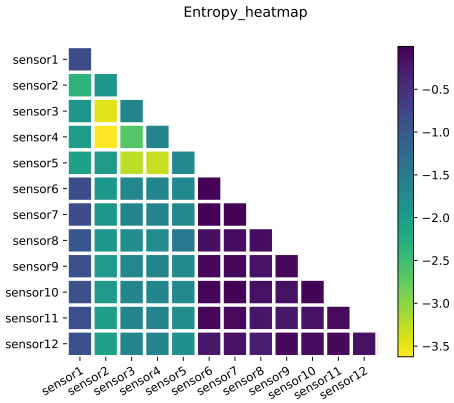

Figure 5.30: Information content using entropy of different pairs.

5

In comparison, the evaluation of information content using the area of credible region is shown in Figure 5.29. It verifies that sensor 2 and 4 is still the most informative pair. Interestingly, similar conclusion that the vertical transducers overwhelmingly outperform the rest sensor type in terms of extracting information for prestress loss. Again, the credible region and entropy perform similarly in this case.

Moving to the most informative sensor pair under different applied damage extent, the best pair varies when the preset damage extent is $[0.2, 0.2]$. Even though the most informative combination has changed, it is still within the scale of the vertical transducer. Another remarkable tendency in figure 5.31 is that the worst pair of sensors could rarely extract effective information regarding the damaged condition as the entropy is around 0 and credible region almost covers the entire support. As can be seen in figure 5.28, it tends to be most of the strain sensors are inefficient to detect the damage caused by prestress loss. In practice, if the prestress loss is suspected, installing the strain sensors might lead to a futile result.

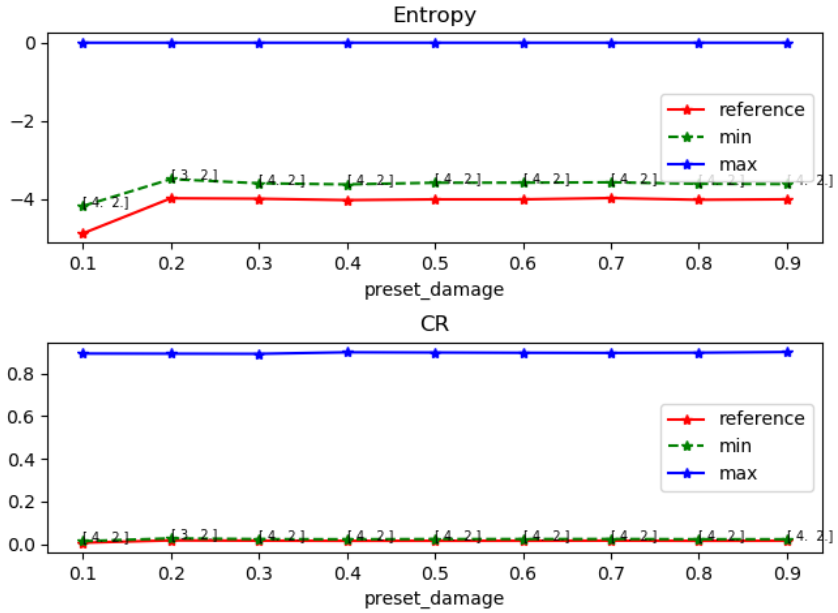

Figure 5.31: Information gain for the most informative pair.

LOSS OF STIFFNESS

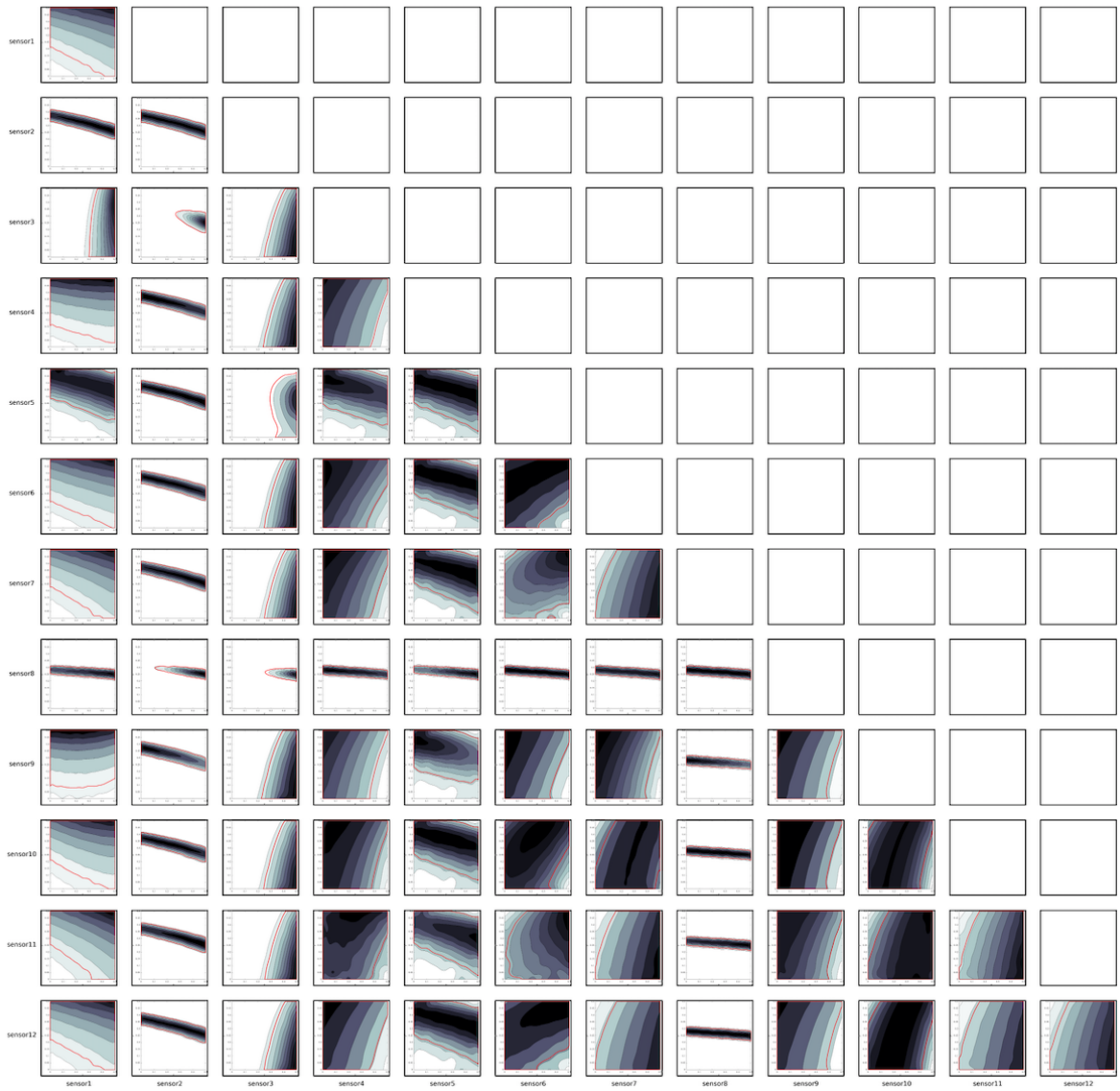

Figure 5.32: Posterior distribution of different pairs

Figure 5.32 shows all details of posteriors and credible region for different sensor pairs if stiffness loss from the cross-section of $TPN - P1$ and above $P1$ is considered. Intuitively, column 2 and column 8 in the matrix plot have a relatively concentrated shape of posterior contours.

Surprisingly, as can be seen in figures below, using sensor 3 and 8 as a pair has the smallest entropy, with one of them measuring the displacement of second span $P1P2$ and the other measuring the strain of midspan from the first segment. As the color scale differentiates from others, sensor 2, 3, and 8 are most efficient in detecting the damage caused by loss of stiffness. In Figure 5.34, column 4 where the sensor of a vertical transducer is contained no longer have a dominating performance than other sensor types. It may be attributed to that the effect of stiffness loss would not be significant to influence the vertical displacement of the midspan of the last segment.

In comparison, the evaluation of information content using the area of credible region is shown in Figure 5.33. It verifies that sensor 2 and 8 is still the most informative pair. Great similarity can be

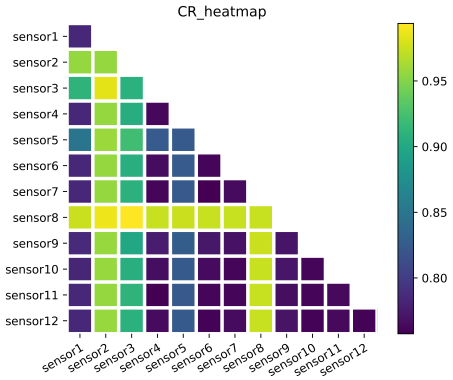

Figure 5.33: Information content using credible region of different pairs

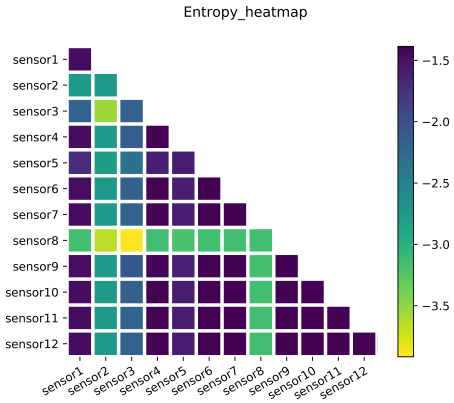

Figure 5.34: Information content using entropy of different pairs

5

observed in the comparison of these two measures of information content.

Turning to the most informative sensor pair under different applied damage extent, an interesting pattern can be observed in Figure 5.35 where for both credible region and information entropy, the best pair appears to alternate between the sensor 2, 3 and 8. It shows the variation of the best sensor pair under different damage severity. As the damage severity increases, measuring the vertical displacement of $P1P2$ where is away from the damaged spot could provide more damage information compared to measuring the displacement of $TPNP1$. It demonstrates that not only the most informative pair is conditional on the damage scenarios, but the severity of damage as well.

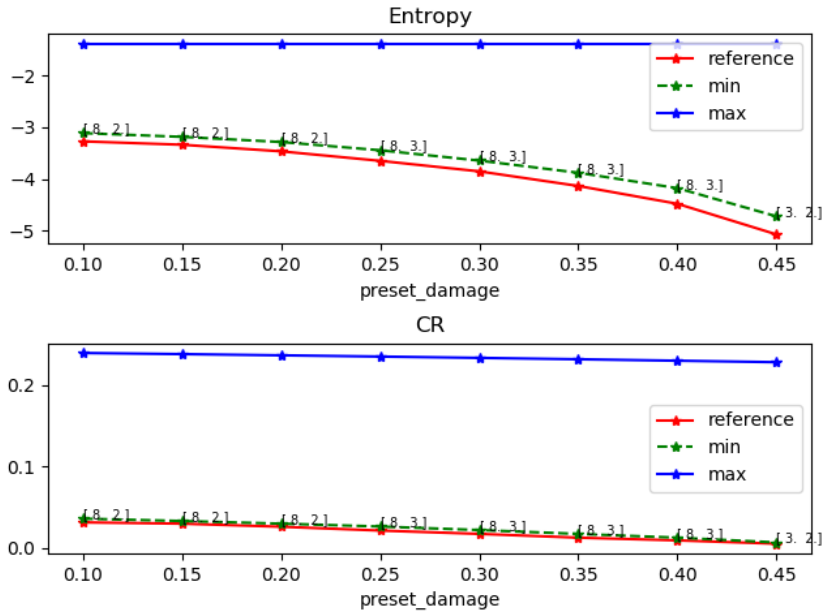

Figure 5.35: Information gain for the most informative pair.

5.6.4. COPULA

Besides analyzing the information carried by the joint distribution of two variables, the dependence of variables is explored through copula. The detailed methodology is introduced in Section 3.6. From the matrix plot of the detailed posteriors for all sensor pairs, there are three patterns of pos-

terior distributions that can be observed frequently, namely, the concentrated pattern, the elliptical pattern, and line-like shape. Because all of them are non-parametric distributions, τ coefficient is evaluated to match their corresponding parametric copula family with the same tau coefficient. The intent of matching its parametric family is to find out the underlying properties of the non-parametric copula. Five commonly used copulas are selected to be matched. Dividing the unit space into four quadrants, the copula density and correlations are plotted.

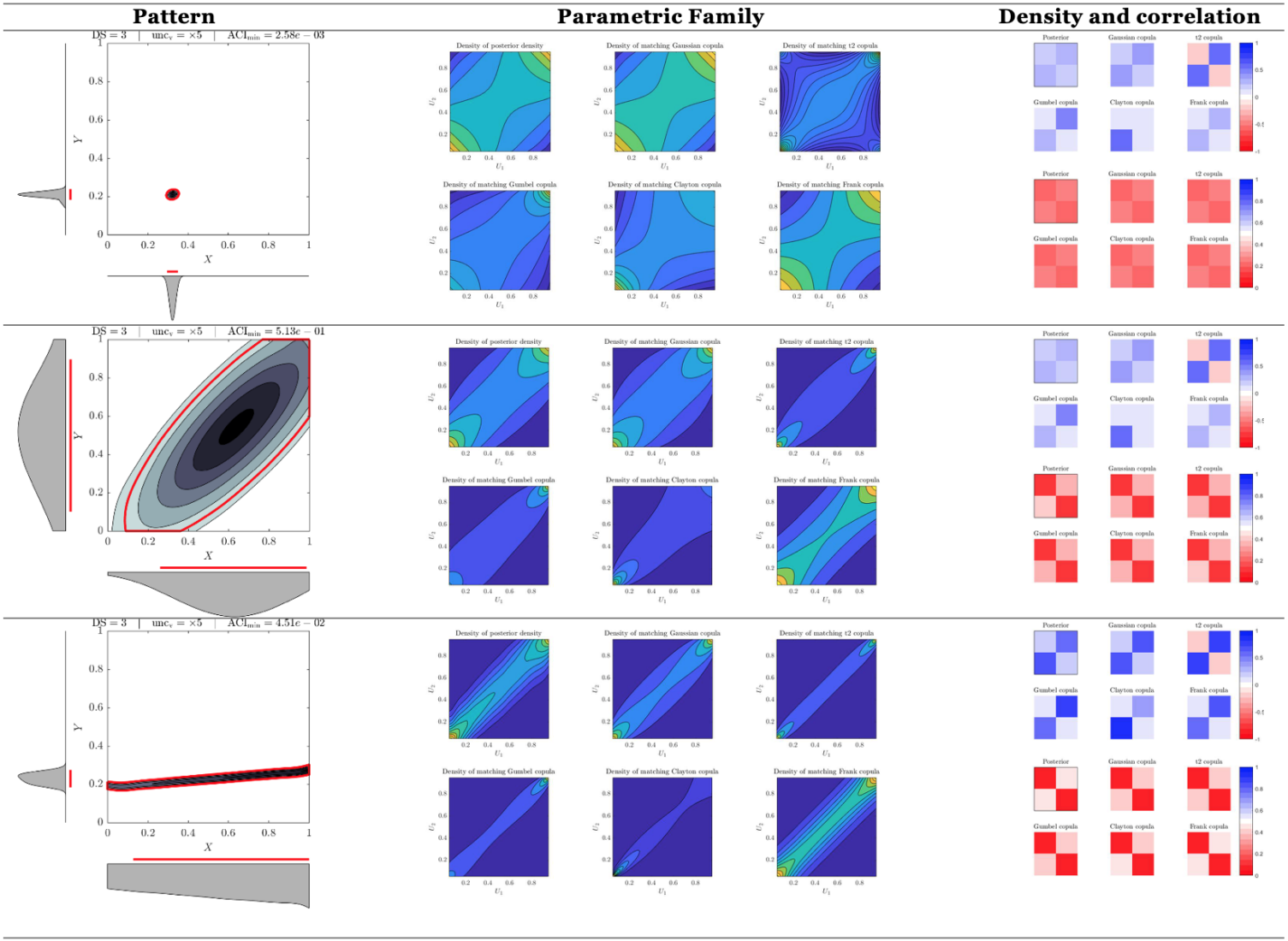

Figure 5.36: Matching parametric copulas for three frequently seen posteriors.

As shown in Figure 5.36, for circle-like posterior in the first row, the closest parametric copula is judged by visualization that the color scale of the density contour should be consistent with the non-parametric copula. Gaussian and Frank copula satisfy this condition with the same coefficient. It also presents both of them are consistent with the non-parametric copula in terms of correlation as well. As for the elliptical-like posterior, even though both the copula density and correlation in four quadrants for Frank copula have the same tendency as the non-parametric copula does, Gaussian copula is the more probable matching parametric family judging by the contour of copula density. The line-like posterior tends to match the Frank copula by checking all the criterion above-mentioned.

This analysis provides an approach to explore the dependency of two parameters with a set of parametric copulas. However, there are plenty of methods which could extend the research of copula, for example, tail dependency, and sampling from copula in higher dimensional. But it is out of the scope of this thesis.

5.7. APPROXIMATE BAYESIAN COMPUTATION

Above sections focus on four damage scenarios considered separately. Nevertheless, in reality, all damage scenarios could occur simultaneously and a single damage scenario can be defined with more parameters, which motivate higher dimensions with more parameters to be probed. The actual damage state might be a combination of the aforementioned damage scenarios. In this section, it is assumed pier settlement and prestress loss can take place together. The intent for DI is expanded to infer both four parameters that describe the combined damage scenarios. The reason for choosing pier settlement and prestress loss is based on the assumption that the bridge is in the elastic phase, the superposition of responses is valid because both of them are under the same loading configurations and the neither stiffness nor the boundary conditions change. The new responses for each sensor can be manipulated as a summation of the responses from each scenario. As mentioned in Section 3.4.3, numerical integration is intractable to obtain the evidence when parameter space extends to higher dimensions. Therefore, the numerical integration would not be feasible anymore, asymptotic approximations of posterior distribution are proposed instead. MCMC algorithms and VI are studied as asymptotic approximation method subsequently. The ability to infer the different types of parameters, performance of the most informative sensor combinations in higher parameters space, and efficiency of different computational methods are explored in this section.

5.7.1. UNCERTAIN PARAMETERS

The actual damage scenario consists of the pier settlement and the prestress loss, so the parameters have been expanded to four, with the first two indicating prestress tendon loss, third and fourth representing the severity of pier settlements. The severity is set the same as previous analysis in Table 5.5.

Damage Scenarios	Parameters	Lower bound (no damage)	Upper bound (full damage)	Normalization (range)
Prestress loss	θ_1: PTD1	1341 MN	0 MN	(0, 1)
	θ_2: PTD2	1270 MN	0 MN	(0, 1)
Pier settlement	θ_3: ΔP_{TD1}	0.0 m	0.5 m	(0, 1)
	θ_4: ΔP_{TD2}	0.0 m	0.5 m	(0, 1)

Table 5.5: Uncertain arameters for each damage scenario.

After specifying the parameters and obtaining new responses which is observed under the combination of damage scenarios, the Bayesian inference can be conducted. As discussed in chapter 4, the hybrid MCMC is more efficient of drawing samples from posterior. Therefore, HMC is applied in this circumstance. Using HMC, with two chains and the first 500 samples burnt in, the inference result is visualized by trace plot, scatter plot and the statistical quantities of samples. A uniform distribution is applied for the prior which is the green dash line in the marginal plot.

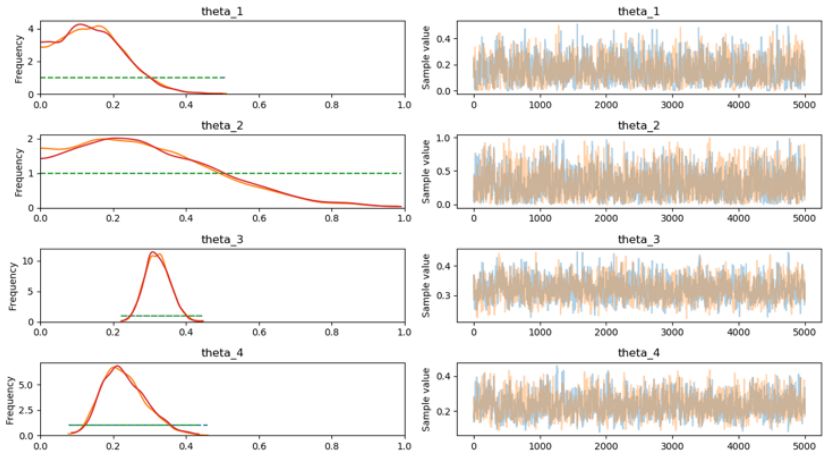

Figure 5.37: Trace plot of parameters.

In general, the figures illustrate that for the combined scenario, pier settlement has a better identifiability than prestress loss. The samples are projected in two separate damage spaces for the scatter plot where samples in pier settlement space have a more concentrated cluster. The trace plot shows the sample marginal distribution of those four parameters where θ_2 has a wider range than the rest. θ_2 is not accurately identified according to Table 5.6 where the deviation of posterior mean estimation has been summarized. To conclude, considering the damage combination of pier settlement and prestress loss, the parameters that define the pier settlement severity tend to be identified more accurately, while the parameters for prestress loss are less sensitive to be identified. Different than the scenario that only prestress loss occurs where both parameters can be inferred precisely, the second parameter that describes the prestress loss between pier $P1P3$ is less identifiable in higher dimension space. The underlying engineering explanation may be the pier settlement has a more significant influence on the monitoring data for this specific case. Table 5.6 confirms that except the second parameter, the rest parameters can be identified reasonably using the uniform prior and MCMC simulation. It also illustrates the availability of Bayesian approach applied in SHM for higher dimensions. Next, the sensor management will be discussed based on the previous analysis.

Notation	Severity	Posterior Mean	Deviation (%)
θ_1	0.14	0.146	4.28
θ_2	0.22	0.301	36.8
θ_3	0.32	0.322	0.625
θ_4	0.21	0.231	10

Table 5.6: Accuracy of posterior mean approximation

5.7.2. THE MOST INFORMATIVE SENSOR TYPE

According to the conclusion of Section 5.6.3, the most informative sensor type for all proposed damage scenarios is the sensor that measures vertical displacement. Either sensor 2,3, or 4 that belongs

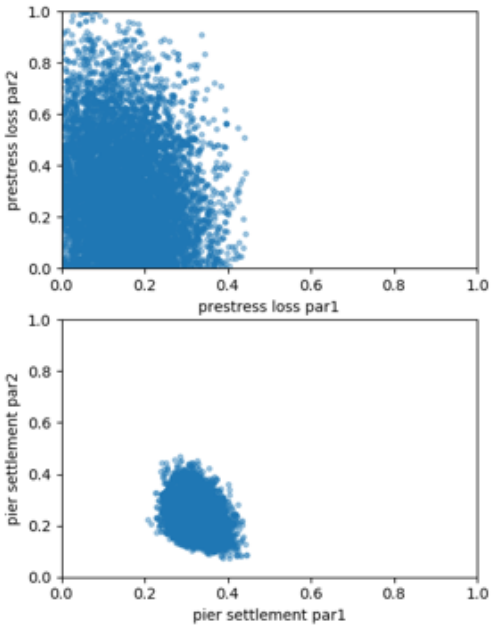

Figure 5.38: Scatter plot of samples.

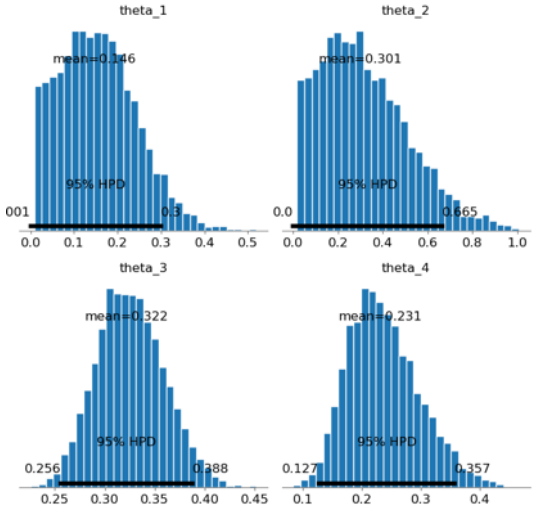

Figure 5.39: Posterior distribution of parameters.

to vertical displacement sensor type has appeared as the one component of the most informative pair. In this session, the comparison between the most informative sensor type and the rest sensors is made in high-dimension parameter space. It aims to test if the most informative type in the 2D case can still extract considerable information in higher dimensions.

The Bayesian inference is conducted twice, the first time using the monitoring data from the vertical displacement sensors, and the second time using the rest of the sensor. The performance is visualized in the Figure 5.40 where using vertical transducers is more informative than the combination of rest sensor types based on the scatter plot of parameters. It shows that using the most informative sensor type is able to identify most parameters. It is visible that for the pier settlement parameters, using vertical transducer monitoring data outperforms the combination of the rest of the sensor types.

It further reveals the information content of a posterior might be attributed mostly to the informative pairs or sensor types. However, the additional information could be captured by the rest of sensors if one looks at trace plot of θ_2 in Figure 5.42. The sample is fluctuating around the uniform distribution which means data barely changes the initial belief. According to the deviation changes which is the ratio of the discrepancy between posterior mean and preset value divided by preset value in Table 5.7, it confirms that using more than the vertical displacement sensor type could only provide limited information. Nevertheless, only installing the displacement sensors are not sensitive to detect the prestress loss in the second segment where complementary sensors should be used to identify the damage.

5.7.3. COMPARISON OF COMPUTATIONAL METHODS

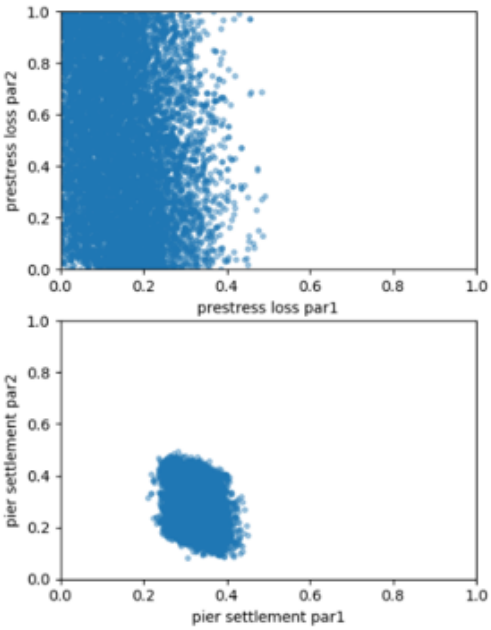

Figure 5.40: Scatter plot of settlement parameters using VD sensor type.

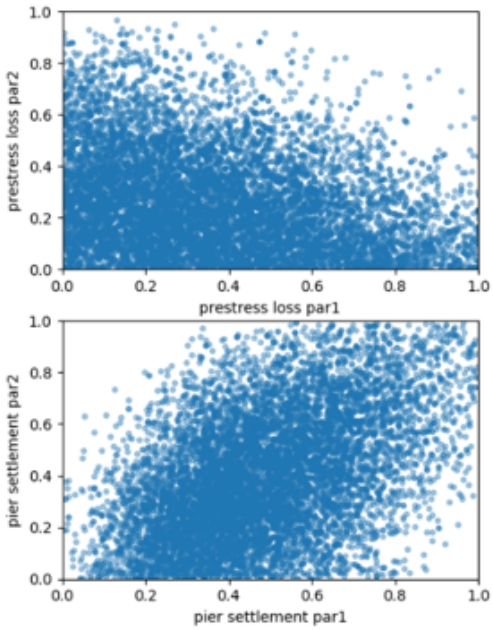

Figure 5.41: Scatter plot of settlement parameters using the rest sensors.

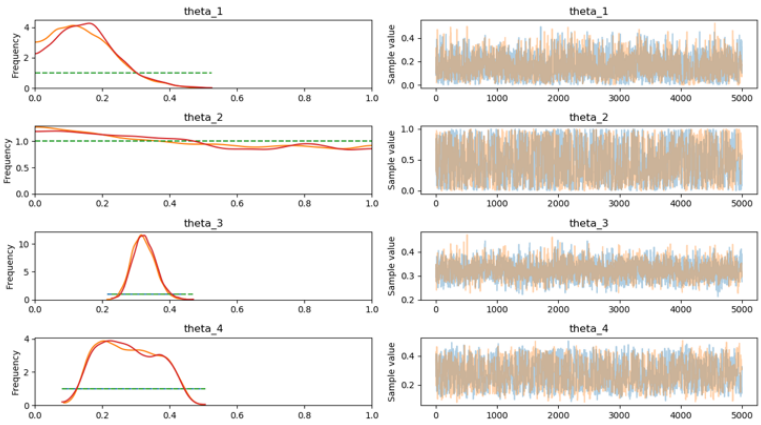

Figure 5.42: Trace plot using vertical displacement sensor.

Notation	Severity	Deviation (%)	Deviation (%) using VD sensors
θ_1	0.14	4.28	7
θ_2	0.22	36.8	112
θ_3	0.32	0.625	9
θ_4	0.21	10	10

Table 5.7: Accuracy of posterior mean approximation.

As a continuation of the benchmark shear frame problem, three different algorithms are tested in this case. First, MH and HMC are compared as the same scheme in section 4. Assumption that HMC evaluates likelihood twice than Metropolis-Hasting is made in consistent with section 4.7. The

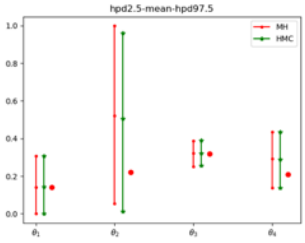

Figure 5.43: 95% credible interval

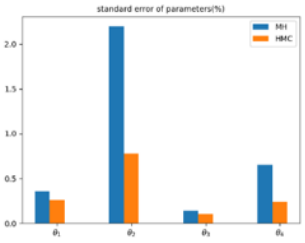

Figure 5.44: Standard error

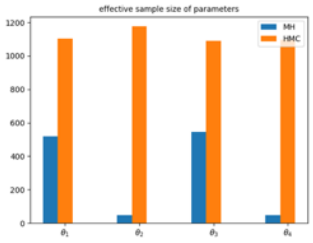

Figure 5.45: Effective sample size

simulation setting is also similar to previous case, with 500 burn-in samples, 5000 draws for HMC and 10000 draws for MH. The results are visualized in terms of credible interval, standard error, and effective sample size as shown below.

Unlike the shear frame case that some standard error from certain parameter drawing by MH might be smaller than HMC, those figures depict HMC outperform MH significantly in other aspects though the credible interval is still close to each other. It is worth noticing that samples drawn by MH have a high autocorrelation, while HMC has consistently better behavior through all the parameters. It again illustrates that HMC is more effective and efficient as the complexity of structure goes high in DI.

Furthermore, variational methods are also important techniques for the approximation of complex distribution. Being applied in statistical physics, data modeling and neural networks [3], ADVI has been tested in this context. The details of ADVI implementation can be found Blei *et al.* [26], only the results are shown in Figure 5.46. As can be seen clearly in this figure, some of the parameters could be properly identified by ADVI. But the deviation for the second parameter is considerably large. This may due to the parametric distribution is still far from the target distribution even though the relative entropy is minimized.

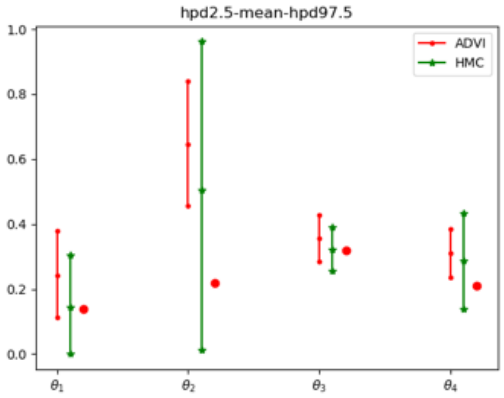

Figure 5.46: Variational inference.

6

CONCLUSION

6.1. CONCLUSIONS RELATED TO THE MAIN RESEARCH QUESTION

Although in practice, deterministic methods where data is used to identify one model to predict structural behavior are commonly used, Bayesian approach is a more robust framework to cope with the uncertainty by assigning appropriate probabilities to a series of possible models. Incorporating model uncertainty and measurement uncertainty, damage identification using Bayesian approach is able to infer parameters of a structure given a specific set of measured data. To answer the main research question:

- *Given a civil engineering structure and responses that can be measured potentially, which responses should be monitored so that the damage identification using Bayesian inference would give the most information on the damaged condition?*

A shear frame is analyzed to capture the clue of this question, after which a realistic bridge is investigated as a follow-up to validate the features obtained from the previous case. The conclusion is summarized in three aspects for each case, specifically, acquisition of monitoring data , evaluation of information content, behavior of different computational algorithms.

6.1.1. DERIVED FROM THE SHEAR FRAME

First of all, using the displacement of each story or natural frequency of the structure as monitoring data for Bayesian inference is able to infer the stiffness scale factors of the column. However, measuring displacement and natural frequency would have a distinctive performance in terms of information carried by the posterior distributions. Using natural frequency as measurable data might yield multimodal posterior, while measuring displacement always generate a unimodal posterior regardless the damage scenarios. This is due to the underlying equations of the stiffness parameter and the measurable responses, specifically, as the measurement uncertainty decreases, the posterior would shrink towards the deterministic solution where there is no uncertainty at all. Given certain frequency responses, sometime there are two pairs of possible solutions which result in the multimodality of posterior distributions. In general, measuring different responses from the structure may significantly affect the information content carried by the posterior distribution of parameters. In this case, measuring displacement outperforms natural frequency in identifying the stiffness reduction of the shear frame. This is not only because it has a smaller area of credible region in all damage scenarios, but the constant unimodality for measuring displacement.

6.1.2. DERIVED FROM THE FULL-SCALE APPLICATION

To validate the findings from the shear frame case, the conclusions related to the monitoring data can be drawn as follows. In general, damage severity can be identified using all available sensors for all possible damage scenarios proposed. Regardless the measurement uncertainty may have a huge influence on the posterior distribution, the applied damage is involved in 90% credible region. Moving to the contribution of monitoring different responses, using the most informative sensor pair could obtain adequate information on the damage state. It is demonstrated that more than the most informative pair provides negligible gain in terms of information entropy. It is also further illustrated in high dimensional space where only using displacement measuring sensors could yield a more informative result than using all the rest sensors. Although this feature may largely depend on the structure itself, it still offers a methodology to prioritize which sensor to be installed.

6.1.3. GENERAL CONCLUSIONS OF BAYESIAN INFERENCE APPLIED TO A REALISTIC STRUCTURE

- Prior analysis is important as some of the inference might be highly conditional on the selected prior, which may significantly influence the result.
- Information entropy is more robust numerically than the credible region to measure the information carried by posteriors.
- The joint distribution of parameters can be analyzed from a statistical point of view to explore the dependency structure of two variables: copula analysis. The dependency properties can be estimated by its matching parametric copula family.
- In higher dimensions, the posterior mean provides an accurate approximation of preset damage, which illustrates that the statistical techniques of Bayesian inference can be successfully implemented for DI of Civil Engineering structures.
- The hybrid Monte Carlo outperforms the random-walk based MCMC in terms of effective sample size and standard error in this context. Despite the complexity of the structure, using responses surface and HMC computational method enables to sample parameters effectively and efficiently.

6.2. CONCLUSIONS RELATED TO SUB RESEARCH QUESTIONS

The sub-research questions are also analyzed through these two cases. The first question is:

- *What is the most versatile criterion to evaluate the information carried by the probability distribution of the parameters that reflect damage state of the structure?*

In this study, credible region and information entropy are applied as the measurement of information content carried by the posterior distributions. Both of them are able to reflect the informativeness of the damage identification results.

As for credible region, it is easy to visualize its shape, which provides intuitive information on the behavior of damage identification. For instance, a circle-like posterior may have an identical area of credible regions with a line-like posterior, which means they have almost the same informativeness in this aspect. However, considering the engineering background of the damage identification, a circle-like posterior tends to be more favorable of determining the damage state of a structure than a line-like posterior with an equal area of credible region. This is because for a circle-like shape, it is easier to estimate the potential damage with a relatively small range. Furthermore, the credible region is able to present the modality of a posterior where multiple modes could be observed. While the deficiency of using credible region is obvious as well. When determining the credible region,

numerical issues may happen where the posterior is a spike shape and the density is concentrated around one point.

Information entropy is introduced as a numerically robust measurement due to this issue. As shown in section 5.6.3, not only entropy tackles evaluation of information content for the spike shape posterior perfectly, but it seems that it has a more distinguishable scale for different posteriors. However, when it comes to posteriors having the identical entropy, information entropy is not capable of recognizing the modality of them which may affect the decision of monitoring data type and sensor management.

Overall, visualizing credible region assists engineers with choosing a more desirable posterior intuitively, while information entropy carries out a series hierarchical value which provides a rigorous scheme to measure the information content of posteriors. Accordingly, although entropy is a more versatile measurement of informativeness considering the numerical robustness, credible region should still be used as a complementary method to support engineers in making decisions.

Moving to the second research question:

- *Which commonly used Bayesian computational algorithms perform better considering the fact that computational demanding FE model is involved in damage identification?*

The MH and HMC are compared in both cases. For the reason that HMC needs to evaluate the gradient of posterior PDF, it assumes that HMC will double the time than MH. The performance is discussed in terms of the 95% credible interval, standard error, and effective sample size. For the credible interval, both of them in two cases include the preset value in the credible region, with the range of the credible region almost same with each other. MH and HMC behave equally well in this aspect. Besides, the posterior mean in the shear frame case provides close approximation of the preset damage severity. But for the standard error and effective sample size, HMC outclasses MH with smaller error and less correlated samples. This is reflected notably in the Leziria bridge case where the effective sample size of MHC is nearly 10 times larger than that of MH with almost the same computational effort. As a result, Hybrid MCMC where the random walk behavior is reduced, the efficiency and effectiveness are both increased in drawing samples of parameters in the context of damage identification using Bayesian approach. In addition, apart from the MCMC family, the variational inference method is tested as well. But the result is not as accurate as MCMC family with only some of the parameters include the preset damage severity in the 95% credible interval.

SUGGESTIONS TO THE ASSET OWNER

- Damage identification for a complex Civil Engineering asset using Bayesian approach is not only available but also promising with uncertainties taken into account.
- Generally, the number and type of sensors are limited in real-life applications. Nevertheless, Bayesian analysis coupled with the measurement of information carried by posteriors aids asset owner to choose the most effective sensor types. The most informative sensor type is able to extract adequate information of the damage state. Moreover, through the analysis of the Leziria bridge, one may generally conclude that the most informative sensors always measure the quantities that are relatively more sensitive to the damage scenario. The sensitivity of monitoring data is reflected by the informativeness of its corresponding posterior distribution.

7

LIMITATIONS & RECOMMENDATIONS

7.1. LIMITATIONS

The limitation is presented in three aspects that associated with the research questions accordingly: data acquisition, information content measurement, and computational methods.

Data acquisition

- The monitoring data of the studied two cases is synthetic, i.e. generated from FE models. In practice, the data is acquired from real structures. Multiple model-measurement uncertainty extents are considered in the simulation studies to cover a wide range of realistic situations. However, it is impossible to cover all situations that can be encountered in practice. A further limitation is the mathematical structure how model-measurement uncertainty is modeled, i.e. additive model.
- The sensor types and locations are fixed, corresponding to the actual monitoring system. The most informative sensor pair is selected from this fixed set of sensors; therefore, the related conclusions likely particular to the Leziria bridge and cannot be generalized.
- The majority of the completed analysis is dealing with 2-dimensional problems (i.e. two parameters to be inferred), and a smaller part is concerning with higher, 4-dimensional problems. The 4-dimensional problems are restricted to the combination of pier settlement and prestress. Further combinations and higher dimensional damage scenario description would be needed to generalize the conclusions.

Measure of Information Content

- Although the process of determining the credible region utilizes the built-in integration methods of Matlab, sometimes the algorithms fail.
- In higher dimensional cases, the comparison of informativeness of different sensor set is made based on the scatter plot, which is obvious to compare. Entropy cab be generalized to higher dimensions, but it is not done in this study.

Computational Methods

- A critical assumption is that the computation of the gradient in case of the HMCMC algorithm doubles the computational effort of the traditional random-walk-based MCMC is made to keep the amount of evaluations of likelihood function or its gradient identical. However, this may be dependent on the custom likelihood functions and samplers.

- Despite the amount of evaluations is identical for comparison, no tuning process is made for different methods. For instance, the performance would be better if the most optimal proposal function is found for MH or the optimal frog step size is set for HMC
- The VI method has not been constrained with the same computational effort due to it calculates the relative entropy as well, only performance with the same amount of samples is presented.
- Only limited computational methods are compared. There are other commonly used algorthms such as transitional MCMC, slice sampling, and Gibbs sampling are not investigated in this study due to the time limit.

7.2. RECOMMENDATIONS

Further study should focus on:

- Using the real monitoring data set of a realistic monitored structure
- Refining the comparison scheme for different computational methods and involving more algorithms
- Improving the calculation of credible region by finding a more robust method to tackle with the concentrated posterior PDF
- Finding the most informative sensor layout by not fixing the sensor location for different considered damage scenarios
- Exploring more in the higher dimensional space where more parameters can be set to describe a more complex damage scenario
- Extending the copula analysis to capture interesting dependency features

BIBLIOGRAPHY

[1] H. Sousa, Árpád Rózsás, A. Slobbe, W. Courage, and A. B. van Vliet, *Development of a novel proactive shm tool devoted to bridge maintenance based on damage identification by fe analysis and probabilistic methods - Application to the Lezíria Bridge* -, Tech. Rep. (TNO, 2018).

[2] J. L. Simon, *Resampling: The new statistics,* (1997).

[3] D. J. MacKay and D. J. Mac Kay, *Information theory, inference and learning algorithms* (Cambridge university press, 2003).

[4] *Leziria bridge,* http://www.datajembatan.com/index.php?g=guest_bridge&m=bridge.detail&b=707, accessed: 2018-09-30.

[5] H. Sousa, C. Félix, J. Bento, and J. Figueiras, *Design and implementation of a monitoring system applied to a long-span prestressed concrete bridge,* Structural concrete **12**, 82 (2011).

[6] A. Gelman, H. S. Stern, J. B. Carlin, D. B. Dunson, A. Vehtari, and D. B. Rubin, *Bayesian data analysis* (Chapman and Hall/CRC, 2013).

[7] M. Hofert, M. Mächler, and A. Mcneil, *Likelihood inference for archimedean copulas in high dimensions under known margins,* Journal of Multivariate Analysis **110**, 133 (2012).

[8] M. W. Vanik, J. L. Beck, and S. Au, *Bayesian probabilistic approach to structural health monitoring,* Journal of Engineering Mechanics **126**, 738 (2000).

[9] S. W. Doebling, C. R. Farrar, M. B. Prime, and D. W. Shevitz, *Damage identification and health monitoring of structural and mechanical systems from changes in their vibration characteristics: a literature review,* (1996).

[10] M. Sanayei and M. J. Saletnik, *Parameter estimation of structures from static strain measurements. i: Formulation,* Journal of Structural Engineering **122**, 555 (1996).

[11] X. Wang, N. Hu, H. Fukunaga, and Z. Yao, *Structural damage identification using static test data and changes in frequencies,* Engineering structures **23**, 610 (2001).

[12] J. L. Beck and L. S. Katafygiotis, *Updating models and their uncertainties. i: Bayesian statistical framework,* Journal of Engineering Mechanics **124**, 455 (1998).

[13] S. Mustafa and Y. Matsumoto, *Bayesian model updating and its limitations for detecting local damage of an existing truss bridge,* Journal of Bridge Engineering **22**, 04017019 (2017).

[14] E. Figueiredo, L. Radu, K. Worden, and C. R. Farrar, *A bayesian approach based on a markov-chain monte carlo method for damage detection under unknown sources of variability,* Engineering Structures **80**, 1 (2014).

[15] D. Straub and I. Papaioannou, *Bayesian updating with structural reliability methods,* Journal of Engineering Mechanics **141**, 04014134 (2014).

[16] H. Sohn and K. H. Law, *A bayesian probabilistic approach for structure damage detection,* Earthquake engineering & structural dynamics **26**, 1259 (1997).

[17] J. L. Beck and S.-K. Au, *Bayesian updating of structural models and reliability using markov chain monte carlo simulation,* Journal of engineering mechanics **128**, 380 (2002).

[18] S. H. Cheung and J. L. Beck, *Bayesian model updating using hybrid monte carlo simulation with application to structural dynamic models with many uncertain parameters,* Journal of engineering mechanics **135**, 243 (2009).

[19] W. Zheng and Y. Yu, *Bayesian probabilistic framework for damage identification of steel truss bridges under joint uncertainties,* Advances in Civil Engineering **2013** (2013).

[20] J. L. Beck and K.-V. Yuen, *Model selection using response measurements: Bayesian probabilistic approach,* Journal of Engineering Mechanics **130**, 192 (2004).

[21] C. Papadimitriou, J. L. Beck, and S.-K. Au, *Entropy-based optimal sensor location for structural model updating,* Journal of Vibration and Control **6**, 781 (2000).

[22] J. Kruschke, *Doing Bayesian data analysis: A tutorial with R, JAGS, and Stan* (Academic Press, 2014).

[23] A. Gelman, D. B. Rubin, *et al.*, *Inference from iterative simulation using multiple sequences,* Statistical science **7**, 457 (1992).

[24] K. Conrad, *Probability distributions and maximum entropy,* Entropy **6**, 10 (2004).

[25] H. Sousa, J. Bento, and J. Figueiras, *Assessment and management of concrete bridges supported by monitoring data-based finite-element modeling,* Journal of Bridge Engineering **19**, 05014002 (2014).

[26] D. M. Blei, A. Kucukelbir, and J. D. McAuliffe, *Variational inference: A review for statisticians,* Journal of the American Statistical Association **112**, 859 (2017).